



Structure functions in the three nucleon system

François René Pierre Bissey

Thesis submitted for the degree of

Doctor of Philosophy

at

The University of Adelaide

(Department of Physics and Mathematical Physics)

18th March 2002

Contents

Contents	i
List of Figures	iii
List of Tables	v
Abstract	vii
Résumé (French summary)	ix
Statement	xi
Acknowledgements	xiii
1 Introduction	1
2 The three nucleon wave function	7
2.1 Introduction	8
2.2 Notation	8
2.3 The partial wave expansion	10
2.4 Separable potential	10
2.5 The three-nucleon wave function	11
2.6 Numerical results	15
3 Structure functions and convolution formalism	19
3.1 The electromagnetic cross section	20
3.2 Particularly interesting cross sections	23
3.2.1 Unpolarised scattering	23
3.2.2 Polarised scattering	23
3.3 The convolution formalism	24
3.3.1 The partial wave impulse approximation	24
3.3.2 Convolution of the structure functions	29

4	Spectral functions and light-cone momentum distributions of the three nucleon system	33
4.1	The spectral function	34
4.2	The case of ^3He	36
4.2.1	Neutron in ^3He	36
4.2.2	Proton in ^3He	39
4.3	Results	40
5	Unpolarised structure functions of the three nucleon system	45
5.1	Parton model	46
5.2	EMC effect	47
5.3	Gottfried sum rule	50
5.4	The neutron structure function F_2^n	52
6	Polarised structure functions of the three nucleon system	59
6.1	Parton model	60
6.2	Off-shell corrections	61
6.3	Non-nucleonic degrees of freedom	62
6.4	The neutron in ^3He	65
6.5	The proton in tritium	70
7	Conclusions	73
A	The kernel of the homogeneous Faddeev equation	79
B	The permutation term	85
	Bibliography	89
	List of Publications	97

List of Figures

2.1	A graphical representation of Eq. (2.1).	9
2.2	Angular momentum and momentum in the three body system.	9
3.1	Scattering of a lepton l on a nucleus A , with one photon exchange.	20
3.2	In PWIA, only one nucleon of the nucleus is struck by the photon.	25
3.3	Handbag diagram.	27
3.4	Cross term diagram.	28
3.5	Higher twist diagram neglected using assumption (3).	28
4.1	Neutron light-cone momentum distribution in ^3He for various potentials.	38
4.2	Neutron polarised light-cone momentum distribution in ^3He for various potentials.	38
4.3	Proton light-cone momentum distribution in ^3He for various potentials.	41
4.4	Proton polarised light-cone momentum distribution in ^3He for various potentials.	41
5.1	The ratio R_3 , given in Eq.(5.9), for ^3He , at $Q^2 = 10 \text{ GeV}^2$, calculated for various potentials using the CTEQ5 quark distributions.	49
5.2	The ratio R_3 , given in Eq.(5.9), for ^3H , at $Q^2 = 10 \text{ GeV}^2$, calculated for various potentials using the CTEQ5 quark distributions.	49
5.3	The ratio R_3 , given in Eq.(5.9), for ^3He , at $Q^2 = 10 \text{ GeV}^2$, calculated for the PEST potential, using various quark distributions for the nucleons.	50
5.4	The difference $F_2^A(x) - F_2^{A'}(x)$ for both the tri-nucleon system and the free nucleon, at $Q^2 = 10 \text{ GeV}^2$, using the CTEQ5 quark distributions.	53

5.5	The difference $(F_2^A(x) - F_2^{A'}(x))/x$ for both the tri-nucleon system and the free nucleon, at $Q^2 = 10 \text{ GeV}^2$, using the CTEQ5 quark distributions.	53
5.6	The ratio of ratios, Eq. (5.19), for various potentials, using the CTEQ5 parametrisation at $Q^2 = 10 \text{ GeV}^2$	55
5.7	The ratio of ratios, Eq. (5.19), using the CTEQ5 quark parametrisation at $Q^2 = 10 \text{ GeV}^2$, for isospin symmetric and non isospin symmetric three-nucleon wave functions.	56
5.8	The ratio of ratios, Eq. (5.19), for various quark distributions, using the PEST potential.	56
6.1	Comparison of several calculations of $xg_1(x)$ for ^3He and the free neutron at $Q^2 = 4 \text{ GeV}^2$	66
6.2	Δ_g , Δ'_g and g_1^n at $Q^2 = 4 \text{ GeV}^2$	68
6.3	Δ_g , Δ'_g and g_1^n , without off-shell corrections, at $Q^2 = 4 \text{ GeV}^2$	68
6.4	Corrections to g_1^n data from E154. White circles represent the original data. Black circles are corrected for binding energy and nuclear effects. Diamonds have all corrections from the black circles as well as off-shell corrections. Squares have all the corrections from the diamonds as well as Δ isobar corrections. The error bars are statistical errors.	69
6.5	Corrections to g_1^n data from HERMES. White circles represent the original data. Black circles are corrected for binding energy and nuclear effects. Diamonds have all corrections from the black circles as well as off-shell corrections. Square have all the corrections from the diamond as well as Δ isobar corrections. The error bars are statistical errors.	69
6.6	The ratio R_g and R'_g of Eqs. (6.22) and (6.23) at 4 GeV^2 , without any off-shell corrections.	72
6.7	The ratio R'_g of Eq. (6.23) at 4 GeV^2 . The dotted line is without off-shell corrections. The dashed line is with off-shell corrections and the solid line include both off-shell corrections and Δ isobar corrections.	72

List of Tables

2.1	Binding energy for a given potential and components of the wave function.	16
4.1	Effective polarisation of the nucleons in ^3He for various potentials.	42
4.2	Effective polarisation of the nucleons in ^3He and ^3H , with two-body interaction adjusted to produce the experimental binding energies.	42

Abstract

In this thesis, we study the structure functions, both polarised and unpolarised, of the three nucleon system and how they can give us information on two aspects of nuclear physics. First, we examine how to extract information on the free neutron structure functions and second we ask how does the nucleon's structure change in nuclei. Starting from a non-relativistic wave function for the three nucleon system, we use the standard convolution formalism to produce both polarised and unpolarised structure functions of ${}^3\text{He}$ and ${}^3\text{H}$. In the unpolarised case we demonstrate a new way of extracting the unpolarised structure function F_2 of the neutron from the measurement of the EMC effects in both ${}^3\text{He}$ and ${}^3\text{H}$. In the polarised case we discuss how close an approximation $g_1^{{}^3\text{He}}$ is to g_1^n . We also study the different corrections which must be included to obtain the best possible estimate for g_1^n . In this case we study the nuclear effects included in the convolution formalism, the contribution of the Δ -resonance and novel off-shell corrections to the free structure functions inside ${}^3\text{He}$ computed in QMC (Quark Meson Coupling model). With respect to the effects of the nuclear medium on nucleons, this thesis presents estimates of the EMC effect in both ${}^3\text{He}$ and ${}^3\text{H}$ and of the nuclear medium on the Gottfried sum rule. Finally, we present a clear signature of off-shell effects on the proton inside ${}^3\text{H}$. In this case off-shell corrections from QMC have been used but the results show that a variety of off-shell effects are, in fact, enhanced by the convolution formalism and consequently, can be similarly identified.

Résumé

Le principal objectif de cette thèse est l'étude des fonctions de structure, polarisées et non-polarisées, des nucléons à partir des fonctions de structure du système à trois nucléons. Un premier aspect de cette étude est consacré à l'extraction des fonctions de structures des nucléons libres, et plus particulièrement du neutron (pour lequel il n'existe pas de cible pure), à partir de celle du système à trois nucléons. Un second point d'intérêt est l'étude des modifications des propriétés des nucléons dans la matière nucléaire légère.

Nous avons commencé ce travail par le calcul de la fonction d'onde non-relativiste du système à trois nucléons. Pour effectuer ce calcul nous avons utilisé les équations de Faddeev. Pour simplifier le problème, nous avons considéré que le système est invariant par symétrie d'isospin et donc composé de particules identiques. Pour simplifier encore plus notre problème, nous avons décomposé la fonction d'onde en ondes partielles et fait appel à un potentiel séparable. Nous avons considéré trois potentiels simples, une version séparable du potentiel de Paris appelé PEST et les décompositions en pôles unitaires des potentiels de Reid à cœur mou et de Yamaguchi.

Nous posons ensuite les bases du formalisme de convolution. Ce formalisme permet d'obtenir les fonctions de structure de noyaux complexes à partir de celles de leurs constituants. Nous avons alors montré comment calculer les distributions d'impulsion sur le cône de lumière des différents nucléons à l'aide de la fonction d'onde du système à trois nucléons que nous avons précédemment calculée. Ces distributions d'impulsion sont les ingrédients fondamentaux du formalisme de convolution.

Armés de nos distributions d'impulsion sur le cône de lumière pour les différents nucléons, nous sommes passés à l'étude des fonctions de structure non-polarisées des noyaux d'hélium 3 et de tritium. Dans un premier temps nous présentons notre prédiction pour l'effet EMC dans ces deux noyaux pour les différents potentiels nucléaires étudiés ainsi que pour plusieurs paramétrisations des fonctions de structure du proton et du neutron. Nous avons ensuite étudié les prédictions de notre modèle pour la règle de somme de Gottfried. Enfin, nous avons terminé cette partie par la présentation d'une nouvelle façon d'accéder à la fonction de structure F_2 du neutron libre à partir des mesures de cette quantité pour les noyaux d'hélium 3 et de tritium. Une telle mesure pourrait être entreprise prochainement à TJNAF aux États Unis et permettrait d'enrichir considérablement notre connaissance du neutron.

Après avoir étudié les fonctions de structure non-polarisées du système à trois nucléons nous sommes passés au cas polarisé. On sait depuis longtemps que la fonction de structure g_1 de l'hélium 3 constitue une bonne approximation de cette même fonction pour le neutron libre. Nous avons

donc étudié les diverses corrections qu'il est nécessaire d'inclure pour avoir la meilleure extraction possible de cette fonction pour le neutron libre à partir des données de l'hélium 3. Ces corrections comprennent les effets nucléaires inclus dans le formalisme de convolution, la contribution de la résonance Δ et enfin une paramétrisation des effets dus au fait que les nucléons impliqués dans le formalisme de convolution ne sont pas sur couche de masse. Cette correction est souvent ignorée parce qu'il n'existe pas de paramétrisation des fonctions de structure pour des nucléons qui ne sont pas sur couche de masse. Ici, nous employons une correction calculée dans le cadre du modèle QMC (Quark Meson Coupling) pour les nucléons dans l'hélium 3. Le tritium est une bonne cible pour étudier le proton comme l'hélium 3 est une bonne cible pour étudier le neutron. Bien sûr, nous avons déjà une bonne cible de proton : le noyau d'hydrogène. Néanmoins le tritium permet d'étudier les effets du milieu nucléaire sur le proton. Nous montrons que les effets de couche de masse mis en jeu dans le formalisme de convolution peuvent être mis en évidence par l'étude de la fonction g_1 du tritium.

Pour finir, nous présentons nos conclusions et les extensions possibles de ce travail dans deux directions : l'étude de la fonction g_2 du neutron et du système à trois nucléons ; les fonctions de structure du noyau de lithium 6 considéré comme un cœur d'hélium et de deux nucléons. L'étude du lithium 6 pourrait compléter les données provenant de l'hélium et du tritium.

Statement

This work contains no material which has been accepted for the award of any other degree or diploma in any university or other tertiary institution and, to the best of my knowledge and belief, contains no material previously published or written by another person, except where due reference has been made in the text.

I give consent to this copy of my thesis, when deposited in the University Library, being made available for loan and photocopying.

Signature:

Name: F. Bissey

Acknowledgements

First of all, I would like to thanks both of my supervisors, Professor Tony Thomas in Adelaide and Jean-François Mathiot in Clermont-Ferrand, for undertaking all the paper work that made my coming to Australia and the completion of this thesis possible.

I must also thanks all the people that contributed to my understanding of physics. Among those people I especially would like to thank: Iraj Afnan, Wally Melnitchouk, Koichi Saito, Kazuo Tsushima, Csaba Boros, Andreas Schreibeir, Vadim Guzey, G. G. Petratos, A. T. Katramatou, Hélène Fonvielle, Vladimir Karmanov, Jean-Jacques Dugne and M. Strickman. A good part of the work presented here, came from collaborations with one or several people mentioned here. A special mention has to given to Iraj Afnan and Wally Melnitchouck who, beside Tony Thomas, gave me a lot of support, made me part of larger efforts and pushed me towards new frontiers.

I also would like to thank all the members and the staff of the CSSM as well as the physics department of the University of Adelaide for the hospitality and friendship they extended to me during my stay in Adelaide. I also have to thank the members and staff of the Laboratoire de Physique Corpusculaire in Clermont-Ferrand for coping with my special situation as a particular breed of exchange student and the support of the "Conseil général de la région Auvergne".

I also would like to thank my family for their ongoing support during the whole length of my thesis. I also have to thank my wife Caroline for being able to stand me and the support gave me when she entered my life. I want to give a special mention for my maternal grand father, Pierre Buillit (1909-1999), who was like a father to me, always supportive, very proud of my accomplishments and who died during the course of this thesis.

1
2
3
4
5
6
7
8
9
10
11
12
13
14
15
16
17
18
19
20
21
22
23
24
25
26
27
28
29
30
31
32
33
34
35
36
37
38
39
40
41
42
43
44
45
46
47
48
49
50
51
52
53
54
55
56
57
58
59
60
61
62
63
64
65
66
67
68
69
70
71
72
73
74
75
76
77
78
79
80
81
82
83
84
85
86
87
88
89
90
91
92
93
94
95
96
97
98
99
100

Chapter 1

Introduction

One the main issue of today's physics, is the understanding of nuclear matter from its most fundamental description – Quantum Chromo-Dynamics (QCD). For years, physicists have been able to describe, with some success, many nuclear phenomenon in terms of hadronic degrees of freedom, that is in terms of baryons and mesons. However, a full understanding of nuclear matter can only be reached by a description in terms of quarks and gluons in interaction.

After the discovery of the nucleus, by E. Rutherford and his students in 1909 [83], what physicists wanted to know was: what, exactly, is a nucleus? Slowly, we learned that the nucleus is a composite object. The first indication of the compositeness of the nucleus came in 1919, when Rutherford discovered the proton. Not long after, in 1921, J. Chadwick and E. S. Bieler concluded that some "strong force" must be holding the nucleus together. Then in 1931, Chadwick discovered the neutron. The central question of nuclear physics then definitely moved to: what is holding these particles, neutrons and protons together in such a compact object? The first theory of this strong interaction, came from H. Yukawa in 1933. It not only explained some features of the interaction, but also made the prediction that there should exist a particle with a mass of about 200 MeV. Such a particle, called pion, was eventually discovered in 1947¹, giving a lot of credibility to Yukawa's theory. Subsequently during the 1950s and 1960s, a wide variety of particles were found, first in cosmic rays and then in ever more powerful accelerators.

This proliferation of particles leads physicists to search for ways to put some order into their bestiary. First, in 1961, they came with a mathematical classification based on the group $SU(3)$ [86]. Then in 1964, M. Gell-Mann and G. Zweig [85] came up with the idea that all hadrons could be made up of smaller particles which would be later be universally known as quarks. This idea was treated more as mathematical scheme to put some order in the increasing number of hadrons rather than a physical reality. This, because of the facts that nobody ever observed a quark and that quarks have fractionary electric charge never found in nature before. In 1965, O. W. Greenberg [97], M. Y. Han and Y. Nambu [87] added the property of colour charge to quarks in order to be able to describe the Δ^{++} particle in terms of quarks. All observed hadrons are colour neutral. In 1968 and 1969, at SLAC in an experiment in which electrons are scattered off protons [88], the electrons appeared to be bouncing off small hard core inside the proton. J. Bjorken and R. P. Feynman [89] suggested that these data reflect the existence of constituent particles inside the proton. This was the first evidence for quarks.

¹In 1937, there was indication of a particle of similar mass. However it was later identified as being a heavy charged lepton: the muon.

Finally, in 1973, QCD was formulated as a gauge theory by H. Fritzsch, M. Gell-Mann and H. Leutwyler [98]. In this theory, quarks exchange colour via new particles called gluons which are similar to the photon of Quantum Electro-Dynamics (QED). It was soon found that QCD has a number of unique features, like "asymptotic freedom" [90]. This means that the effective coupling constant of the strong interaction becomes small at short distances, so that one can make use of perturbation theory to describe short-distance processes – or equivalently, processes involving large momentum transfer. This property is responsible for the fact that one cannot observe quarks directly outside a hadron. Perturbative QCD, which deals with the behaviour of QCD at high energy and small distance is quite reliable. However, tools that would be able to unveil the secrets of QCD in "normal" nuclear matter, like lattice QCD, are still in their infancy and need further development and ever more computing power.

To help us build an understanding of nuclear matter we need to have a good knowledge of its properties and of its behaviour. There are several aspects to the study of the properties of nuclear matter. First, one can study the properties of the fundamental building blocks of the nucleus, that is the proton and neutron. Then one can also study the properties of more complex nuclear matter like light, or even heavy. One can also probe a nuclear target with different probes or under different physical conditions (unpolarised or polarised scattering for example).

If we had a complete understanding of QCD, we could precisely predict the cross-section of a probe of any kind on a nuclear target. While we are not able to make such predictions, we know, from first principles, how to write such a cross-section as a function of unknown quantities. These quantities could be computed from QCD, if we had a complete understanding of it. While we cannot compute them, they can be measured experimentally. These quantities called either form factors, in elastic scattering (at low energy transfer), or structure functions, in deep inelastic scattering (at high energy transfer), contain all the information one can extract from the target with a given probe. In the electromagnetic scattering of a lepton off a nuclear target of spin 1/2, that is a nucleon or ^3He and ^3H for example, the behaviour of the target is completely described by four structure functions called F_1 , F_2 , g_1 and g_2 [59, 60, 18]². Nuclear targets with higher spin have more structure functions, however the four mentioned above are the dominant ones.

A point-like target does not have any form factors (structure functions), its behaviour is entirely determined by kinematic variables. The observation

²Or equivalently by four form factors: W_1 , W_2 , G_1 and G_2 or by some combinations of the above.

of a form factor is a proof of the fact that the target has a complex structure and is not point-like. From 1953 to 1957, various experiments of electron scattering off of nuclei [84] revealed that both proton and neutron have a "charge density", that is they do have form factors. At that time it was not interpreted as a sign that the nucleons were composite objects, but rather that nucleons were surrounded by a cloud of pions or other mesons constantly in interaction with the nucleon. This interpretation in terms of hadronic degrees of freedom can explain the existence of nucleon form factors and can give a somewhat accurate description of the hadronic system at low energy. However, at high momentum transfer, the picture is different. In this regime, experiments at SLAC in 1968 and 1969 [88] showed that the measured structure functions of the nucleon exhibit scaling and are become almost independent of the momentum transfer. This phenomenon is the clear signature of the presence of smaller elementary objects inside the nucleon, the quarks. In deep inelastic scattering, one probes directly the quarks inside nuclear matter, as if they were quasi-free. Thus, deep inelastic scattering, offers a clear picture of the quark structure of nuclear matter.

Since then, experimentalist have continued to probe nuclear matter under different conditions. The properties of the proton are still studied to this day. As there is no such thing as a pure neutron target, it is not possible to access to the properties of the neutron directly. To study the neutron one has to make experiment on a nucleus and extract the neutron information from the nucleus data. The target of choice to study the structure functions of the neutron in unpolarised has for a long time been the deuteron. This nucleus, made of only one proton and one neutron weakly bound, was usually thought to be very simple and the extraction of the neutron straightforward. However, recent analysis has cast a new light on the extraction of neutron information from deuterium data in some kinematic regions [66]. Experiments have also been performed on heavier targets, leading to the discovery in 1983, to what is now known as the "EMC effect" by the Electron Muon Collaboration [42]. It was followed by the discovery of two other effects known as "shadowing" and "anti-shadowing". These effects show that the the properties of the neutron and proton inside a nucleus are changed in a non trivial way and that some physical phenomenon have more importance than was previously thought. Several models have been put forward to explain these effects. The EMC effect in particular, may be dealt with using convolution formalism, see Ref. [17] for a review of the various experiment and of some models.

In their investigation of proton and neutron, physicists have, for a long time, focused on unpolarised (or "spin averaged") experiments (at least in electromagnetic scattering). In these kind of experiments F_1 and F_2 are the only structure functions contributing to the cross-section. F_1 and F_2 are for

this reason called the unpolarised, or spin averaged, structure functions while on the other hand g_1 and g_2 are called polarised, or spin, structure functions. To access g_1 and g_2 , one needs to devise an experiment where both the target and the probe are polarised [18, 19]. The first experiment of this kind took place at SLAC in 1976 and was, of course, probing the proton [91]. Several experiments followed after that throughout the 1980s and lead to at least two unexpected results. First, the strange quark from the "sea" are polarised and contribute to the spin of the proton [92]. The other unexpected result, is the fact that the quark contribute little to the total spin of the proton [92, 99].

Like we already said, there is no such thing as a pure neutron target. To extract the polarised structure functions of the neutron, experimentalists have to use more complex nuclear target. Like for the unpolarised case, one can extract the information from the deuteron. However, for the measurement of polarised structure functions of the neutron we have a better target: ^3He . The nucleus of ^3He is made up of one neutron and two protons and in first approximation the spin of the nucleus is entirely carried by the neutron while the two protons must have opposite spin. Of course, this is only an approximation, but a very good one as the neutron polarisation is about 87% while the polarisation of the protons is about -2.5% . The first experiment measuring the structure function g_1 of the neutron were conducted 1992 [93] using a ^3He target. These results were then combined with the previous results from the proton to get a new estimate of the fraction of nucleon spin carried by the quarks [51]. Since then, several new experiments have measured the structure functions of ^3He to extract information on the neutron, among those we can mention HERMES at DESY, E154 and E155 at SLAC.

This thesis has several goal. First we want to show how it is possible to extract information on the neutron from ^3He and even, in one occurrence, from ^3He and its mirror nucleus, ^3H . The other aim of this thesis, which is closely related to the first one, is to try to understand how the properties of nucleons change in light nuclear matter. This thesis has five main parts:

- First we will show how to compute the wave function of ^3He with the help of Faddeev equations and of separable potentials. Since we will use isospin symmetry to simplify the problem, we will really compute wave functions for the three nucleon system and our results will be applicable to ^3H . We will compute wave functions for four different potentials in order to isolate any model dependence from the potential.
- Then we will turn on the definition of the structure functions for a spin $1/2$ target and to the derivation of the convolution formalism. The convolution formalism will enable us to link structure functions of the free nucleons to structure functions of more complex nuclei. We

will also discuss the domain of applicability and the limitations of this formalism.

- In the next part, we will show how one can extract the fundamental ingredient of the convolution formalism from the three nucleon wave function we computed in the first part. The fundamental quantity needed in the convolution formalism is the light-cone momentum distribution. We will examine the dependence of this quantity to the kind of potential used to compute the wave function.
- In this fourth part we will apply our knowledge of the convolution formalism and of the light-cone momentum distribution to study unpolarised structure functions of the three nucleon system and of the nucleon themselves. First we will show our prediction for the EMC effects in both ^3He and ^3H and its dependence to various parameters like the potential and the parton distributions used to compute the free nucleons structure functions. We will also apply our results to the computation of the Gottfried sum rule in the ^3He - ^3H system. Finally, we will show how one can extract unpolarised neutron structure functions from measurements of both ^3He and ^3H structure functions.
- Lastly, we will study the polarised structure functions of the three nucleon system and their relationship with free nucleon structure functions. Since one usually wants to extract neutron information from ^3He , we will study very carefully different kinds of corrections that must be included in such a computation. We will then study the effects of our corrections to experimental results. Finally, ^3H is a perfect target to study the effect of nuclear medium on the polarised structure functions of the proton. So we will investigate how to single out such effects.

Finally, we will summarise and make some concluding remarks.

Chapter 2

The three nucleon wave function

2.1 Introduction

For the three-nucleon problem we can determine the non-relativistic wave function by solving the Faddeev equations exactly for any realistic two-body interaction. However, to simplify the computational aspects of the problem, with no sacrifice in the quality of the wave function, we turn to separable expansions that have been extensively tested [7, 8]. This will result in a three-nucleon wave function that can be used to calculate the spectral function and the light-cone momentum distribution. In the present chapter we detail the three-nucleon formalism required to evaluate the wave functions for ^3He and ^3H .

2.2 Notation

With the extensive literature on the Faddeev equations [12] and their use in the three-nucleon system, we restrict ourselves here to a summary of the notation used in the present analysis. The Faddeev decomposition of the three-nucleon wave function is given by

$$|\Psi\rangle = |\varphi_1\rangle + |\varphi_2\rangle + |\varphi_3\rangle = \{e + (123) + (132)\} |\varphi_3\rangle. \quad (2.1)$$

Here “ e ”, “ (123) ” and “ (132) ” are members of the permutation group of three objects, with e being the unit element (*i.e.* $e|\varphi_\alpha\rangle = |\varphi_\alpha\rangle$) and the other two being cyclic permutations of $\{1, 2, 3\}$. The second equality results from the requirement that we have identical particles, the wave function is then invariant under any cyclic permutation of our particles. Since we have a system of identical fermions, the total wave function must also be antisymmetric under the exchange of any two particles in the system. This requirement leads to following conditions

$$\begin{aligned} (\alpha\beta) |\varphi_\alpha\rangle &= -|\varphi_\beta\rangle, \\ (\alpha\beta) |\varphi_\beta\rangle &= -|\varphi_\alpha\rangle, \\ (\alpha\beta) |\varphi_\gamma\rangle &= -|\varphi_\gamma\rangle. \end{aligned} \quad (2.2)$$

In the above equations α , β and γ are indices running from 1 to 3, and always different from each other, and $(\alpha\beta)$ is again a member of the permutation group of three objects which exchange particles α and β leaving the third one unchanged. Since we are dealing with a three-body problem, there will be only two independent momenta in the centre of mass frame. All the particles have spin and isospin $\frac{1}{2}$ and one must account for their orbital angular momentum. We briefly summarise the quantum numbers and momenta used throughout this chapter:

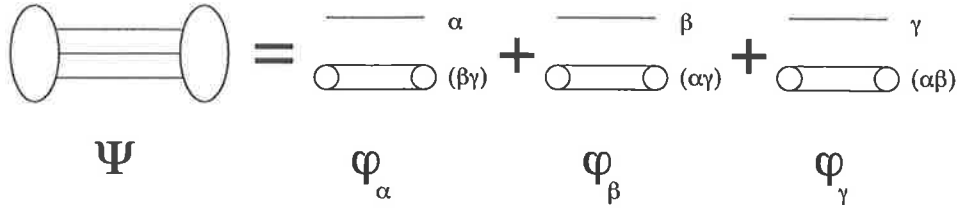


Figure 2.1: A graphical representation of Eq. (2.1).

- N_α is a set of quantum numbers describing a three body channel from the point of view of the particle α , which is the spectator; the set is unique for each channel.
- $\vec{\ell}_\alpha$ is the orbital angular momentum between particles β and γ (see Fig. 2.2).
- \vec{L}_α is the orbital angular momentum between particle α and the centre of mass of the system consisting of particles β and γ (see Fig. 2.2).
- $\vec{j}_\alpha, \vec{j}_\beta, \vec{j}_\gamma$ are the spins of each particle.
- $\vec{i}_\alpha, \vec{i}_\beta, \vec{i}_\gamma$ are the isospins of each particle.
- \vec{p}_α is the momentum of particle α in the centre of mass frame.
- \vec{q}_α is the relative momentum of the pair of particles β and γ , defined as $\vec{q}_\alpha = (\vec{p}_\gamma - \vec{p}_\beta)/2$.
- \vec{I} and \vec{J} are respectively the total isospin and total angular momentum of the system.

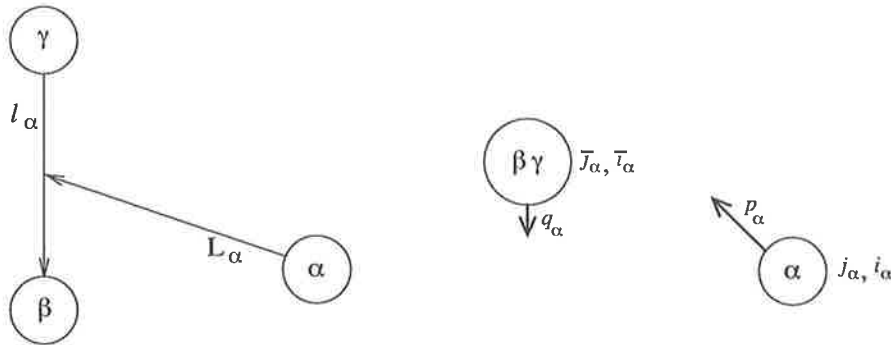


Figure 2.2: Angular momentum and momentum in the three body system.

2.3 The partial wave expansion

We now turn to the partial wave expansion of our wave function. To minimise the number of coupled Faddeev equations, having truncated the interaction to a set of partial waves, we have used the following coupling scheme:

$$\begin{aligned} \vec{j}_\beta + \vec{j}_\gamma &= \vec{s}_\alpha, & \vec{\ell}_\alpha + \vec{s}_\alpha &= \vec{j}_\alpha, & \vec{j}_\alpha + \vec{j}_\alpha &= \vec{S}_\alpha, & \vec{L}_\alpha + \vec{S}_\alpha &= \vec{J}, \\ \vec{i}_\beta + \vec{i}_\gamma &= \vec{i}_\alpha, & \vec{i}_\alpha + \vec{i}_\alpha &= \vec{I}, \end{aligned}$$

which is known as the channel coupling scheme. With this coupling scheme the complete set of quantum numbers N_α describing a three body channel is; $N_\alpha = \{\bar{i}_\alpha, s_\alpha, \bar{j}_\alpha, S_\alpha, L_\alpha\}$. A subset of these quantum numbers that describes the two-body channels is; $n_\alpha = \{\bar{i}_\alpha, s_\alpha, \bar{j}_\alpha\}$, and therefore $N_\alpha = \{n_\alpha, S_\alpha, L_\alpha\}$. We have not included ℓ_α in the set of quantum numbers since the tensor force mixes values of ℓ_α . This allows us to define the angular momentum and isospin basis as

$$|\Omega_{\ell_\alpha N_\alpha}^{JI}\rangle = |\{L_\alpha, [(\ell_\alpha, (j_\beta, j_\gamma) s_\alpha) \bar{j}_\alpha, j_\alpha] S_\alpha\} J\rangle |[(i_\beta, i_\gamma) \bar{i}_\alpha, i_\alpha] I\rangle, \quad (2.3)$$

These basis states satisfy the following orthogonality relation $\langle \Omega_{\ell_\alpha N_\alpha}^{JI} | \Omega_{\ell_\beta N_\beta}^{JI} \rangle = \delta_{\ell_\alpha, \ell_\beta} \delta_{N_\alpha, N_\beta}$.

We are now in a position to write the partial wave expansion of the total three-nucleon wave function as

$$|\Psi\rangle = \sum_{\ell_\alpha N_\alpha} |\Omega_{\ell_\alpha N_\alpha}^{JI}\rangle |\mathcal{U}_{\ell_\alpha N_\alpha}^{IJ}\rangle, \quad (2.4)$$

where $|\mathcal{U}_{\ell_\alpha N_\alpha}^{IJ}\rangle$ is defined as the radial part of the wave function corresponding to the partial wave $\{\ell_\alpha, N_\alpha\}$.

2.4 Separable potential

To reduce the dimensionality of the Faddeev integral equations (after partial wave expansion) from two to one, and in this way simplify the three-body wave function, we have employed a separable expansion of the nucleon-nucleon interaction. Our potential for the interaction of particles β and γ in a given partial wave is of the form [9]

$$V_{\ell_\alpha, \ell'_\alpha}^{n_\alpha} = |g_{\ell_\alpha}^{n_\alpha}\rangle \lambda_{\ell_\alpha \ell'_\alpha}^{n_\alpha} \langle g_{\ell'_\alpha}^{n_\alpha}|, \quad (2.5)$$

where $|g_{\ell_\alpha}^{n_\alpha}\rangle$ is a “form factor” and $\lambda_{\ell_\alpha \ell'_\alpha}^{n_\alpha}$ is the strength of the potential in that partial wave. By taking $\ell_\alpha \neq \ell'_\alpha$ we can accommodate a tensor interaction,

as in the case of the 3S_1 - 3D_1 nucleon-nucleon channel. The above expression for the potential is for a rank one potential. To incorporate higher rank potentials, we turn the strength $\lambda_{\ell_\alpha \ell'_\alpha}^{n_\alpha}$ into a matrix and as a result $|g_{\ell_\alpha}^{n_\alpha}\rangle$ is a row matrix. In resorting to separable expansions, we have taken the view that the expansion is a numerical procedure analogous to the use of quadratures. The main problem with the use of a separable expansion is that the resulting potential is non-local. However, the use of a low order expansion, such as the UPA (Unitary Pole Approximation [9, 95, 13]) or of a separable potential, is justified on the grounds that it generates the same analytic structure in the amplitude (*i.e.*, bound or anti-bound state poles) as a corresponding realistic potential [13]. Thus, we can assume it is safe to use a separable expansion. The use of a separable potential gives rise to a separable t -matrix that satisfies the Lippmann-Schwinger (LS) equation;

$$t_\alpha(E) = V_\alpha + V_\alpha G_0(E) t_\alpha(E) = (1 - G_0(E) V_\alpha)^{-1} V_\alpha, \quad (2.6)$$

with $G_0(E) = (E - H_0)^{-1}$ the two-body Green's function. It is simple to show that the separable t -matrix in a given partial wave, resulting from a solution of the LS equation, is of the form

$$t_{\ell_\alpha, \ell'_\alpha}^{n_\alpha}(E) = |g_{\ell_\alpha}^{n_\alpha}\rangle \tau_{\ell_\alpha \ell'_\alpha}^{n_\alpha}(E) \langle g_{\ell'_\alpha}^{n_\alpha}|, \quad (2.7)$$

where the form factor $|g_{\ell_\alpha}^{n_\alpha}\rangle$ is identical to that used in the separable potential. The function $\tau_{\ell_\alpha \ell'_\alpha}^{n_\alpha}(E)$, in a given channel, can be written in matrix form as

$$[\tau^{n_\alpha}(E)]^{-1} = [\lambda^{n_\alpha}]^{-1} - \langle g^{n_\alpha} | G_0(E) | g^{n_\alpha} \rangle. \quad (2.8)$$

This separability of the t -matrix will allow us to reduce the dimensionality of the Faddeev integral equations from two to one after the partial wave expansion described in Eq. (2.4).

2.5 The three-nucleon wave function

Having determined the structure of the two-body amplitude, we now turn to the wave function for the three-nucleon system. The Schrödinger equation for this system is

$$(E - H_0) |\Psi\rangle = V |\Psi\rangle = \sum_{\alpha=1}^3 V_\alpha |\Psi\rangle. \quad (2.9)$$

This can be rewritten in a form that suggests the Faddeev decomposition stated in Eq. (2.1), *i.e.*,

$$|\Psi\rangle = G_0(E) V |\Psi\rangle = \sum_{\alpha=1}^3 G_0(E) V_{\alpha} |\Psi\rangle = \sum_{\alpha=1}^3 |\varphi_{\alpha}\rangle. \quad (2.10)$$

Here, $G_0(E) = (E - H_0)^{-1}$ is the three-body Green's function. We now can write an equation for the Faddeev components of the wave function as

$$|\varphi_{\alpha}\rangle = G_0(E) V_{\alpha} |\Psi\rangle = G_0(E) V_{\alpha} |\varphi_{\alpha}\rangle + \sum_{\gamma \neq \alpha} G_0(E) V_{\alpha} |\varphi_{\gamma}\rangle. \quad (2.11)$$

With the help of Eq. (2.6), the set of coupled integral equations for the Faddeev components of the wave function, $|\varphi_{\alpha}\rangle$, becomes

$$|\varphi_{\alpha}\rangle = G_0(E) T_{\alpha}(E) (|\varphi_{\beta}\rangle + |\varphi_{\gamma}\rangle). \quad (2.12)$$

Here $T_{\alpha}(E)$ is the t -matrix for particles β and γ in the three-particle Hilbert space, which is related to the two-body amplitude considered in the last section by

$$T_{\alpha}(E) = t_{\alpha}(E - \epsilon_{\alpha}), \quad (2.13)$$

where ϵ_{α} is the energy of the spectator particle α in the three-body centre of mass.¹

Eq. (2.12) is in fact a set of three coupled integral equations, known as the Faddeev equations, for the three-body bound state. In their most general form one can write in a matrix form

$$\begin{bmatrix} \varphi_{\alpha} \\ \varphi_{\beta} \\ \varphi_{\gamma} \end{bmatrix} = G_0(E) \begin{bmatrix} 0 & T_{\alpha}(E) & T_{\alpha}(E) \\ T_{\beta}(E) & 0 & T_{\beta}(E) \\ T_{\gamma}(E) & T_{\gamma}(E) & 0 \end{bmatrix} \begin{bmatrix} \varphi_{\alpha} \\ \varphi_{\beta} \\ \varphi_{\gamma} \end{bmatrix}. \quad (2.14)$$

Eq. (2.11) tells us that the component φ_{α} describes the three body system when the particles β and γ are interacting together with α as a spectator. The Faddeev equation, Eq. (2.12) and Eq. (2.14), tell us how the Faddeev components are linked together. It tells how to exchange a spectator particle with an interacting one in the system. For the three-nucleon system, where we have identical Fermions, we can take advantage of the anti-symmetry, as given in Eq. (2.2), and the fact that $(\beta\gamma)T_{\alpha} = T_{\alpha}(\beta\gamma) = -T_{\alpha}$, to reduce the Faddeev equations to

$$|\varphi_{\alpha}\rangle = G_0(E) T_{\alpha}(E) (1 - (\beta\gamma)) |\varphi_{\beta}\rangle = 2 G_0(E) T_{\alpha}(E) |\varphi_{\beta}\rangle, \quad (2.15)$$

¹For the three-nucleon system in a non-relativistic formulation, $\epsilon_{\alpha} = \frac{3}{4m} p_{\alpha}^2$, where m is the nucleon mass.

with $\alpha \neq \beta$. To recast this equation into a form that will admit numerical solutions, we need to first partial wave decompose the Faddeev equations and take into consideration the separability of the two-body amplitudes. This can all be achieved by partial wave expanding the two-body amplitude in three-body Hilbert space in terms of the angular momentum states defined in Eq. (2.3) [14]

$$\begin{aligned} T_\alpha(E) &= \sum_{\substack{\ell_\alpha \ell'_\alpha \\ N_\alpha J I}} \int_0^\infty dp_\alpha p_\alpha^2 \left| \Omega_{\ell_\alpha N_\alpha}^{JI}; p_\alpha \right\rangle t_{\ell_\alpha \ell'_\alpha}^{n_\alpha}(E - \epsilon_\alpha) \left\langle p_\alpha; \Omega_{\ell'_\alpha N_\alpha}^{JI} \right| \\ &= \sum_{\substack{\ell_\alpha \ell'_\alpha \\ N_\alpha J I}} \int_0^\infty dp_\alpha p_\alpha^2 \left| \Omega_{\ell_\alpha N_\alpha}^{JI}; g_{\ell_\alpha}^{n_\alpha} \right\rangle \tau_{\ell_\alpha \ell'_\alpha}^{n_\alpha}(E - \epsilon_\alpha) \left\langle g_{\ell'_\alpha}^{n_\alpha}; \Omega_{\ell'_\alpha N_\alpha}^{JI} \right| \end{aligned} \quad (2.16)$$

where $\epsilon_\alpha = \frac{3}{4m} p_\alpha^2$ and

$$\left| \Omega_{\ell_\alpha N_\alpha}^{JI}; g_{\ell_\alpha}^{n_\alpha} \right\rangle = \left| \Omega_{\ell_\alpha N_\alpha}^{JI} \right\rangle \left| g_{\ell_\alpha}^{n_\alpha}; p_\alpha \right\rangle. \quad (2.17)$$

We now can write Eq. (2.15) as

$$\begin{aligned} |\varphi_\alpha\rangle &= 2 G_0(E) \sum_{\substack{\ell_\alpha \ell'_\alpha \\ N_\alpha J I}} \int_0^\infty dp_\alpha p_\alpha^2 \left| \Omega_{\ell_\alpha N_\alpha}^{JI}; g_{\ell_\alpha}^{n_\alpha} \right\rangle \tau_{\ell_\alpha \ell'_\alpha}^{n_\alpha}(E - \epsilon_\alpha) \left\langle g_{\ell'_\alpha}^{n_\alpha}; \Omega_{\ell'_\alpha N_\alpha}^{JI} \right| \varphi_\beta \rangle \\ &\equiv 2 G_0(E) \sum_{\substack{\ell_\alpha \ell'_\alpha \\ N_\alpha J I}} \int_0^\infty dp_\alpha p_\alpha^2 \left| \Omega_{\ell_\alpha N_\alpha}^{JI}; g_{\ell_\alpha}^{n_\alpha} \right\rangle \tau_{\ell_\alpha \ell'_\alpha}^{n_\alpha}(E - \epsilon_\alpha) X_{N_\alpha \ell'_\alpha}^{JI}(p_\alpha), \end{aligned} \quad (2.18)$$

with the spectator function, $X_{N_\alpha \ell_\alpha}^{JI}(p_\alpha)$, satisfying the equation

$$\begin{aligned} X_{N_\alpha \ell_\alpha}^{JI}(p_\alpha) &\equiv \left\langle g_{\ell_\alpha}^{n_\alpha}; \Omega_{\ell_\alpha N_\alpha}^{JI} \right| \varphi_\beta \rangle \\ &= 2 \sum_{\substack{\ell_\beta \ell'_\beta \\ N_\beta}} \int_0^\infty dp_\beta p_\beta^2 Z_{\ell_\alpha N_\alpha; \ell_\beta N_\beta}^{JI}(p_\alpha, p_\beta; E) \tau_{\ell_\beta \ell'_\beta}^{n_\beta}(E - \epsilon_\beta) X_{N_\beta \ell'_\beta}^{JI}(p_\beta), \end{aligned} \quad (2.19)$$

where

$$Z_{\ell_\alpha N_\alpha; \ell_\beta N_\beta}^{JI}(p_\alpha, p_\beta; E) \equiv \left\langle g_{\ell_\alpha}^{n_\alpha}; \Omega_{\ell_\alpha N_\alpha}^{JI} \right| G_0(E) \left| \Omega_{\ell_\beta N_\beta}^{JI}; g_{\ell_\beta}^{n_\beta} \right\rangle, \quad (2.20)$$

with $\alpha \neq \beta$. We give a succinct derivation of $Z_{\ell_\alpha N_\alpha; \ell_\beta N_\beta}^{JI}$ for the coupling scheme used in the present analysis in appendix A [12, 14]. In Eq. (2.19) we have a set of coupled, homogeneous, integral equations for the spectator wave function, $X_{N_\alpha \ell_\alpha}^{JI}(p_\alpha)$, which we can use to construct the total wave function. Here, we note that the spectator wave function is only a function of the momentum of the spectator particle and the energy of the system, which is the binding energy of ${}^3\text{He}$ or ${}^3\text{H}$. We now turn to the total wave function for the three-nucleon system. Making use of the orthogonality of the angular functions, $|\Omega_{\ell_\alpha N_\alpha}^{JI}\rangle$, we can write the total radial wave function, defined in Eq. (2.4), as

$$\begin{aligned} |\mathcal{U}_{N_\alpha \ell_\alpha}^{JI}\rangle &= \langle \Omega_{\ell_\alpha N_\alpha}^{JI} | \Psi \rangle \\ &= \langle \Omega_{\ell_\alpha N_\alpha}^{JI} | \varphi_\alpha \rangle + \langle \Omega_{\ell_\alpha N_\alpha}^{JI} | \varphi_\beta + \varphi_\gamma \rangle \\ &= |\eta_{\ell_\alpha N_\alpha}^{JI1}\rangle + |\eta_{\ell_\alpha N_\alpha}^{JI2}\rangle, \end{aligned} \quad (2.21)$$

where

$$\begin{aligned} \eta_{\ell_\alpha N_\alpha}^{JI1}(p_\alpha, q_\alpha) &\equiv \langle p_\alpha q_\alpha | \eta_{\ell_\alpha N_\alpha}^{JI1} \rangle \\ &= \langle p_\alpha q_\alpha; \Omega_{\ell_\alpha N_\alpha}^{JI} | \varphi_\alpha \rangle \\ &= 2G_0(q_\alpha, p_\alpha; E) g_{\ell_\alpha}^{n_\alpha}(q_\alpha) \sum_{\ell'_\alpha} \tau_{\ell_\alpha \ell'_\alpha}^{n_\alpha}(E - \epsilon_\alpha) X_{N_\alpha \ell'_\alpha}^{JI}(p_\alpha), \end{aligned} \quad (2.22)$$

with $G_0(q_\alpha, p_\alpha; E) = [E - \frac{1}{m}(q_\alpha^2 + \frac{3}{4}p_\alpha^2)]^{-1}$. The second component of the radial wave function in Eq. (2.21) is given by

$$\begin{aligned} \eta_{\ell_\alpha N_\alpha}^{JI2}(p_\alpha, q_\alpha) &\equiv \langle p_\alpha q_\alpha | \eta_{\ell_\alpha N_\alpha}^{JI2} \rangle, \\ &= \langle p_\alpha q_\alpha; \Omega_{\ell_\alpha N_\alpha}^{JI} | \varphi_\beta + \varphi_\gamma \rangle, \\ &= \langle p_\alpha q_\alpha; \Omega_{\ell_\alpha N_\alpha}^{JI} | \{1 - (\beta\gamma)\} |\Omega_{\ell_\beta N_\beta}^{JI}\rangle |\eta_{\ell_\beta N_\beta}^{JI1}\rangle, \\ &= 2 \sum_{\ell_\beta N_\beta} \langle p_\alpha q_\alpha; \Omega_{\ell_\alpha N_\alpha}^{JI} | \Omega_{\ell_\beta N_\beta}^{JI} \rangle |\eta_{\ell_\beta N_\beta}^{JI1}\rangle. \end{aligned} \quad (2.23)$$

The exact form of this equation, which we call the permutation term, will be the object of section B. We can write the last line because we have $(\beta\delta)|\Omega_{\ell_\alpha N_\alpha}^{JI}\rangle = -|\Omega_{\ell_\alpha N_\alpha}^{JI}\rangle$ from Eq. (2.2), since the permutation operator acts through the angular part of $|\varphi_\alpha\rangle$. The normalisation of the total wave function is then given by

$$\begin{aligned} \langle \Psi | \Psi \rangle &= 3\langle \varphi_\alpha | \varphi_\alpha \rangle + 6\langle \varphi_\alpha | \varphi_\beta \rangle \\ &= 3 \sum_{\ell_\alpha N_\alpha} [\langle \eta_{\ell_\alpha N_\alpha}^{JI1} | \eta_{\ell_\alpha N_\alpha}^{JI1} \rangle + 2\langle \eta_{\ell_\alpha N_\alpha}^{JI1} | \eta_{\ell_\alpha N_\alpha}^{JI2} \rangle]. \end{aligned} \quad (2.24)$$

Here the sum is restricted by the two-body partial waves included in the Faddeev equations. Since the partial wave expansion of the total wave function involves an infinite sum, we need to truncate this sum such that the normalisation evaluated by the truncated sum, that is:

$$\langle \Psi | \Psi \rangle = \sum_{\ell_\alpha N_\alpha} \langle \mathcal{U}_{N_\alpha \ell_\alpha}^{II} | \mathcal{U}_{N_\alpha \ell_\alpha}^{II} \rangle, \quad (2.25)$$

agrees with the result of Eq. (2.24). In this way we ensure that our total wave function includes all the partial waves dictated by the two-body interaction.

2.6 Numerical results

As a first step in the determination of our wave function, we calculate the binding energy of the three-nucleon system for the class of potentials being considered. For the UPA to the Reid Soft core (RSC)[10] and the Yamaguchi (YAM) potentials [11] the interaction is restricted to the 1S_0 and 3S_1 - 3D_1 channels. This reduces the homogeneous Faddeev equations to five coupled integral equations for the spectator wave function. For the PEST (a multi-rank separable expansion of the Paris potential)[5, 6] potentials the number of coupled channels depends on the rank of the interaction in a given channel and the number of partial waves included. To get the optimal representation of the Paris potential we need to have achieved convergence in the rank. This varies from channel to channel. In all cases the rank has been chosen in such a way that the binding energy for a given number of channels has converged and is in agreement with the results of calculations using the Paris potential directly [8].

In Table 2.1 we present the result for the binding energy for the three classes of potentials. The experimental binding energy of ^3He is -7.72 MeV while the binding energy of ^3H is -8.48 MeV. The difference in binding energy between the two nucleus is caused by isospin symmetry breaking and Coulomb forces. Since we did not include any of those our results should be compared to the binding energy of ^3H . For the PEST potentials we have taken the 5, 10, and 18 channel potentials. The 18 channel calculation corresponds to including all nucleon-nucleon channels with $J \leq 2$. This will allow us to examine the contribution to the spectral function from higher partial waves. We observe that the Yamaguchi potentials over-bind the three-nucleon system, while the UPA and PEST potentials under-bind. Since the binding energy determines the long range part of the wave function, this difference allows us to examine the sensitivity of the structure functions to the binding energy and therefore to the tail of the wave function.

Table 2.1: Binding energy for a given potential and components of the wave function.

Potential	number of channels	binding energy (MeV)	$P(S)$ %	$P(S')$ %	$P(D)$ %
RSC	5	-7.15	88.37%	1.88%	8.89%
YAM4	5	-9.12	93.08%	1.58%	4.97%
YAM7	5	-8.05	89.1%	1.59%	8.71%
PEST	5	-7.27	89.3%	1.88%	8.11%
PEST	10	-7.10	89.72%	1.71%	7.85%
PEST	18	-7.32	89.56%	1.66%	8.07%
PARIS	—	-7.31	89.88%	1.62%	8.43%
PEST (^3He)	5	-7.72	89.52%	1.6%	8.11%
PEST (^3H)	5	-8.48	89.95%	1.23%	8.1%

A comparison of the PEST five channel and the UPA suggests that the difference between these two models is minimal. In fact, that is the case for most realistic potentials that do not include energy dependence. The higher partial waves in the PEST potential seem to have a small but significant contribution to the binding energy. Here again, this potential, in common with all realistic potentials, tends to under-bind the three nucleon system. As we can see from Table 2.1 the result from PEST and RSC potential are more than 1 MeV short (more than 10%). This is also the case of the PARIS potential we give as comparison to PEST and also other potential. A review of the triton binding energy given by recent potentials can be found in Ref. [96]. In [96], the value of the binding energy for potential from the Nijmegen group (Nijm-I and Nijm-II) and the Argonne group (V_{18}) are between -7.6 and 7.7 MeV. The solution to this under-binding problem may involve the short-range, velocity dependence of the two-nucleon force [15], as well as a genuine three-body force [16].

Table 2.1 also gives the contribution of the three dominant kind of partial waves (S , S' and D waves) to the wave function. The fundamental distinction between the different kind of waves is based on the total angular momentum of the system $\vec{\mathcal{L}} = \vec{L} + \vec{\ell}$ which can only have the following value $\mathcal{L} = 0, 1$ or 2 (S , P or D wave)². Further distinction between S and S' wave are based on other properties of symmetry of the different waves, a complete and accurate description of the classification of the different kind of waves

²The spin of the three nucleons add up to either $\frac{1}{2}$ or $\frac{3}{2}$. The total angular momentum of the tri-nucleon system is $\frac{1}{2}$, this requirement limits \mathcal{L} to the above values.

in the tri-nucleon system can be found in [80]. The figures for the different kind of waves are similar for all potential, with the exception of YAM4 which presents an excess of S waves and a depletion of D waves.

Since we have neglected the Coulomb contribution to the energy of ${}^3\text{He}$, and our more realistic potentials under-bind the three nucleon system, we have chosen to adjust the strength of the 1S_0 interaction to reproduce the experimental binding energy of both ${}^3\text{He}$ and ${}^3\text{H}$. This procedure does not affect the deuteron wave function, but could have some influence on the continuum wave function in the 1S_0 . In this way, we may estimate the error in neglecting the Coulomb energy for ${}^3\text{He}$, and the possible error in the tail of the wave function due to under-binding of the three nucleon system. The contribution of this correction will be discussed when considering the spectral functions and light-cone momentum distributions.

Chapter 3

Structure functions and convolution formalism

3.1 The electromagnetic cross section

The cross section for the scattering of a charged lepton with a nucleus, assuming we exchange only one photon, as in Fig. 3.1, is proportional to the product of the leptonic tensor $L_{\mu\nu}$ with the hadronic tensor $W_{\mu\nu}$. In the following we consider a lepton of mass m , initial (final) four momentum k (k') and s (s') its covariant polarisation vector, such that $s \cdot k = 0$ ($s' \cdot k' = 0$) and $s \cdot s = -1$ ($s' \cdot s' = -1$). The hadronic system will have a mass M and four momentum and polarisation P and S . In the laboratory frame we consider that $P = (M, \vec{0})$, $k = (E, \vec{k})$ and $k' = (E', \vec{k}')$. Then the differential cross section for detecting a final lepton in a solid angle $d\Omega$ and in the energy range $(E', E' + dE')$ is

$$\frac{d^2\sigma}{d\Omega dE'} = \frac{\alpha^2}{q^4} \frac{E'}{E} L_{\mu\nu} W^{\mu\nu}, \quad (3.1)$$

where $q = k - k'$ is the momentum of the exchanged photon and α is the fine structure constant. The leptonic tensor has the following form in the case of

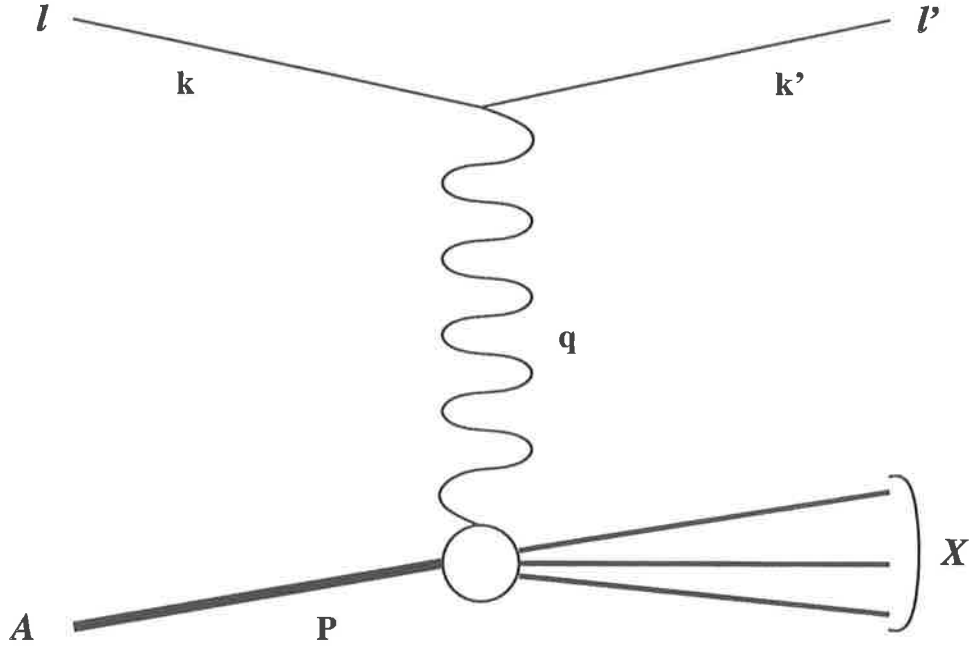


Figure 3.1: Scattering of a lepton l on a nucleus A , with one photon exchange.

an electromagnetic current

$$\begin{aligned} L_{\mu\nu}(k, s; k', s') &= [\bar{u}(k', s')\gamma_\mu u(k, s)]^\dagger [\bar{u}(k', s')\gamma_\nu u(k, s)] \\ &= L_{\mu\nu}^{(S)}(k; k') + L_{\mu\nu}^{(A)}(k, s; k') + L_{\mu\nu}'^{(S)}(k, s; k', s') + L_{\mu\nu}'^{(A)}(k; k', s'). \end{aligned} \quad (3.2)$$

Here the leptonic tensor is a sum of four parts because we consider the possibility of a different polarisation for the final state of the lepton. In practice, the measurement of the polarisation of the final lepton is difficult and never done. So one sums over the polarisation of the final lepton, s' , and the leptonic tensor is reduced to a sum of two terms: $2L_{\mu\nu}^{(S)}(k; k') + 2L_{\mu\nu}^{(A)}(k, s; k')$. Finally if we average over initial polarisation, to consider the use of an unpolarised lepton probe, the leptonic tensor is reduced to only one, symmetric, component: $L_{\mu\nu}^{(S)}(k; k')$. We have

$$L_{\mu\nu}^{(S)}(k; k') = k_\mu k'_\nu + k'_\mu k_\nu + g_{\mu\nu}(k \cdot k' - m^2) \quad (3.3)$$

$$L_{\mu\nu}^{(A)}(k, s; k') = im\epsilon_{\mu\nu\alpha\beta}s^\alpha(k - k')^\beta \quad (3.4)$$

$$\begin{aligned} L_{\mu\nu}'^{(S)}(k, s; k', s') &= k \cdot s' (k'_\mu s_\nu + s_\mu k'_\nu - g_{\mu\nu}s \cdot k') \\ &\quad - (k \cdot k' - m^2) (s_\mu s'_\nu + s'_\mu s_\nu - g_{\mu\nu}s \cdot s') \\ &\quad + k' \cdot s (s'_\mu k_\nu + k_\mu s'_\nu) - s \cdot s' (k_\mu k'_\nu + k'_\mu k_\nu) \end{aligned} \quad (3.5)$$

$$L_{\mu\nu}'^{(A)}(k; k', s') = im\epsilon_{\mu\nu\alpha\beta}s'^\alpha(k - k')^\beta. \quad (3.6)$$

Since leptons are point like objects, the leptonic tensor is very simple and depends only on the kinematics. The hadronic tensor, on the other hand, represents a composite object. It depends on how the composite object is made, and how it is bound. However, from general principles one can write the general form of the electromagnetic current for the hadronic system. For an hadronic system of spin $\frac{1}{2}$ (*i.e.* free nucleon, ^3He , ^3H etc.) the hadronic tensor has the following form [17, 18, 19]

$$\begin{aligned} \mathcal{W}_{\mu\nu}(q; P, S) &= \int d^4\xi e^{iq\xi} \langle PS | J_\mu(\xi) J_\nu(0) | PS \rangle \\ &= \mathcal{W}_{\mu\nu}^{(S)}(q; P) + \mathcal{W}_{\mu\nu}^{(A)}(q; P, S), \end{aligned} \quad (3.7)$$

where J^μ is the electromagnetic current. Here we have separated the hadronic tensor into symmetric and antisymmetric parts. As in the case of the leptonic tensor, if one averages over the initial polarisation only the symmetric component, $\mathcal{W}_{\mu\nu}^{(S)}$, remains. Each of these components depends on two form

factors:

$$\begin{aligned} \mathcal{W}_{\mu\nu}^{(S)}(q; P) = & \left(-g_{\mu\nu} + \frac{q_\mu q_\nu}{q^2} \right) W_1(P \cdot q, q^2) \\ & + \left(P_\mu - \frac{P \cdot q}{q^2} q_\mu \right) \left(P_\nu - \frac{P \cdot q}{q^2} q_\nu \right) \frac{W_2(P \cdot q, q^2)}{M^2}, \end{aligned} \quad (3.8)$$

and

$$\begin{aligned} \mathcal{W}_{\mu\nu}^{(A)}(q; P, S) = & i\epsilon_{\mu\nu\alpha\beta} q^\alpha \left[MS^\beta G_1(P \cdot q, q^2) \right. \\ & \left. + [(P \cdot q) S^\beta - (S \cdot q) P^\beta] \frac{G_2(P \cdot q, q^2)}{M} \right], \end{aligned} \quad (3.9)$$

where W_1 , W_2 , G_1 and G_2 are the form factors of the hadronic system. All the dependence of the cross section on the internal structure of the hadronic system is included in the form factors. Therefore these form factors may be used as a probe of the structure of the hadronic system. The deep inelastic scattering (DIS) or Bjorken limit is given by the following conditions, in the rest frame of the target

$$-q^2 = Q^2 \rightarrow \infty, \quad \nu = E - E' \rightarrow \infty \quad \text{and} \quad x = \frac{Q^2}{2P \cdot q} = \frac{Q^2}{2M\nu}, \text{ fixed.} \quad (3.10)$$

Note that Q^2 and x are defined covariantly while ν is defined in the laboratory frame. In the deep inelastic (Bjorken) regime, one prefers to use the structure functions which are known to approximately scale as functions of x (to logarithmic corrections in Q^2):

$$\begin{aligned} \lim_{Bj} MW_1(P \cdot q, Q^2) &= F_1(x), \\ \lim_{Bj} \nu W_2(P \cdot q, Q^2) &= F_2(x), \\ \lim_{Bj} \frac{(P \cdot q)^2}{\nu} G_1(P \cdot q, Q^2) &= g_1(x), \\ \lim_{Bj} \nu (P \cdot q) G_2(P \cdot q, Q^2) &= g_2(x). \end{aligned} \quad (3.11)$$

3.2 Particularly interesting cross sections

3.2.1 Unpolarised scattering

In unpolarised scattering one has to sum over the final polarisations and average over the initial polarisations. The cross section becomes

$$\begin{aligned}
 \frac{d^2\sigma^{unp}}{d\Omega dE'} &= \frac{1}{4} \frac{\alpha^2}{q^4} \frac{E'}{E} \sum_{s,s',S} L_{\mu\nu} \mathcal{W}^{\mu\nu}, \\
 &= \frac{\alpha^2}{q^4} \frac{E'}{E} 2L_{\mu\nu}^{(S)} \mathcal{W}^{\mu\nu(S)}, \\
 &= \frac{4\alpha^2 E'^2}{q^4} \left[2W_1 \sin^2 \frac{\theta}{2} + W_2 \cos^2 \frac{\theta}{2} \right],
 \end{aligned} \tag{3.12}$$

or

$$\frac{d^2\sigma^{unp}}{dx dQ^2} = \frac{4\pi\alpha^2 E'^2}{xQ^4} \frac{E'}{E} \left[F_2 \cos^2 \frac{\theta}{2} + 2 \frac{\nu}{M} F_1 \sin^2 \frac{\theta}{2} \right], \tag{3.13}$$

where θ is the scattering angle of the lepton. So in unpolarised scattering the cross section depends only on the two first form factors, or in DIS the two first structure functions F_1 and F_2 . This is why they are often called unpolarised form factors (structure functions).

3.2.2 Polarised scattering

To measure the polarised structure function g_1 and g_2 one needs not only a polarised target but also a polarised probe as one can tell by the structure of the hadronic and leptonic tensors. To access precisely the two polarised structure functions one forms the difference of the cross sections between a polarised probe and two targets of opposite polarisation. That is

$$\begin{aligned}
 \frac{d^2\sigma^{s,S}}{d\Omega dE'} - \frac{d^2\sigma^{s,-S}}{d\Omega dE'} &= \frac{\alpha^2}{q^4} \frac{E'}{E} \sum_{s'} L_{\mu\nu}(k, s; k', s') [\mathcal{W}^{\mu\nu}(q; P, S) - \mathcal{W}^{\mu\nu}(q; P, -S)] \\
 &= \frac{\alpha^2}{q^4} \frac{E'}{E} 4L_{\mu\nu}^{(A)}(k, s; k') \mathcal{W}^{\mu\nu(A)}(q; P, S) \\
 &= \frac{8m\alpha^2 E'}{q^4 E} \left\{ [(q \cdot S)(q \cdot s) + Q^2(s \cdot S)] M G_1 \right. \\
 &\quad \left. + Q^2 [(s \cdot S)(P \cdot q) - (q \cdot S)(P \cdot s)] \frac{G_2}{M} \right\}.
 \end{aligned} \tag{3.14}$$

In particular, if we polarise the probe longitudinally (\rightarrow) and then polarise the target, first in the same direction as the probe (\Rightarrow), then in the opposite direction (\Leftarrow), we have (to the first order in m/E)

$$\frac{d^2\sigma^{\rightarrow\Rightarrow}}{d\Omega dE'} - \frac{d^2\sigma^{\rightarrow\Leftarrow}}{d\Omega dE'} = -\frac{4\alpha^2}{Q^2} \frac{E'^2}{E} [(E + E' \cos \theta)MG_1 - Q^2G_2]. \quad (3.15)$$

The structure of Eq. (3.15) is such that it is mainly sensitive to G_1 . Another set up, which is important if one wishes to measure the polarised G_2 structure function, is to polarise the hadronic target transversely (\uparrow or \downarrow) while the probe is polarised longitudinally (\rightarrow). In this case Eq. (3.14) leads to

$$\frac{d^2\sigma^{\rightarrow\uparrow}}{d\Omega dE'} - \frac{d^2\sigma^{\rightarrow\downarrow}}{d\Omega dE'} = -\frac{4\alpha^2}{Q^2} \frac{E'^2}{E} \sin \theta \cos \phi (MG_1 + 2EG_2), \quad (3.16)$$

where ϕ is the angle between the scattering plane, (\vec{k}, \vec{k}') , and the polarisation plane, (\vec{k}, \vec{S}) .

3.3 The convolution formalism

3.3.1 The partial wave impulse approximation

As we have said the hadronic tensor has the same form for both the nucleon and tri-nucleon system. What we are looking at now is how one can relate the free nucleon structure functions to the structure functions of a nucleus. We will use the plane wave impulse approximation (PWIA) to derive a relation between the hadronic tensor of nucleus and its constituent nucleons. The PWIA involves the following assumptions:

1. Only the sum of single-nucleon currents contributes to the inclusive cross section.
2. Interference between different constituent nucleons does not contribute.
3. The effect of final-state interactions between the products of the struck nucleon and the residual hadronic state is neglected.

Assumption (1) implies that we will neglect multiple rescattering. It is justified by the fact that at high Q^2 we expect to be in the perturbative regime of QCD. Consequently, the contribution from multiple scattering should be low. However, this does not apply at small Bjorken- x . x is a measure of the

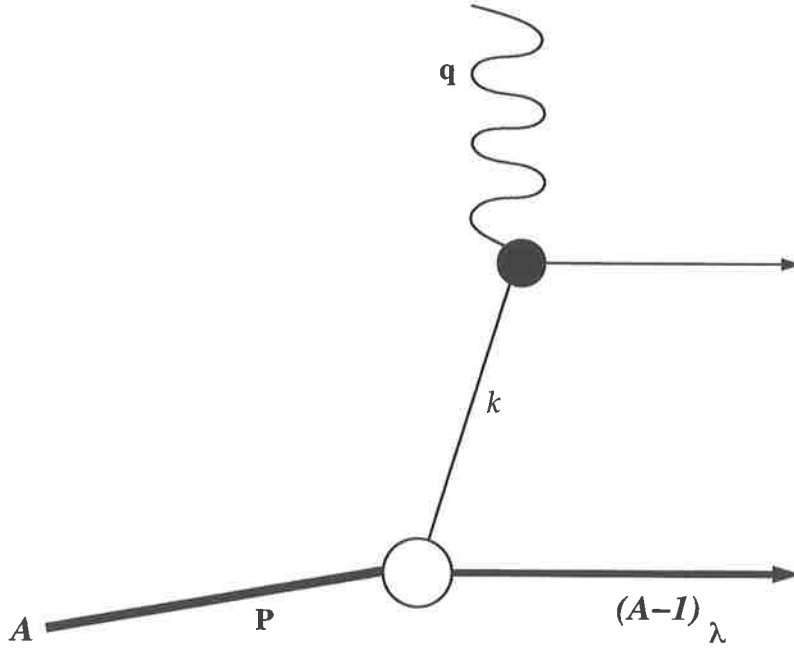


Figure 3.2: In PWIA, only one nucleon of the nucleus is struck by the photon.

momentum of the struck nucleon along the impulsion of the photon. A low value of x means that the interaction between the photon and the nucleus occurs at a low energy scale, outside the perturbative regime.

(2) implies that the nucleon constituents are quasi-free, which is expected in DIS as the energy of interaction is far greater than the binding energy of the constituent. So from the point of view of the probe, the constituent nucleons are quasi-free.

Finally (3) means that we consider the final state as the product of a wave function describing the products of the struck nucleon with an independent wave function describing the spectators. This supposes that the products of the collision will not interact or that the contribution of such interaction will be very small. We checked the validity of this assumption for the neutron in ^3He and we found that indeed the contribution of this interaction was very small in this case.

Using (1) we can write the electromagnetic current of the nucleus as the sum of the individual particle currents, so in the three nucleon system

$$J^\mu = \sum_{\alpha=1}^3 j_\alpha^\mu, \quad (3.17)$$

where j_α^μ is the electromagnetic current of the nucleon α in the nucleus. Note that in the previous equation we assumed that the nucleus did not have any other constituents beside the nucleons. However, one can easily extend the derivation of the convolution formalism to include other components of the nucleus if needed. So now we can write the hadronic tensor for the three nucleon system as

$$\mathcal{W}^{\mu\nu}(q; P_A, S_A) = \sum_{\alpha=1}^3 \int d^4\xi e^{iq\xi} \langle P_A S_A | j_\alpha^\mu(\xi) j_\alpha^\nu(0) | P_A S_A \rangle, \quad (3.18)$$

note that here we used (2) to get rid of the possibility of cross terms of the kind $j_\alpha^\mu(\xi) j_\beta^\nu(0)$. This hadronic tensor arises from the reaction depicted in Fig. 3.3, cross terms would arise from a diagram of the form of Fig. 3.4. Assumption (3) also gets rid of the diagram represented in Fig. 3.5, thanks to this assumption we can write the final state as a product $|p_\alpha s_\alpha\rangle |P_{A-1} S_{A-1} f\rangle$, where f is an index over all $A-1$ states having same P_{A-1} and S_{A-1} . We can then write the hadronic tensor as

$$\begin{aligned} \mathcal{W}^{\mu\nu}(q; P_A, S_A) = & \sum_{\alpha=1}^3 \sum_{\text{final states}} \int d^4\xi e^{iq\xi} \langle P_A S_A | p_\alpha s_\alpha \rangle |P_{A-1} S_{A-1} f\rangle \delta^4(P_A - (p_\alpha + P_{A-1})) \\ & \times \langle P_{A-1} S_{A-1} f | \langle p_\alpha s_\alpha | j_\alpha^\mu(\xi) j_\alpha^\nu(0) | p'_\alpha s'_\alpha \rangle |P'_{A-1} S'_{A-1} f'\rangle \\ & \times \langle P'_{A-1} S'_{A-1} f' | \langle p'_\alpha s'_\alpha | P_A S_A \rangle \delta^4(P_A - (p'_\alpha + P'_{A-1})). \end{aligned} \quad (3.19)$$

In Eq. (3.19) the sum over all final states refers to both $|p_\alpha s_\alpha\rangle |P_{A-1} S_{A-1} f\rangle$ and $|p'_\alpha s'_\alpha\rangle |P'_{A-1} S'_{A-1} f'\rangle$, and where it is needed an integral over 4-momentum as well. If the set of $A-1$ states is complete then we have

$$\langle P_{A-1} S_{A-1} f | P'_{A-1} S'_{A-1} f' \rangle = \delta^4(P_{A-1} - P'_{A-1}) \delta(S_{A-1} - S'_{A-1}) \delta_{f,f'}. \quad (3.20)$$

Since the current operators in Eq. (3.19) act only on the particle labeled α leaving the $A-1$ state untouched we can use Eq. (3.20) to simplify Eq. (3.19)

$$\begin{aligned} \mathcal{W}^{\mu\nu}(q; P_A, S_A) = & \sum_{\alpha=1}^3 \sum_{\text{final states}} \int d^4\xi e^{iq\xi} \langle p_\alpha s_\alpha | j_\alpha^\mu(\xi) j_\alpha^\nu(0) | p_\alpha s_\alpha \rangle \\ & \times \langle P_A S_A | p_\alpha s_\alpha \rangle |P_{A-1} S_{A-1} f\rangle \delta^4(P_A - (p_\alpha + P_{A-1})) \\ & \times \langle P_{A-1} S_{A-1} f | \langle p_\alpha s_\alpha | P_A S_A \rangle. \end{aligned} \quad (3.21)$$

In the previous equation we can easily spot the nucleon hadronic tensor times a term defined as the spectral function for the nucleon α . This term is

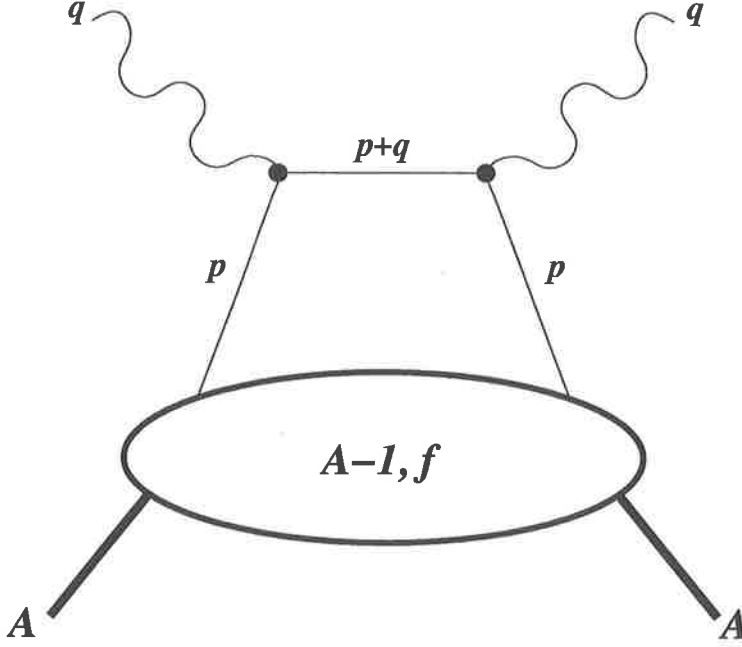


Figure 3.3: Handbag diagram.

interpreted as being the number density of the given nucleon α , with given momentum p and polarisation s , while the remaining system is in a state f with momentum P_{A-1} and polarisation S_{A-1} multiplied by a delta-function:

$$S_f^\alpha(p, s, P_A, S_A) = \sum_{\substack{P_{A-1} \\ S_{A-1}}} |\langle P_A S_A | ps \rangle \langle P_{A-1} S_{A-1} f \rangle|^2 \delta^4(P_A - (p + P_{A-1})) . \quad (3.22)$$

In instant form dynamic the sum over the state of momentum P_{A-1} is an integral over \vec{P}_{A-1} . We can split the delta-function of Eq. (3.22) in two parts: $\delta^4(P_A - (p + P_{A-1})) = \delta(P_A^0 - (p^0 + P_{A-1}^0)) \delta^3(\vec{P}_A - (\vec{p} + \vec{P}_{A-1}))$, using the spatial part of this delta-function one can integrate the integral over \vec{P}_{A-1} in Eq. (3.22). Since from assumption (2) we consider the constituent nucleons to be quasi-free, we will consider that the struck nucleon can be described by a plane wave. Therefore, we can replace $|ps\rangle$ by $a_s^\dagger(\vec{p})|0\rangle$, where $a_s^\dagger(\vec{p})$ is the creation operator of the nucleon of spin s and momentum \vec{p} . We can now rewrite Eq. (3.22) as:

$$S_f^\alpha(p, s, P_A, S_A) = \sum_{S_{A-1}} \langle P_A S_A | a_{s,\alpha}^\dagger(\vec{p}) | 0 \rangle \langle P_{A-1} S_{A-1} f \rangle \\ \times \langle P_{A-1} S_{A-1} f | \langle 0 | a_{s,\alpha}(\vec{p}) | P_A S_A \rangle \delta(P_A^0 - p^0 - P_{A-1}^0) , \quad (3.23)$$

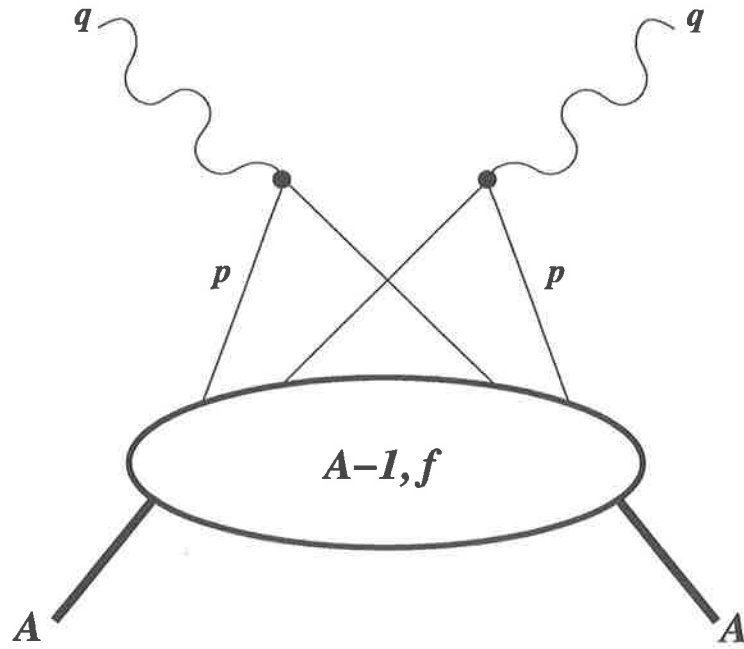


Figure 3.4: Cross term diagram.

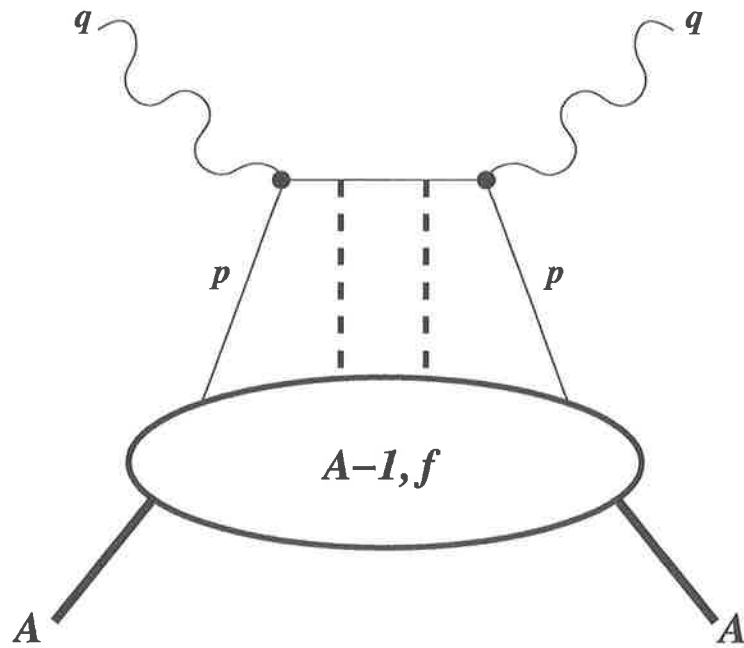


Figure 3.5: Higher twist diagram neglected using assumption (3).

with $\vec{P}_{A-1} = \vec{P}_A - \vec{p}$. In the previous equation, the index α in the creation and destruction operators indicates that we act on the nucleon labelled α inside the nucleus. If we suppose that for a given value of P_{A-1} and label f , the set of state $|P_{A-1}S_{A-1}f\rangle$ is complete, we can replace the sum over those states by the identity. In the end the spectral function is expressed by:

$$S_f^\alpha(p, s, P_A, S_A) = \langle P_A S_A | a_{s,\alpha}^\dagger(\vec{p}) a_{s,\alpha}(\vec{p}) | P_A S_A \rangle \delta(p^0 - (P_A^0 - P_{A-1}^0)) . \quad (3.24)$$

Alternatively the energy p^0 of the nucleon in Eq. (3.24) can also be expressed phenomenologically [17] as the sum of the nucleon mass, m , plus the separation energy of this nucleon, ϵ_f^1 , and minus the recoil kinetic energy, Tr_f , of the remaining $A - 1$ state. In this case we have $p^0 = m + \epsilon_f - Tr_f$. As we will see later, one can find ϵ_f and Tr_f in terms of P_A and P_{A-1} . So one can write Eq. (3.24) in the following way:

$$S_f^\alpha(p, s, P_A, S_A) = \langle P_A S_A | a_{s,\alpha}^\dagger(\vec{p}) a_{s,\alpha}(\vec{p}) | P_A S_A \rangle \delta(p^0 - (m + \epsilon_f - Tr_f)) . \quad (3.25)$$

It is easier to express the spectral function as well as the nucleon electromagnetic tensor in terms of protons and neutrons rather than particle α . In the following we will introduce an isospin index t for the spectral function and the nucleon electromagnetic tensor. So we have:

$$\mathcal{W}_{\mu\nu}(q; P_A, S_A) = \sum_{t=-\frac{1}{2}}^{\frac{1}{2}} \sum_{s,f} \int d^4p S_f^t(p, s, P_A, S_A) \mathcal{W}_{\mu\nu}^t(q; p, s) . \quad (3.26)$$

Of course, because of momentum conservation, the electromagnetic tensor of the nucleon actually involves an off-shell particle. We only have measurements and parametrisations of structure functions for on-shell nucleons. There are several ways to deal with this problem. One is to develop the convolution formalism on the light front, where particles are always on-shell – the drawback being that the hadronic system has to be described as a sum of Fock-states. We have also to be careful of the fact that the electromagnetic tensor of the nucleus is defined in terms of q , P_A and S_A , while the nucleon one is defined in terms of q , p and s . In the following we extend the hadronic tensor off-shell by assuming that the off-shell structure functions of the nucleons are equal to the on-shell ones.

3.3.2 Convolution of the structure functions

With Eq. (3.24) and Eq. (3.26), we have all the necessary ingredients for the convolution formalism for the hadronic tensor. However we are ultimately

¹ ϵ_f is defined as $\epsilon_f = M_A - M_f - m$ where M_f is the mass of the remaining $A - 1$ remaining hadronic system in the state f .

interested in observable quantities like the structure functions. So, now that we have a convolution formula for the hadronic tensor we will derive convolution formulas for the structure functions. There are several ways to access individual structure functions from the hadronic tensor, see for example Refs. [24, 20]. Before proceeding we will introduce some new notation and some definitions. First the Bjorken variable x , as defined in Eq. (3.10), is not always very convenient, so from now on we will use a new definition for x :

$$x = \frac{Q^2}{2P_A \cdot q} \frac{M_A}{M_N} = \frac{Q^2}{2M_N \nu}, \quad (3.27)$$

where M_A is the mass of the target and M_N is the nucleon mass. For the nucleon both definitions of x give the same results. The Bjorken limit is defined in the same way for both definitions and gives the same physics. In our system we want to know the nuclear structure functions, which are given as functions of $x = Q^2/(2M_N \nu)$ and Q^2 , as a combination of nucleon structure functions given in terms of $\tilde{x} = Q^2/(2p \cdot q)$ and Q^2 . For the convolution formula to be useful we also need to know how to link x and \tilde{x} .

In the nuclear rest frame we define the z -axis as being along the direction of the virtual photon. In this frame we have the nuclear momentum $P_A = (M_A, 0, 0, 0)$, and the virtual photon momentum, $q = (\nu, 0, 0, -\sqrt{\nu^2 + Q^2})$. In the Bjorken limit we have $q \rightarrow (\nu, 0, 0, -\nu - M_N x)$. We will now move to light-cone coordinates which we define as $a^\pm = (a^0 \pm a^3)/\sqrt{2}$, a^1 and a^2 being unchanged and denoted as \vec{a}_\perp . In this coordinate system we have $a \cdot b = a^+ b^- + a^- b^+ - \vec{a}_\perp \cdot \vec{b}_\perp$. Finally we have $P_A^+ = P_A^- = M_A/\sqrt{2}$, $q^+ = -M_N x/\sqrt{2}$ and $q^- = (2\nu + M_N x)/\sqrt{2}$. In the Bjorken limit we have $q^- \rightarrow \sqrt{2}\nu$ which is infinite. So in the Bjorken limit Eq. (3.27) becomes $x \rightarrow M_A Q^2/(2M_N P_A^+ q^-)$ and is dominated by q^- . We now define the quantity y by:

$$y = \frac{p^+}{P_A^+} \frac{M_A}{M_N} = \frac{\sqrt{2}p^+}{M_N}. \quad (3.28)$$

Thus y is the fraction of the momentum of the nucleus carried by the struck nucleon, defined so it runs from 0 to approximately $A(\approx M_A/M_N)$, like x . With this definition, we can now express both p^+ and p^- in terms of y :

$$p^+ = y P_A^+ \frac{M_N}{M_A} = \frac{y M_N}{\sqrt{2}}, \quad (3.29)$$

$$p^- = \frac{M_N^2 - \vec{p}_\perp^2}{2p^+} = \frac{M_N^2 - \vec{p}_\perp^2}{\sqrt{2}y M_N}. \quad (3.30)$$

If we suppose that the transverse momentum of the struck nucleon cannot become very big, then p^- will remain finite and the dot-product $p \cdot q$ will be

dominated by the term p^+q^- which goes to infinity in the Bjorken limit while p^-q^+ stays finite. Consequently we have $p \cdot q \approx p^+q^- = yP_A^+q^-M_N/M_A \approx yP_A \cdot qM_N/M_A$, and the argument of the structure function needed in the nuclear calculation, $\tilde{x} = Q^2/(2p \cdot q)$, is:

$$\tilde{x} = \frac{x}{y}. \quad (3.31)$$

We now can express the convolution formula for the various structure functions, in the Bjorken limit:

$$F_1^A(x, Q^2) = \sum_{t=-\frac{1}{2}}^{\frac{1}{2}} \sum_{s,f} \int d^4p S_f^t(p, s, P_A, S_A) \frac{M_A}{M_N} F_1^t\left(\frac{x}{y}, Q^2\right), \quad (3.32)$$

$$F_2^A(x, Q^2) = \sum_{t=-\frac{1}{2}}^{\frac{1}{2}} \sum_{s,f} \int d^4p S_f^t(p, s, P_A, S_A) y F_2^t\left(\frac{x}{y}, Q^2\right), \quad (3.33)$$

$$g_1^A(x, Q^2) = \sum_{t=-\frac{1}{2}}^{\frac{1}{2}} \sum_{s,f} \int d^4p S_f^t(p, s, P_A, S_A) \frac{M_A(q \cdot s)}{y M_N(q \cdot S_A)} g_1^t\left(\frac{x}{y}, Q^2\right). \quad (3.34)$$

The ratio of masses in Eq. (3.32) comes from the fact that $W_1 = F_1/M$. In Eq. (3.33) this ratio is in fact included in the definition of y . We did not include a convolution formula for g_2 as it is quite complex compared to the other structure functions and we will not study it in the following. As one can notice the structure function of the nucleon on the right hand side depends only on y , which is in fact a measure of p^+ . Consequently we can simplify the integrals in the Eqs. (3.32) to (3.34) to the form:

$$F_1^A(x, Q^2) = \sum_{t=-\frac{1}{2}}^{\frac{1}{2}} N_t \int dy \frac{f^t(y)}{y} F_1^t\left(\frac{x}{y}, Q^2\right), \quad (3.35)$$

$$F_2^A(x, Q^2) = \sum_{t=-\frac{1}{2}}^{\frac{1}{2}} N_t \int dy f^t(y) F_2^t\left(\frac{x}{y}, Q^2\right), \quad (3.36)$$

$$g_1^A(x, Q^2) = \sum_{t=-\frac{1}{2}}^{\frac{1}{2}} N_t \int dy \frac{\Delta f^t(y)}{y} g_1^t\left(\frac{x}{y}, Q^2\right). \quad (3.37)$$

In those equations N_t is the number of particles of isospin t in the nucleus and we have:

$$f^t(y) = \frac{1}{N_t} \sum_{s,f} \int d^4p S_f^t(p, s, P_A, S_A) \frac{p^0 + p^3}{p^0} \delta\left(y - \frac{p^0 + p^3}{M_N}\right). \quad (3.38)$$

$f^t(y)$ is called the (unpolarised) light-cone momentum distribution for the nucleon of isospin t . It is in fact the probability of finding a nucleon of isospin t and fraction of momentum y in the nucleus. The division by N_t is necessary because the spectral function is not a probability but a number density. For the definition of Δf^t we have to remember that a spin 1/2 particle only has two possible spin projections along any given axis, we will call them “+” and “-”. We also have the choice of the polarisation S_A , which we will take as being positive (+), so:

$$\Delta f^t(y) = \frac{1}{N_t} \sum_f \int d^4p \left(S_f^t(p, +, P_A, +) - S_f^t(p, -, P_A, +) \right) \times \frac{p^0 + p^3}{p^0} \delta\left(y - \frac{p^0 + p^3}{M_N}\right). \quad (3.39)$$

$\Delta f^t(y)$ is known as the polarised light-cone momentum distribution of the nucleon of isospin t . It is interpreted as the probability of finding a nucleon of given isospin t with the same spin projection as the nucleus along the z -axis, minus the probability of finding the same nucleon with opposite spin projection to that of the nucleus along the z -axis.

Chapter 4

Spectral functions and light-cone momentum distributions of the three nucleon system

4.1 The spectral function

As we saw in the last chapter, to compute the nuclear structure functions, we ultimately need to know the light-cone momentum distributions of the various nucleons. To determine these light-cone momentum distributions we need to know how to compute the spectral function. As we have seen previously in section 3.3.1, the spectral function is proportional to a number density. As one can see in Eqs. (3.38) and (3.39) the light-cone momentum distributions depend on combinations of spectral functions. Those combinations of spectral functions are not dependent on the nuclear polarisation, S_A (up to a sign in the case of Δf). So one can replace the combination of spectral functions in Eqs. (3.38) and (3.39) by spectral functions that have been "averaged" over polarisation. That is:

$$f^t(y) = \frac{1}{N_t} \sum_f \int d^4p \bar{S}_f^t(p, P_A) \frac{p^0 + p^3}{p^0} \delta\left(y - \frac{p^0 + p^3}{M_N}\right), \quad (4.1)$$

$$\Delta f^t(y) = \frac{1}{N_t} \sum_f \int d^4p \Delta \bar{S}_f^t(p, P_A) \frac{p^0 + p^3}{p^0} \delta\left(y - \frac{p^0 + p^3}{M_N}\right), \quad (4.2)$$

with:

$$\bar{S}_f^t(p, P_A) = \frac{1}{2J_A + 1} \sum_{s, S_A} S_f^t(p, s, P_A, S_A), \quad (4.3)$$

$$\Delta \bar{S}_f^t(p, P_A) = \frac{1}{2J_A + 1} \sum_{\pm} (S_f^t(p, \pm, P_A, \pm) - S_f^t(p, \mp, P_A, \pm)) . \quad (4.4)$$

The quantity $\bar{S}_f^t(p, P_A)$, called the "diagonal spectral function" in Refs. [30, 31], can be interpreted as the number density of particles of isospin t inside the nucleus (while the remaining hadronic system is in a state f). On the other hand, $\Delta \bar{S}_f^t(p, P_A)$ is interpreted as the number density of particles of isospin t , with spin aligned with the spin of the nucleus, minus the number density of the same particles, with spin anti-aligned with the spin of the nucleus (while the remaining hadronic system is in a state f). Since we are summing over all polarisations, we can replace sums over polarisation by sums over spin states, which is easier to use. Note also, that those spectral functions are sometimes defined in terms of E and \vec{k} rather than the four vector k (see for example Refs. [28, 29]). Then E is the energy of the state λ , that is, what has been called P_{A-1}^0 in Eqs. (3.24) and (3.25). E and k^0 are, of course, related by energy conservation.

One can define two extra polarised spectral functions, $\bar{S}_f^{t,+}$ and $\bar{S}_f^{t,-}$. $\bar{S}_f^{t,+}$ ($\bar{S}_f^{t,-}$) is the number density of particle of isospin t , with spin aligned (anti-

aligned) with the spin of the nucleus, while the remaining hadronic system is in a state f . They are defined by:

$$\bar{S}_f^{t,+}(p, P_A) = \frac{1}{2J_A+1} \sum_{\pm} S_f^t(p, \pm, P_A, \pm) , \quad (4.5)$$

$$\bar{S}_f^{t,-}(p, P_A) = \frac{1}{2J_A+1} \sum_{\pm} S_f^t(p, \mp, P_A, \pm) . \quad (4.6)$$

We can also define the corresponding light-cone momentum distributions $f^{t,+}$ and $f^{t,-}$ with equations similar to Eqs. (4.1) and (4.2). We have the following relations between the various spectral functions defined by Eqs. (4.3) through (4.6): $\bar{S}_f^t = \bar{S}_f^{t,+} + \bar{S}_f^{t,-}$ and $\Delta \bar{S}_f^t = \bar{S}_f^{t,+} - \bar{S}_f^{t,-}$.

In the following we will denote the product $a_{\sigma,N}^\dagger(\vec{k}) a_{\sigma,N}(\vec{k})$ – where σ is a spin index – as the familiar number density operator $\rho_{\sigma,N}(\vec{k})$ and we will define it in a way similar to Ref. [33]. For example, the density of protons with spin $+\frac{1}{2}$ along the z -axis and momentum \vec{k} , $\langle \rho_p^+(\vec{k}) \rangle$, in a tri-nucleon with wave function $|\Psi\rangle$ and spin projection σ , is defined by

$$\begin{aligned} \langle \rho_p^+(\vec{k}) \rangle &= \frac{1}{2} \sum_{\sigma} \langle \Psi^\sigma | \rho_p^+(\vec{k}) | \Psi^\sigma \rangle \\ &= \frac{1}{2} \sum_{\sigma} \sum_{i=1}^3 \int d^3\vec{p} d^3\vec{q} \langle \Psi^\sigma(\vec{p}, \vec{q}) | \rho_{p,i}^+ | \Psi^\sigma(\vec{p}, \vec{q}) \rangle \delta^3(\vec{p}_i - \vec{k}) , \end{aligned} \quad (4.7)$$

with

$$\rho_{p,i}^+ = \frac{(1+\tau_{3,i})}{2} \frac{(1+\sigma_{z,i})}{2} . \quad (4.8)$$

In Eq. (4.8), $\tau_{3,i}$ is the projection operator of the particle i on the third axis in the isospin space, likewise $\sigma_{z,i}$ is the spin projection operator for the same particle on the z -axis. \vec{p}_i is the momentum of the particle i in the nucleus, by default \vec{p} and \vec{q} are understood as being \vec{p}_1 and \vec{q}_1 . In Eq. (4.8) one can recognise the number density, in the sense of Ref. [33]. The other density operators which we may use are

$$\rho_{p,i}^- = \frac{(1+\tau_{3,i})}{2} \frac{(1-\sigma_{z,i})}{2} , \quad (4.9)$$

$$\rho_{n,i}^+ = \frac{(1-\tau_{3,i})}{2} \frac{(1+\sigma_{z,i})}{2} , \quad (4.10)$$

$$\rho_{n,i}^- = \frac{(1-\tau_{3,i})}{2} \frac{(1-\sigma_{z,i})}{2} . \quad (4.11)$$

Using the notation of section 2, and more specifically Eq. (2.4), we can rewrite Eq. (4.7) in a slightly different way, showing explicitly how the calculation is

performed with our three body wave function

$$\begin{aligned} \langle \rho_p^+(\vec{k}) \rangle = & \frac{1}{2} \sum_{\substack{\ell_1, N_1 \\ \ell_1', N_1'}} \sum_{i, \sigma} \int d^3\vec{p}_1 d^3\vec{q}_1 \langle \Omega_{\ell_1 N_1}^{JJ}, \sigma(\hat{p}_1, \hat{q}_1) | \rho_{p,i}^+ | \Omega_{\ell_1' N_1'}^{JJ}, \sigma(\hat{p}_1, \hat{q}_1) \rangle \\ & \times \langle \mathcal{U}_{\ell_1 N_1}^{IJ}(p_1, q_1) | \mathcal{U}_{\ell_1' N_1'}^{IJ}(p_1, q_1) \rangle \delta^3(\vec{p}_i - \vec{k}) . \end{aligned} \quad (4.12)$$

Since this definition of the number density is averaged over the nuclear spin, it may be used to compute the spectral functions defined in Eqs. (4.3) to (4.6).

4.2 The case of ^3He

^3He is one of simplest nuclei, along with ^3H and deuterium. It consists of 2 protons and 1 neutron. If we compute the light-cone momentum distribution of the neutron, the remaining two protons can only be in a scattering state, since there is no bound state of two protons. On the other hand, if we compute the light-cone momentum distribution of the proton, the remaining two nucleons are a proton and a neutron, which can be in either a bound state, the deuteron, or a scattering state. We will therefore study first the simpler case of the neutron momentum distribution and then turn to the more difficult proton momentum distribution. In the following equations ρ_N will mean the following $\sum_{i,\pm} \rho_{N,i}^\pm$. Whenever we omit the index i it means that we implicitly sum over all three particles.

4.2.1 Neutron in ^3He

In this case, the remaining two-body system is made up of two protons in a scattering state. The scattering state is characterised by a specific energy distribution. The two scattering protons are on-shell and consequently the neutron is off-shell. As a result the neutron does not satisfy the on-mass-shell relation $E^2 = \vec{p}^2 + m^2$. Since we are using a non-relativistic wave function for ^3He we will use a non-relativistic approximation for the relation between the energy and the momentum. We then define the binding energy of the nucleus, E , by the relation $M = 3m + E$, where m is the mass of a nucleon. Since we are working with a non-relativistic wave function, we make use of the approximation $p^0 \approx m + \vec{p}^2/(2m)$. Since we are working in the frame of

the centre of mass of the nucleus we have the following

$$\begin{aligned} M &= p_\alpha^0 + p_\beta^0 + p_\gamma^0, \\ p_\alpha^0 &= M - p_\beta^0 - p_\gamma^0, \\ p_\alpha^0 &= m + E - \frac{\vec{p}_\beta^2}{2m} - \frac{\vec{p}_\gamma^2}{2m}, \\ p_\alpha^0 &= m + E - \frac{\vec{p}_\alpha^2}{2\mu} - \frac{\vec{q}_\alpha^2}{2\nu}, \end{aligned}$$

where ν is the reduced of the mass of the interacting pair and μ is their total mass¹. If we compare this result with the expression given in Eq. (3.25), then the recoil energy Tr is $\vec{p}_\alpha^2/(2\mu)$, while the separation energy, ϵ , is $E - \vec{q}_\alpha^2/(2\nu)$. So the unpolarised spectral function for the neutron in ${}^3\text{He}$ is given by

$$\begin{aligned} \bar{S}^n(k) &= \frac{1}{2} \sum_\sigma \sum_i \int d^3\vec{p} d^3\vec{q} \langle \Psi^\sigma(\vec{p}, \vec{q}) | \rho_{n,i} | \Psi^\sigma(\vec{p}, \vec{q}) \rangle \\ &\quad \times \delta^3(\vec{k} - \vec{p}_i) \delta\left(k^0 - \left(m + E - \frac{\vec{p}_i^2}{2\mu} - \frac{\vec{q}_i^2}{2\nu}\right)\right). \end{aligned} \quad (4.13)$$

We stress that Eqs. (3.23) and (3.24) are equivalent and should give the same results. In order to demonstrate this we computed the light-cone momentum distribution:

$$f_n(y) = \int d^4k \left(1 + \frac{k^3}{k^0}\right) \delta\left(y - \frac{k^0 + k^3}{m}\right) \bar{S}^n(k), \quad (4.14)$$

with the two equations. To compute the light-cone momentum distribution with Eq. (3.23), the final state $|P_{A-1}S_{A-1}\rangle$ was taken to be a plane wave plus a pair of protons interacting in the 1S_0 channel. This is by far the most important channel for the final state interaction. We found that the light-cone momentum distributions computed with Eqs. (3.23) and (3.24) were identical, within numerical precision.

For the polarised case we have:

$$\begin{aligned} \Delta\bar{S}^n(k) &= \frac{1}{2} \sum_\pm \sum_i \int d^3\vec{p} d^3\vec{q} \langle \Psi^\pm(\vec{p}, \vec{q}) | (\rho_{n,i}^\pm - \rho_{n,i}^\mp) | \Psi^\pm(\vec{p}, \vec{q}) \rangle \\ &\quad \times \delta^3(\vec{k} - \vec{p}_i) \delta\left(k^0 - \left(m + E - \frac{\vec{p}_i^2}{2\mu} - \frac{\vec{q}_i^2}{2\nu}\right)\right). \end{aligned} \quad (4.15)$$

This spectral function can then be used in Eq. (4.2) to compute the polarised light-cone momentum distribution.

¹Note that here, in the case of two identical particles we have $\nu = m/2$ and $\mu = 2m$.

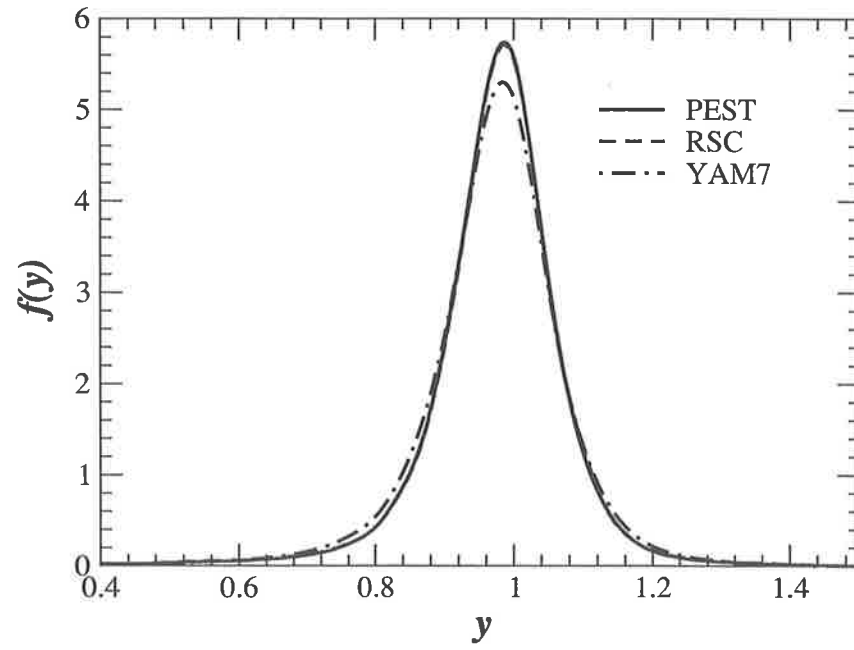


Figure 4.1: Neutron light-cone momentum distribution in ${}^3\text{He}$ for various potentials.

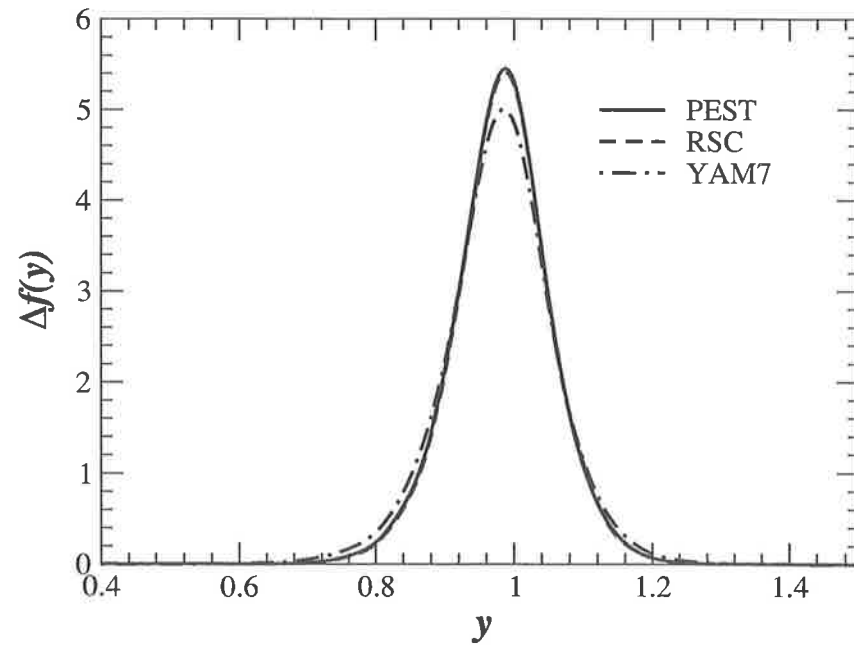


Figure 4.2: Neutron polarised light-cone momentum distribution in ${}^3\text{He}$ for various potentials.

4.2.2 Proton in ${}^3\text{He}$

In the case of the proton we have two possibilities for the final state, so we also have two spectral functions to compute for each light-cone momentum distribution. The first state is a scattering state similar to the final state encountered in the neutron case, with which it shares the formula for p^0 . The second possible final state is made of a scattered proton and a deuteron. We can find the form of the proton energy in the same way we did for the scattering state, only it is now much more simple as we have only two particles in the final state and not three. With the same non relativistic approximation as before, one easily finds that in this case: $p_\alpha^0 = M - M_d - \vec{p}_\alpha^2/(2M_d)$, where M_d is the deuteron mass. Defining the binding energy of the deuteron, E_d , in same way we did for the tri-nucleon we have $M_d = 2m + E_d$ and finally, $p_\alpha^0 = m + E - E_d - \vec{p}_\alpha^2/(2M_d)$.

Because there are two states, it is more practical to use the formulation of Eq. (3.23). To use Eq. (3.23), we have to separate the contributions to each final state by taking the projections of the tri-nucleon wave function over the two-body wave function of the corresponding final state. Here, we can separate the tri-nucleon wave function in two orthogonal parts, one in which the system is a proton plus a deuteron, and one in which the system is a proton plus a proton and a neutron in a scattering state. That is:

$$|\Psi^\pm\rangle = |\Psi_{p,(pn)}^\pm\rangle + |\Psi_{p,d}^\pm\rangle, \quad (4.16)$$

where we have:

$$|\Psi_{p,d}^\pm\rangle = \sum_{\sigma=-1}^{+1} |\Phi_d^\sigma\rangle \langle \Phi_d^\sigma | \Psi^\pm \rangle. \quad (4.17)$$

In Eq. (4.17), $|\Phi_d^\sigma\rangle$ is the wave function of the deuteron with spin projection σ on the z -axis. The deuteron has a spin equal to 1, so σ can run from -1 to $+1$. One can access $|\Psi_{p,(pn)}^\pm\rangle$ by subtracting $|\Psi_{p,d}^\pm\rangle$ from the total wave function. That is: $|\Psi_{p,(pn)}^\pm\rangle = |\Psi^\pm\rangle - |\Psi_{p,d}^\pm\rangle$. In momentum space Eq. (4.17) becomes:

$$|\Psi_{p,d}^\pm(\vec{p}_i, \vec{q}_i)\rangle = \sum_{\sigma=-1}^{+1} |\Phi_d^\sigma(\vec{q}_i)\rangle \int d^3\vec{p}_1' d^3\vec{q}_1' \langle \Phi_d^\sigma(\vec{q}_i) | \Psi^\pm(\vec{p}_1', \vec{q}_1') \rangle \delta^3(\vec{p}_i - \vec{p}_1') . \quad (4.18)$$

We can now write the two spectral functions for the unpolarised case:

$$\begin{aligned} \bar{S}_d^p(k) = \frac{1}{2} \sum_{\pm} \sum_i \int d^3\vec{p}_i d^3\vec{q}_i \langle \Psi_{p,d}^\pm(\vec{p}_i, \vec{q}_i) | \rho_{p,i} | \Psi_{p,d}^\pm(\vec{p}_i, \vec{q}_i) \rangle \\ \times \delta^3(\vec{k} - \vec{p}_i) \delta\left(k^0 - \left(m + E - E_d - \frac{\vec{p}_i^2}{2M_d}\right)\right), \end{aligned} \quad (4.19)$$

$$\bar{S}_s^p(k) = \frac{1}{2} \sum_{\pm} \sum_i \int d^3\vec{p}_i d^3\vec{q}_i \left\langle \Psi_{p,(pn)}^{\pm}(\vec{p}_i, \vec{q}_i) \left| \rho_{p,i} \right| \Psi_{p,(pn)}^{\pm}(\vec{p}_i, \vec{q}_i) \right\rangle \\ \times \delta^3(\vec{k} - \vec{p}_i) \delta\left(k^0 - \left(m + E - \frac{\vec{p}_i^2}{2\mu} - \frac{\vec{q}_i^2}{2\nu}\right)\right) . \quad (4.20)$$

In term of these spectral functions we can write the light-cone momentum distribution of the proton

$$f_p(y) = \frac{1}{2} \int d^4k \left(1 + \frac{k^3}{k^0}\right) \delta\left(y - \frac{k^0 + k^3}{m}\right) (\bar{S}_s^p(k) + \bar{S}_d^p(k)) . \quad (4.21)$$

In the preceding equation we introduced factor one-half because there are two protons in a ^3He nucleus. This is the coefficient N_t , ensuring the normalisation of the light-cone momentum distribution, we introduced in Eqs. (3.35) to (3.37).

One can easily compute the various polarised spectral functions by substituting the appropriate combination of number densities in Eqs. (4.19) and (4.20). It is then possible to compute the corresponding polarised light-cone momentum distributions, following the procedure outlined in Eq. (4.21).

4.3 Results

Using the formalism presented above, we have computed light-cone momentum distributions for some of our three nucleon wave functions. For all those distributions we used only the first 42 three body channels. This is because the computation of the polarised distributions involves some complicated matrix elements. However, for all these wave functions the 42 first channels add up to more than 99% of the total normalisation, so one can safely assume that the contribution of the remaining channels is negligible. For the unpolarised distribution the matrix elements are quite simple, so one can easily check, in this case, that the contribution from higher channels is indeed small. We compared the light-cone momentum distribution for a proton and a neutron in ^3He for respectively 42 and 130 channels and found that for all purposes they were indistinguishable. For the PEST potential we also compared wave functions including 5 and 18 three-body channels and found that they were also indistinguishable.

In Figs. 4.1 and 4.2 we show the proton and neutron light-cone momentum distributions for our potentials (PEST, RSC and YAM7). The light-cone momentum distributions given by the RSC and PEST potentials are almost indistinguishable and they cannot be separated on these figures. The YAM7 potential, however, shows some differences, probably because this potential

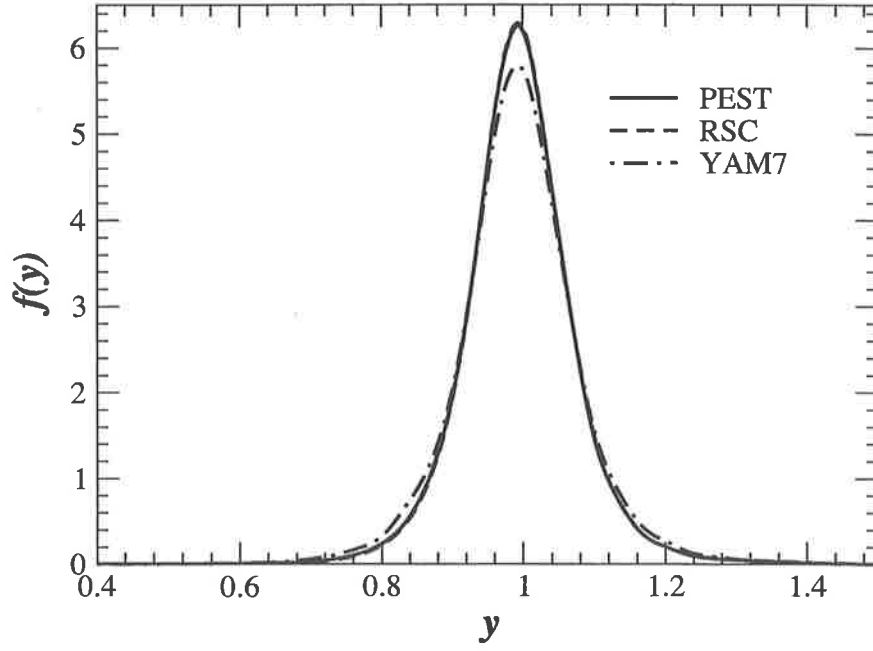


Figure 4.3: Proton light-cone momentum distribution in ${}^3\text{He}$ for various potentials.

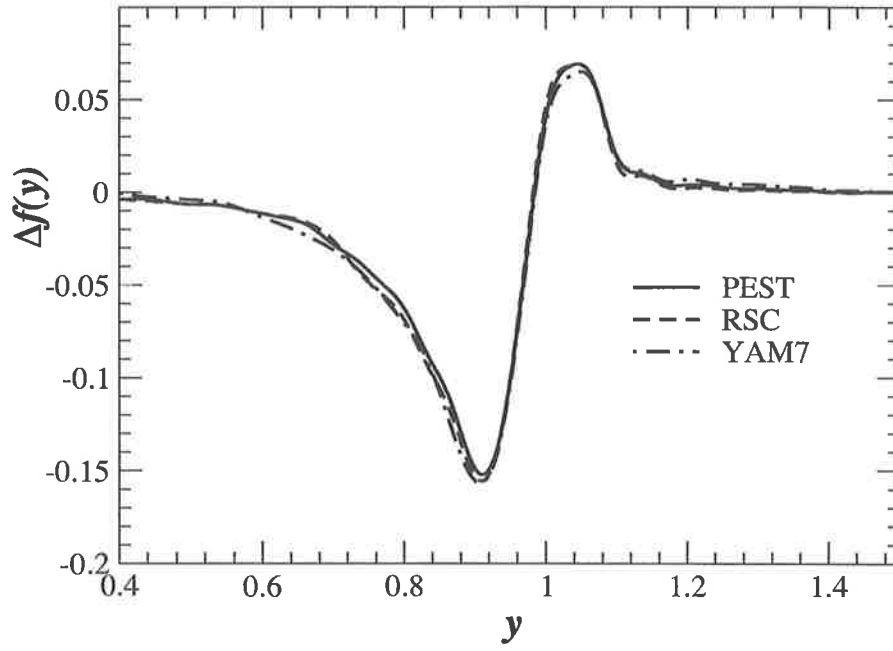


Figure 4.4: Proton polarised light-cone momentum distribution in ${}^3\text{He}$ for various potentials.

Table 4.1: Effective polarisation of the nucleons in ^3He for various potentials.

	$\sum P(X)$				$\int f(y)$			
	n^+	n^-	p^+	p^-	n^+	n^-	p^+	p^-
PEST	93.97%	6.03%	48.96%	51.04%	93.62%	6.32%	48.98%	50.96%
RSC	93.45%	6.55%	48.83%	51.17%	92.92%	6.79%	48.76%	50.95%
YAM7	93.66%	6.34%	48.81%	51.19%	93.25%	6.35%	48.69%	50.92%

Table 4.2: Effective polarisation of the nucleons in ^3He and ^3H , with two-body interaction adjusted to produce the experimental binding energies.

	$\sum P(X)$				$\int f(y)$			
	n^+	n^-	p^+	p^-	n^+	n^-	p^+	p^-
^3He	93.97%	6.03%	48.91%	51.09%	93.73%	6.24%	48.94%	51.02%
^3H	48.85%	51.15%	93.45%	6.55%	48.89%	51.10%	93.86%	6.13%

does not include short range repulsion. It is also important to note that to have consistent results one needs to use a deuteron wave function computed with the same potential as the three nucleon system. In Figs. 4.3 and 4.4 we show the proton and neutron polarised light-cone momentum distributions for the same potentials used in Figs. 4.1 and 4.2. The polarised neutron light-cone momentum distribution shows the same behaviour and is similar in size to its unpolarised counterpart. However, for the proton the polarised momentum distribution is far smaller than its unpolarised counterpart. In this case all the potentials give very similar results. We note that one can extract more information from the polarised momentum distributions. While in the unpolarised case the distributions are normalised to one, in the polarised case they are normalised to the polarisation of the given nucleon. From Ref. [33] one can compute these polarisations analytically in terms of the S , S' and D waves probabilities (neglecting the small contribution of the P waves). One can compute those probabilities from the wave function and then compare them with the values extracted from the momentum distributions. From Ref. [33] we have the following relations

$$n^+ = \int dy f_n^+(y) = 1 - \frac{1}{3} (P(S') + 2P(D)), \quad (4.22)$$

$$n^- = \int dy f_n^-(y) = \frac{1}{3} (P(S') + 2P(D)), \quad (4.23)$$

$$p^+ = \int dy f_p^+(y) = \frac{1}{2} - \frac{1}{6} (P(D) - P(S')), \quad (4.24)$$

$$p^- = \int dy f_p^-(y) = \frac{1}{2} + \frac{1}{6} (P(D) - P(S')). \quad (4.25)$$

In Table 4.1 we compare the numerical values of these two expressions in ^3He , for our various potentials. The results are in quite good agreement, with the small discrepancies arising from numerical errors in the computation of many nested integrals. (Note, for example, that the overall normalisation is correct to about 0.06%.) In Table 4.2 we make the same comparison but with wave functions in which we have adjusted the binding energies to the experimental values.

Chapter 5

Unpolarised structure functions of the three nucleon system

5.1 Parton model

As we explained in chapter 3, in the unpolarised deep inelastic scattering of a charged lepton on a nuclear target, all the target information is included in the two structure functions F_1 and F_2 . In our computations we will use a simple quark parton model (QPM) for the structure functions of the free nucleon. One can find a derivation of the QPM in various text books and lectures such as Refs. [19, 59, 60, 61]. We will not derive the QPM here, but we will recall its main assumptions and results regarding structure functions.

The relevant time scale involved in DIS is $\mathcal{O}(1/\sqrt{Q^2})$ and is far shorter than the time scale which characterises strong interactions. Therefore the virtual photon probes a frozen nucleon, where the partons (*i.e.* quarks and gluons) are quasi-free and do not interact. The last two assumptions constitute the impulse approximation on which the QPM is based.

Those assumptions are similar to the ones we have seen in Section 3.3.1, describing the PWIA, when we were studying the convolution formalism. The derivation of the formulae for the structure functions of the free nucleon have some similarity with the derivation of the convolution formalism. The hadronic tensor for the nucleon is a convolution of the probability of finding a given parton with the tensor for the parton. The main difference between the QPM and the convolution formalism, is that the quarks and gluons, like the leptons, are elementary particles and their tensor is easy to write down. In the end, if one neglects the transverse momentum of the quarks, we have:

$$F_1(x, Q^2) = \frac{1}{2} \sum_i e_i^2 q_i(x, Q^2), \quad (5.1)$$

$$F_2(x, Q^2) = 2xF_1(x, Q^2) = x \sum_i e_i^2 q_i(x, Q^2). \quad (5.2)$$

In the previous equations $q_i(x, Q^2)$ is usually interpreted as the number density of quarks of flavour i and fraction of the nucleon momentum x^1 at the momentum scale Q^2 . e_i is the electric charge of the parton of flavour i . The first part of Eq. (5.2) is called the Callan-Gross relation [62]. This relation is valid for a simple parton model if one neglects the transverse momentum of the partons and if they have spin 1/2. A more general relation between F_1 and F_2 [17] is:

$$F_2(x, Q^2) = 2xF_1(x, Q^2) \frac{1+R}{1+2xm_N/\nu}, \quad (5.3)$$

¹Here x is defined by $x = k^+/p^+$, where k is the four-momentum of the struck quark inside the nucleon of four-momentum p . In the QPM this quantity is equal to the Bjorken variable x , defined by Eq. (3.10).

where R is the ratio of the cross section for absorbing a longitudinal photon to that for a transverse photon. Given the relation between F_1 and F_2 , most studies concentrate on the latter and we will do so as well using, Eq. (5.2) to compute F_2 in this study.

5.2 EMC effect

The convolution formula between the free and in medium structure functions [17, 25] are

$$\tilde{F}_1^N(x, Q^2) = \int_x^{\frac{M_A}{m}} dy \frac{f_N(y)}{y} F_1^N\left(\frac{x}{y}, Q^2\right), \quad (5.4)$$

$$\tilde{F}_2^N(x, Q^2) = \int_x^{\frac{M_A}{m}} dy f_N(y) F_2^N\left(\frac{x}{y}, Q^2\right). \quad (5.5)$$

Hence the F_2 structure function of a nucleus of mass number A and proton number Z is given by

$$F_2^A(x, Q^2) = \int_x^{\frac{M_A}{m}} dy \left(Z f_p(y) F_2^p\left(\frac{x}{y}, Q^2\right) + (A-Z) f_n(y) F_2^n\left(\frac{x}{y}, Q^2\right) \right). \quad (5.6)$$

In comparing the F_2 structure functions on various targets, the European Muon Collaboration (Aubert et al. [42]) discovered what is now called the “EMC” effect. We define a theoretical EMC ratio as the ratio of the F_2 structure function of the nucleus to the sum of the free structure functions of the nucleons in this nucleus:

$$R_t = \frac{F_2^A}{Z F_2^p + (A-Z) F_2^n}. \quad (5.7)$$

On the other hand, it is more common to compare the ratio of the F_2 structure function of the nucleus to that of deuterium:

$$R_x = \frac{F_2^A/A}{F_2^D/2}. \quad (5.8)$$

This should be close to R_t if the deuteron is a quasi-free system of a proton and a neutron and if the nucleus studied is symmetric, or almost, in its

content of neutrons and protons. ${}^3\text{He}$ and ${}^3\text{H}$ are highly asymmetric nuclei, as their content in one type of nucleon is twice as much as the other. To take this into account, it is common to add an isosymmetric correction so that the ratio studied is [25]:

$$R_A(x, Q^2) = \frac{F_2^A(x, Q^2)}{F_2^D(x, Q^2)} I(x, Q^2), \quad (5.9)$$

with:

$$I(x, Q^2) = \frac{F_2^p(x, Q^2) + F_2^n(x, Q^2)}{ZF_2^p(x, Q^2) + (A - Z)F_2^n(x, Q^2)}. \quad (5.10)$$

This ratio is, strictly speaking, the ratio of the EMC ratios of the nucleus A and the deuteron. Following the same kind of procedure used in the previous section, one can compute the light-cone momentum distribution of a nucleon in the deuteron. To be consistent, this ratio has to be computed with the same interaction for both the three nucleon system and the deuteron. To compute R_A we used several parametrisations for the quark distributions:

- The parametrisation “CTEQ5” from the CTEQ collaboration [37]. This collaboration gives several parametrisations, but we mainly used the one called “leading order”, and it will be the one used when we talk about the CTEQ5 parametrisation, unless explicitly stated otherwise.
- The “GRV” parametrisation from Glück, Reya and Vogt [43].
- The “DOLA” parametrisation from Donnachie and Landshoff [44].

These distributions are usually given for quarks in a proton and in order to compute neutron structure functions we used charge symmetry² [45]. In Figs. 5.1 and 5.2 one can see the ratio R_3 for ${}^3\text{He}$ and ${}^3\text{H}$, with the CTEQ5 parametrisation at $Q^2 = 10 \text{ GeV}^2$, for the three potentials studied. In Fig. 5.3 we show R_3 in ${}^3\text{He}$ for the PEST potential alone but for all three quark distributions (again at $Q^2 = 10 \text{ GeV}^2$). We also studied the effect of adjusting the binding energy as described at the end of the first section but did not include it in Figs. 5.1 and 5.2 because it would have confused the plot. This adjustment of the binding energy caused a slightly deeper EMC effect in both ${}^3\text{He}$ and ${}^3\text{H}$ and also a slightly steeper increase at high x .

²With the exception of the DOLA distribution which gives proton and deuteron distributions. In this case we took the neutron as the difference between the deuteron and the proton.

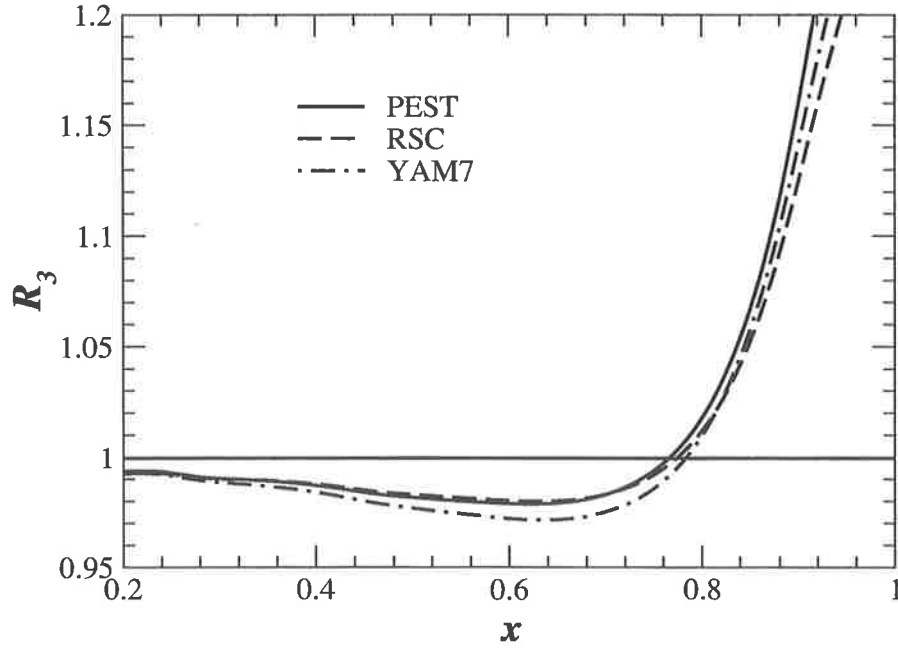


Figure 5.1: The ratio R_3 , given in Eq.(5.9), for ${}^3\text{He}$, at $Q^2 = 10 \text{ GeV}^2$, calculated for various potentials using the CTEQ5 quark distributions.

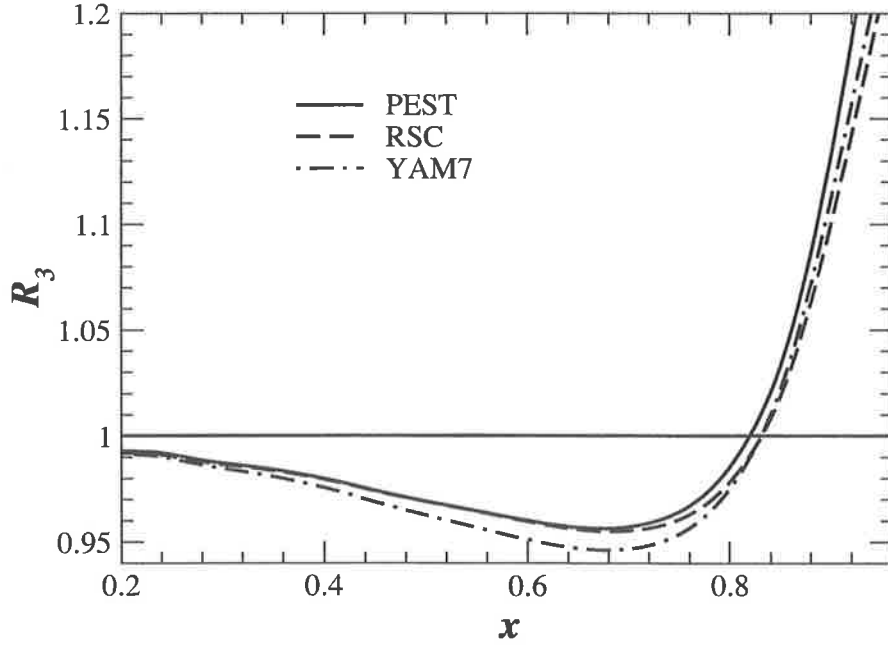


Figure 5.2: The ratio R_3 , given in Eq.(5.9), for ${}^3\text{H}$, at $Q^2 = 10 \text{ GeV}^2$, calculated for various potentials using the CTEQ5 quark distributions.

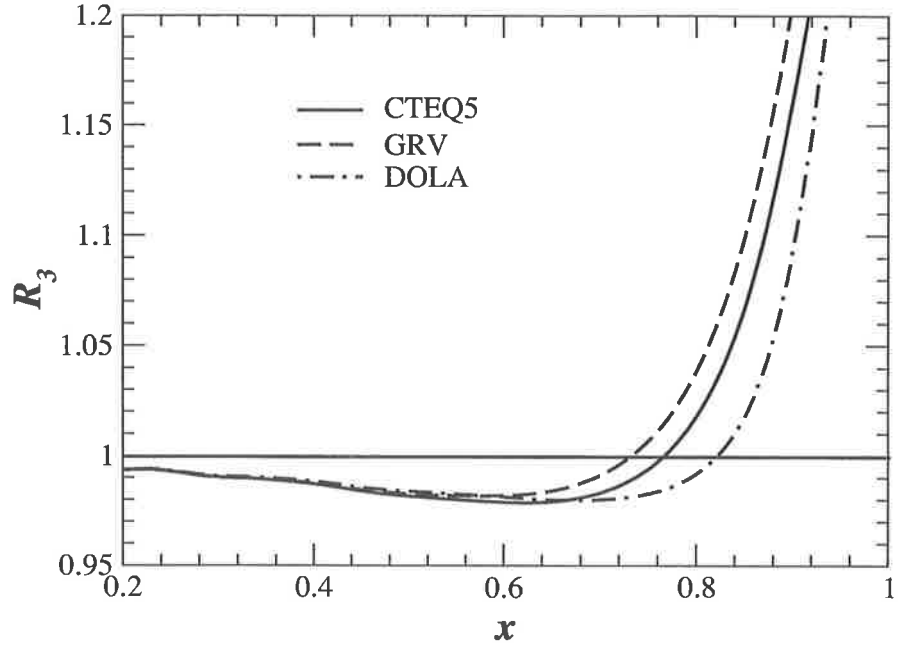


Figure 5.3: The ratio R_3 , given in Eq.(5.9), for ${}^3\text{He}$, at $Q^2 = 10 \text{ GeV}^2$, calculated for the PEST potential, using various quark distributions for the nucleons.

5.3 Gottfried sum rule

Since we have computed the structure functions for both ${}^3\text{He}$ and ${}^3\text{H}$ we can investigate the Gottfried sum rule (GSR) in the tri-nucleon system. The GSR provides a way to probe the flavour asymmetry of the quark. For example, in a simple parton model where we assume charge symmetry, we have

$$\begin{aligned} F_2^p(x) - F_2^n(x) &= \frac{1}{3}x [u(x) - d(x)] + \frac{1}{3}x [\bar{u}(x) - \bar{d}(x)] , \\ &= \frac{1}{3}x [u_v(x) - d_v(x)] + \frac{2}{3}x [\bar{u}(x) - \bar{d}(x)] . \end{aligned} \quad (5.11)$$

In Eq. (5.11), q_v is the valence distribution of the quark q and we have $q_v = q - \bar{q}$. This is why we have a factor 2 in front of the anti-quark distribution in the second line. The difference expressed in Eq. (5.11), divided by x and integrated, gives the Gottfried sum, I_G^N . For the nucleon it gives

$$I_G^N(z) = \int_z^1 dx \frac{F_2^p(x) - F_2^n(x)}{x} . \quad (5.12)$$

Using the normalisation of the valence quark distributions in the proton immediately leads to

$$I_G^N(0) = \frac{1}{3} + \frac{2}{3} \int_0^1 dx [\bar{u}(x) - \bar{d}(x)]. \quad (5.13)$$

This quantity provides a measure of flavour asymmetry. If the sea was flavour symmetric, *i.e.* $\bar{u}(x) = \bar{d}(x)$, the GSR would simply give $I_G^N(0) = 1/3$. However, the experimental value obtained by the NMC collaboration [38] was $I_G^N(0) = 0.235 \pm 0.026$ (at $Q^2 = 4 \text{ GeV}^2$). This value is clearly less than $1/3$, and it implies that $\bar{d}(x)$ exceeds $\bar{u}(x)$ in the proton [38, 39]:

$$\int_0^1 dx [\bar{d}(x) - \bar{u}(x)] = 0.148 \pm 0.039. \quad (5.14)$$

The origin of the flavour asymmetry in the proton may be attributed to either the pion cloud required by chiral symmetry [34, 100] or to the Pauli exclusion principle at the quark level [35, 36, 100], or both. The existence of a pion cloud around the proton can generate pairs of $d\bar{d}$ quarks. For example, in the pion cloud picture the proton can undergo the following process: $p \rightarrow n + \pi^+$. The proton, on the left hand side, has the following quark content: (uud) , while the neutron and pion on the right hand side have the following quark content: $(udd) + (u\bar{d})$. One can immediately see that a $d\bar{d}$ pair is generated in the process. The Pauli exclusion principle would also favour the creation of $d\bar{d}$ pair over $u\bar{u}$ in the proton, as the two u quarks are already filling more degrees of freedom than the single d quark.

Our point of interest here is to see how the GSR changes in a nucleus, and especially in the three nucleon system. The study of the flavour asymmetry of a bound nucleon may gives us insight into the non-perturbative structure of the nucleon in nuclear matter. We will now consider the "nuclear Gottfried sum" defined on a pair of mirror nuclei as

$$I_G^{A,A'}(z) = \int_z^A dx \frac{F_2^A(x) - F_2^{A'}(x)}{x}, \quad (5.15)$$

where A and A' are mirror nuclei, A being proton rich (here ${}^3\text{He}$) while A' is neutron rich (here ${}^3\text{H}$). To compute the nuclear Gottfried sum we have used the wave function given by the PEST potential, adjusted to reproduce the binding energy of the corresponding nuclei. However, it turns out that

the difference of structure functions is not very sensitive to this change in the wave function, so we can expect the charge symmetry breaking to be very small in our study. We have used the CTEQ5 parametrisation for the free nucleon structure functions. This incorporates the measured flavour asymmetry in the free nucleon [37]. We restrict ourselves to $x \geq 0.1$ because the study of the small x region should include correction to take into account nuclear shadowing and physics neglected in the convolution formalism.

The effect of charge symmetry breaking is to break the nuclear Gottfried sum rule:

$$I_G^{A,A'}(0) = Y \times I_G^N(0), \quad (5.16)$$

where Y is the excess proton (neutron) number in A (A') – in our case $Y = 1$. Eq. (5.16) should hold if the nuclear environment does not affect the flavour asymmetry. In Fig. 5.4 we show $F_2^A(x) - F_2^{A'}(x)$ for both the tri-nucleon system and the free nucleon. The curve that one gets using an isosymmetric wave function for the three nucleon system is identical. We can see in Fig. 5.4 that the difference between the free nucleon and three nucleon system case is very small. In the present calculation we find that for $Q^2 = 10 \text{ GeV}^2$, we have $I_G^N(0.1) = 0.152$ whereas $I_G^{^3\text{He}, ^3\text{H}}(0.1) = 0.150^3$, so charge symmetry breaking in the $A = 3$ system gives very little change in the distribution $\bar{d} - \bar{u}$, at least for $x \geq 0.1$. As one can see in Fig. 5.5 there may be an increase in the difference between the free case and the three nucleon case at small x .

5.4 The neutron structure function F_2^n

One of the most interesting things about the tri-nucleon system is the fact that we can extract data on the free neutron. Either by experiments on ^3He alone, as we will see in the next chapter, or by combining results from experiments on both ^3He and ^3H , as we will see here. So far most parametrisations of the structure functions of the nucleon use data from proton and deuteron experiments and several assumptions, like, but not limited to, charge symmetry. The charge symmetry assumption seems to be valid in most cases, however the extraction of neutron data from deuteron experiments is at best problematic for values of x that are not small ($x \gtrsim 0.4$), see for example [63, 64, 65, 66]. We present here another way to access the structure func-

³If we use isosymmetric wave functions for ^3H and ^3He we have $I_G^{^3\text{He}, ^3\text{H}}(0.1) = 0.153$.

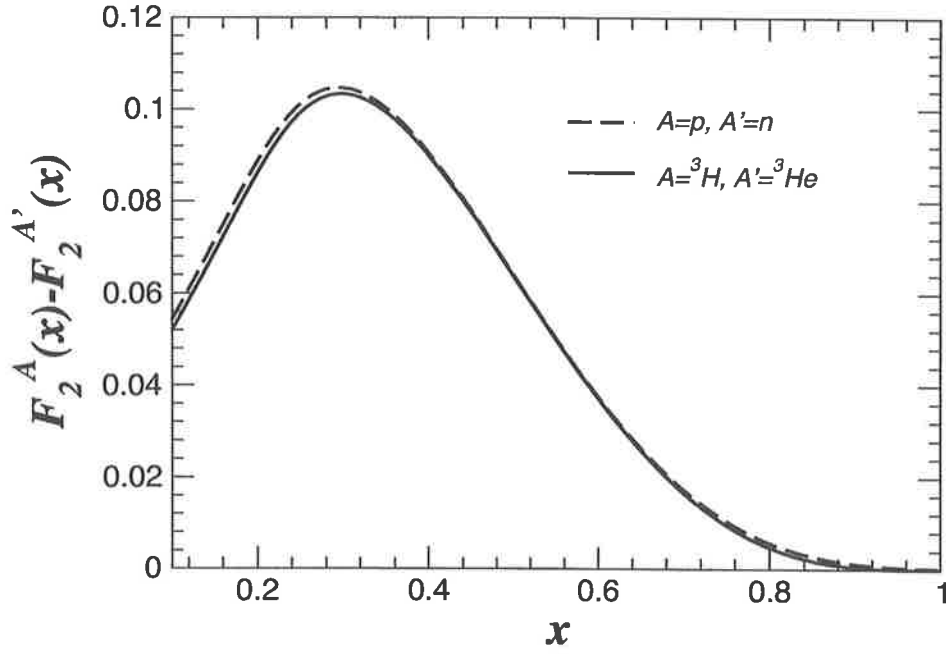


Figure 5.4: The difference $F_2^A(x) - F_2^{A'}(x)$ for both the tri-nucleon system and the free nucleon, at $Q^2 = 10 \text{ GeV}^2$, using the CTEQ5 quark distributions.

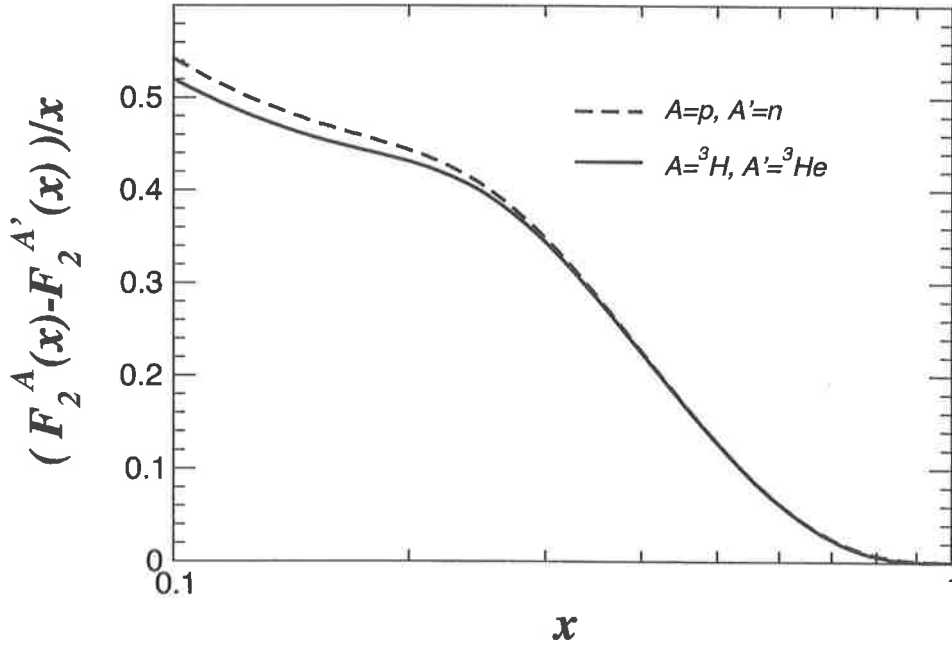


Figure 5.5: The difference $(F_2^A(x) - F_2^{A'}(x))/x$ for both the tri-nucleon system and the free nucleon, at $Q^2 = 10 \text{ GeV}^2$, using the CTEQ5 quark distributions.

tion F_2^n of the neutron. From Eq. (5.7) we have:

$$R_t(^3\text{He}) = \frac{F_2^{^3\text{He}}}{2F_2^p + F_2^n}, \quad (5.17)$$

$$R_t(^3\text{H}) = \frac{F_2^{^3\text{H}}}{F_2^p + 2F_2^n}. \quad (5.18)$$

Now we can form the ratio of EMC ratios:

$$\mathcal{R} = \frac{R_t(^3\text{He})}{R_t(^3\text{H})} = \frac{F_2^{^3\text{He}}}{F_2^{^3\text{H}}} \frac{F_2^p + 2F_2^n}{2F_2^p + F_2^n}. \quad (5.19)$$

This expression can now be inverted to give us the ratio of the free neutron to proton structure functions as a function of \mathcal{R} :

$$\frac{F_2^n}{F_2^p} = \frac{2\mathcal{R} - F_2^{^3\text{He}}/F_2^{^3\text{H}}}{2F_2^{^3\text{He}}/F_2^{^3\text{H}} - \mathcal{R}}. \quad (5.20)$$

The ratio $F_2^{^3\text{He}}/F_2^{^3\text{H}}$ can be measured experimentally in the same way one measures the ratio R_x of Eq. (5.8). So the extracted ratio F_2^n/F_2^p depends, not on the size of the EMC effect in either ^3He or ^3H , but on the ratio of the EMC effects in ^3He and ^3H . If the neutron and proton distributions in tri-nucleon system are not dramatically different, one can expect $\mathcal{R} \approx 1$. Incidentally one can see that we have $\mathcal{R} = R_3(^3\text{He})/R_3(^3\text{H})$, so by studying Figs. 5.1 and 5.2 we can already see that indeed \mathcal{R} is close to 1, within a few percent up to $x \approx 0.8$, the variation with x is quite rapid.

We computed \mathcal{R} in our approach for various potentials for the light cone momentum distributions and various quark parametrisations for the structure functions. What we want to establish is that we can set \mathcal{R} to “a central value” from which it deviates only a few percent, independent of the chosen model. The smaller the deviation the better the extraction of the ratio F_2^n/F_2^p .

Figs. 5.6 to 5.7 show the super-ratio, \mathcal{R} , for various potentials and quark distributions. In Fig. 5.6 we plot \mathcal{R} computed using our three different kinds of potential and the CTEQ5 quark distribution at $Q^2 = 10 \text{ GeV}^2$. As one can see on this figure, \mathcal{R} seems to depend very little on the potential and is very close to unity. In Fig. 5.7 we investigate the effect on the isospin breaking in the three-nucleon wave function. The curve labelled PEST is identical to the one labelled PEST in Fig. 5.6 and corresponds to the use of an isospin symmetric wave function for ^3He and ^3H . The curve labelled PEST(E) corresponds to the use of binding energy adjusted wave functions for ^3He and ^3H , which are not isospin symmetric anymore. The effect observed here is

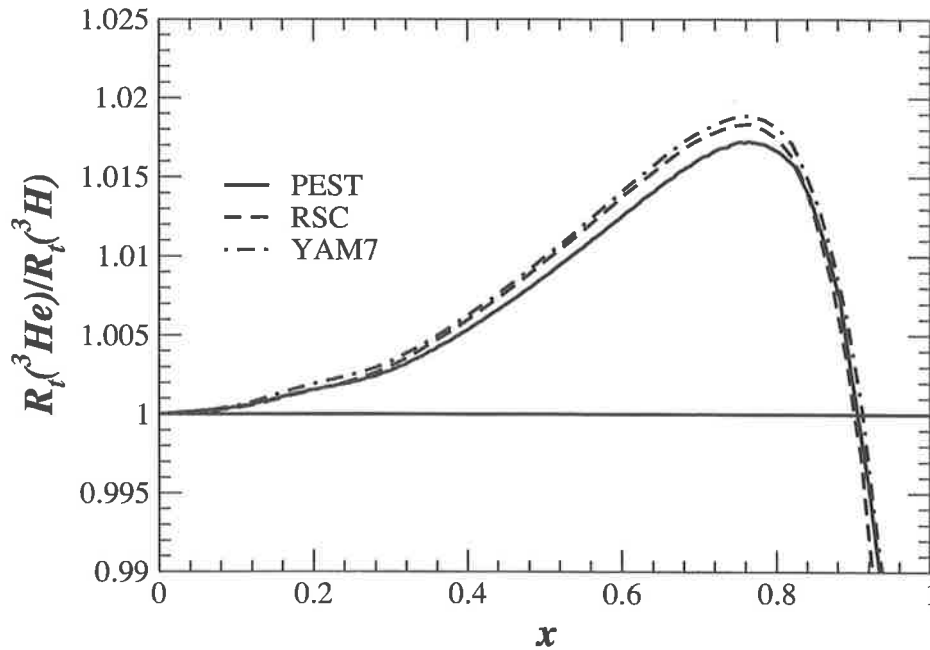


Figure 5.6: The ratio of ratios, Eq. (5.19), for various potentials, using the CTEQ5 parametrisation at $Q^2 = 10 \text{ GeV}^2$.

much greater than those observed in Fig. 5.6. So the extraction of the ratio F_2^n/F_2^p may have some dependence on the model used for the wave functions of ^3He and ^3H .

In Fig. 5.8 we show \mathcal{R} for various quark distributions using the PEST potential for the convolution formula. This figure is again at $Q^2 = 10 \text{ GeV}^2$ except for the curve labelled BBS which is at $Q^2 = 4 \text{ GeV}^2$. The solid curve is for CTEQ5 at leading order, the dash-dotted curve is the GRV parametrisation. There are two dashed curves for the DOLA parametrisation (labelled DL). The first one labelled DL(HT) includes a higher twist contribution to the structure function F_2 , while none of the other parametrisations, including the one simply labelled DL, has it. This is why this curve behaves differently from the others. The curve labelled BBS uses the parametrisation of Ref. [76]. Most fits of parton distributions assume that the ratio $d/u \rightarrow 0$ as $x \rightarrow 1$, however that assumption can be questioned on theoretical and phenomenological grounds [77]. The BBS parametrisation incorporates constraints from perturbative QCD and forces the ratio $d/u \rightarrow 0.2$ as $x \rightarrow 1$.

As one can see, the dependence on the parton distributions is rather weak at low x but becomes large at high x . However this dependence is actually artificial and reflects the lack of knowledge of the neutron structure function

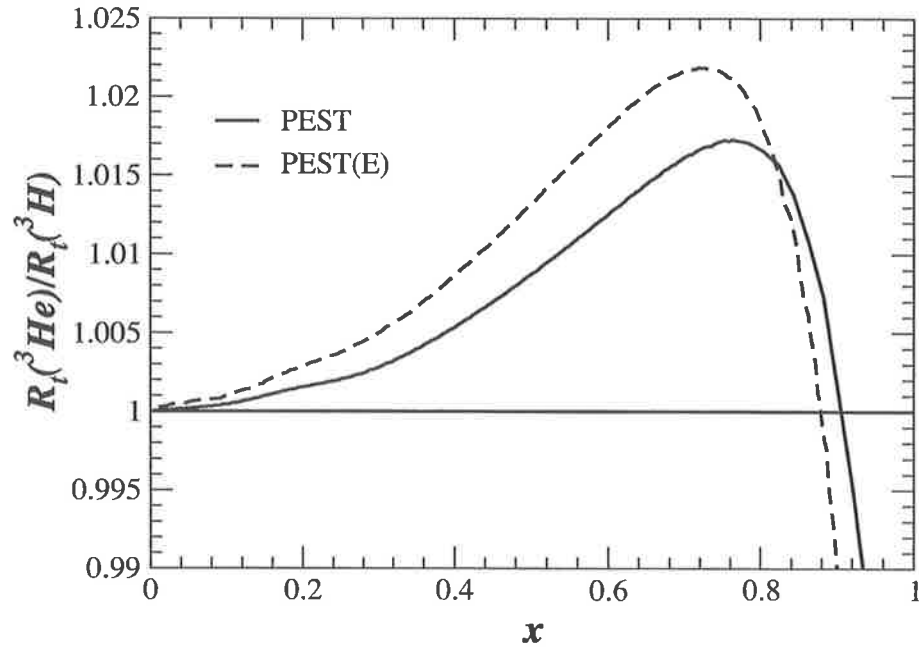


Figure 5.7: The ratio of ratios, Eq. (5.19), using the CTEQ5 quark parametrisation at $Q^2 = 10 \text{ GeV}^2$, for isospin symmetric and non isospin symmetric three-nucleon wave functions.

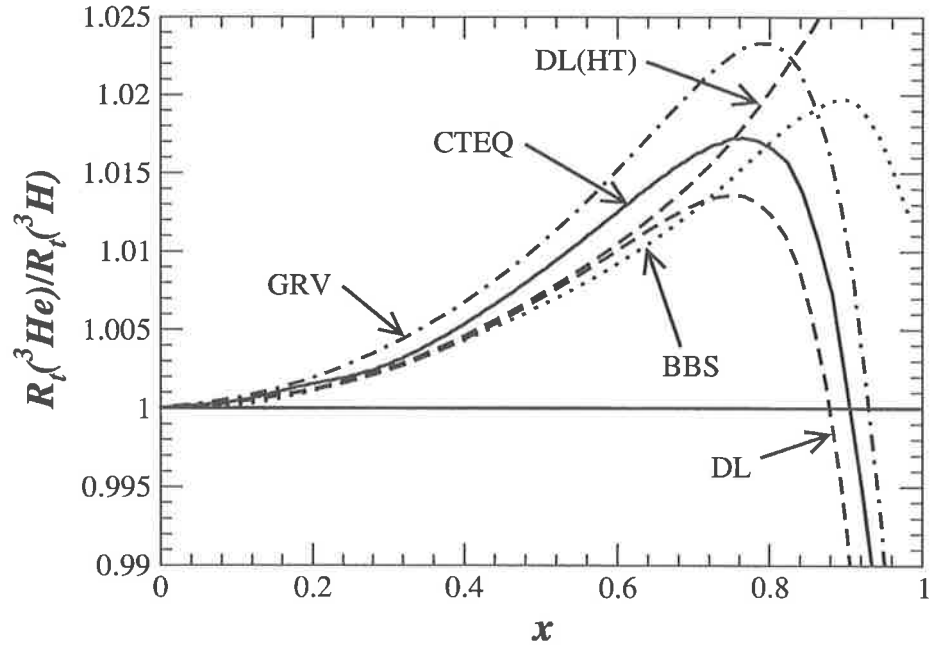


Figure 5.8: The ratio of ratios, Eq. (5.19), for various quark distributions, using the PEST potential.

F_2^n . In practice, once the ratio $F_2^{3\text{He}}/F_2^{3\text{H}}$ is measured one can use an iterative procedure to eliminate this dependence altogether. After extracting F_2^n/F_2^p for some \mathcal{R} one can use the resulting F_2^n to compute a new \mathcal{R} and extract a new F_2^n . This procedure is iterated until convergence is achieved and a self-consistent solution for F_2^n/F_2^p and \mathcal{R} is obtained.

So from this study it appears that main dependence in the extracted ratio F_2^n/F_2^p may come from the model used for the tri-nucleon wave function. But even this dependence as shown in Fig. 5.7 is not very strong and the ratio \mathcal{R} still deviates only by approximately 2% from unity. This shows that the measurement of the ratio $F_2^{3\text{He}}/F_2^{3\text{H}}$ would enable us to have an accurate estimate of the neutron structure function F_2 .

Chapter 6

Polarised structure functions of the three nucleon system

6.1 Parton model

If one does experiments with both a polarised lepton beam and a polarised spin $\frac{1}{2}$ nuclear target, one needs two more structure functions, g_1 and g_2 , to completely describe the target. As we have mentioned in Section 3.2.2 it is possible to isolate the contribution of the polarised structure functions by using combinations of cross sections measured with different polarisations of the target and the beam. If we use the same QPM as in the previous chapter and neglect again the transverse momentum of the quarks one finds that [18, 19, 46, 47]:

$$g_1(x, Q^2) = \frac{1}{2} \sum_i e_i^2 \Delta q_i(x, Q^2), \quad (6.1)$$

$$g_2(x, Q^2) = 0. \quad (6.2)$$

In Eq. (6.1), x , Q^2 and e_i are the same as in Eqs. (5.1) and (5.2). The meaning of Δq_i is less trivial, we have [18, 19]:

$$q_i(x, Q^2) = q_i^+(x, Q^2) + q_i^-(x, Q^2), \quad (6.3)$$

$$\Delta q_i(x, Q^2) = q_i^+(x, Q^2) - q_i^-(x, Q^2), \quad (6.4)$$

where q_i^+ is the probability of finding a quark of flavour i with the same helicity as the nucleon and q_i^- is the probability of finding a quark of flavour i with opposite helicity compared to the nucleon. So the probability of finding a quark of flavour i , which we used in Eqs. (5.1) and (5.2), is just the sum of q_i^+ and q_i^- . On the other hand, in g_1 we need the difference of those probabilities. Eq. (6.2) shows that, at leading order in the QPM, $g_2 = 0$. In fact, g_2 does not have a simple, consistent parton model interpretation [18, 69], but from the previous facts, we can say it is small.

The polarised structure functions are smaller than their unpolarised counterparts, g_2 in particular, as we have just seen, is very small and very difficult to measure (see for example Refs. [67, 68] for such measurements). In practice, in most experiments measuring g_1 , the contribution of g_2 is suppressed by a factor x^2/Q^2 [18] and so it is neglected. We will not study g_2 at all. As we have already seen in Section 4.3 and Tables 4.1 and 4.2, the figures for the polarisation of the various nucleons in the tri-nucleon system indicate that the contribution from the doubly represented nucleon will be considerably suppressed. Therefore the system should be a good approximation to a pure target of the singlet nucleon.

The following computation will be made with a next to leading order (NLO) parametrisation of the parton distribution and a NLO formula for g_1 ,

as found in Refs. [48, 70]. We will use hereafter the standard NLO scenario of the parton distribution given in [70] (GSRV00 hereafter). In Ref. [71] we made those computations with the previous version of this parametrisation (GSRV96 [48] hereafter) and the conclusions were similar.

6.2 Off-shell corrections

As we have mentioned at the end of Section 3.3.1, in the convolution formula (6.5) we should not use the free nucleon structure functions as the parametrisations we have of them are for on-shell nucleons, while in our present formalism the struck nucleons are off-shell. Because of our lack of knowledge on the off-shell structure functions, we have so far used on-shell structure functions for off-shell ones. Here we will also study the impact of the off-shell corrections for g_1 , calculated within the QMC model [50] in Ref. [49]. This off-shell correction was calculated using a local density approximation to estimate the change of the parton distributions in a bound nucleon. This off-shell correction has only been given for polarised parton distributions, which is why we did not study the impact of this model on unpolarised structure functions earlier.

In this model we have the following relation between the polarised quark distribution in a free nucleon and in a nucleon in ^3He :

$$\frac{\delta\tilde{q}_v(x)}{\delta q_v(x)} = \frac{1}{a_q x^{b_q} + c_q x^{d_q} (1-x)^{e_q}}, \quad (6.5)$$

where $\delta\tilde{q}_v$ is the quark distribution in a nucleon in ^3He and the parameters are the following:

$$\begin{aligned} a_u &= 118.41 & , & & a_d &= 8.964, \\ b_u &= 18.97 & , & & b_d &= 7.5848, \\ c_u &= 1.0758 & , & & c_d &= 1.0515, \\ d_u &= 0 & , & & d_d &= -0.0048, \\ e_u &= 0.0335 & , & & e_d &= 0.01086. \end{aligned} \quad (6.6)$$

Notice that in Eq. (6.5) the relation is between valence quark distributions and that we do not have any corrections for quarks from the sea. So, this correction is most useful for the the region of x dominated by valence quarks, namely for $0.2 \leq x \leq 0.8$. (The upper limit is determined by uncertainties in the structure functions calculated for the MIT bag, which underlies the QMC model.) However, since we will be using NLO formula in the $\overline{\text{MS}}$ scheme for the parton distribution [48, 70] for g_1 , a correction applied on a limited range

of x for the quark distribution will have an impact on all x for g_1 . This is not true for a leading order calculation in any scheme, but we should note that the use of this correction is scheme dependent in NLO. While those corrections have been initially computed for ^3He we will apply them to the case of ^3H as well.

6.3 Non-nucleonic degrees of freedom

The convolution formula we will use to produce ^3He and ^3H polarised structure functions are the following:

$$g_1^{^3\text{He}}(x, Q^2) = \int_x^{\frac{M_A}{m}} \frac{dy}{y} \left(\Delta f_n(y) \tilde{g}_1^n\left(\frac{x}{y}, Q^2\right) + 2\Delta f_p(y) \tilde{g}_1^p\left(\frac{x}{y}, Q^2\right) \right), \quad (6.7)$$

$$g_1^{^3\text{H}}(x, Q^2) = \int_x^{\frac{M_A}{m}} \frac{dy}{y} \left(\Delta f_n(y) \tilde{g}_1^p\left(\frac{x}{y}, Q^2\right) + 2\Delta f_p(y) \tilde{g}_1^n\left(\frac{x}{y}, Q^2\right) \right), \quad (6.8)$$

where it is assumed that the polarised light-cone momentum distribution of the proton (neutron) in ^3H is equal to the light-cone momentum distribution of the neutron (proton) in ^3He , thanks to isospin symmetry. In these equations \tilde{g}_1 stands for the off-shell structure function of the corresponding nucleon in medium.

As has been already mentioned in section 3.3.1, a nucleus is more than just a collection of protons and neutrons and can contain other particles which should also be taken into account in the convolution formalism. We have here a perfect example of such a thing with the tri-nucleon system [72]. The Bjorken sum rule [73] relates the difference of the first moments of the proton and neutron polarised structure function g_1 , to the axial vector coupling constant of the neutron β -decay g_A , with $g_A = 1.2670 \pm 0.0035$ [74]:

$$\int_0^1 (g_1^p(x, Q^2) - g_1^n(x, Q^2)) dx = \frac{1}{6} g_A \left(1 + \mathcal{O}\left(\frac{\alpha_s}{\pi}\right) \right). \quad (6.9)$$

In the previous equation $\mathcal{O}(\alpha_s/\pi)$ represents a standard QCD radiative correction. This sum rule can be generalised to the ^3He - ^3H system:

$$\int_0^{\frac{M_A}{m}} (g_1^{^3\text{H}}(x, Q^2) - g_1^{^3\text{He}}(x, Q^2)) dx = \frac{1}{6} g_A(^3\text{H}) \left(1 + \mathcal{O}\left(\frac{\alpha_s}{\pi}\right) \right), \quad (6.10)$$

where $g_A(^3\text{H}) = 1.211 \pm 0.002$ [75] is the axial vector coupling constant measured in ^3H β -decay. Taking the ratio of the two previous equations one gets:

$$\frac{\frac{M_A}{\int_0^m \left(g_1^{^3\text{H}}(x, Q^2) - g_1^{^3\text{He}}(x, Q^2) \right) dx}}{\int_0^1 \left(g_1^p(x, Q^2) - g_1^n(x, Q^2) \right) dx} = \frac{g_A(^3\text{H})}{g_A} = 0.956 \pm 0.004, \quad (6.11)$$

Note that the QCD corrections to both Eqs. (6.9) and (6.10) cancels exactly. We can now compare the experimental value of Eq. (6.11) with the prediction we get using the convolution formalism and Eqs. (6.7) and (6.8). Using the following property of the convolution formalism:

$$\int_0^A dx \int_x^A \frac{dy}{y} C(y) f\left(\frac{x}{y}\right) = \int_0^A dy C(y) \int_0^1 dx f(x), \quad (6.12)$$

and remembering Eqs. (4.15) to (4.18), we define $P_n = n^+ - n^- = \int dy \Delta f_n(y)$ and $P_p = p^+ - p^- = \int dy \Delta f_p(y)$, which are the effective polarisations of the neutron and proton (proton and neutron) in ^3He (^3H). We also define the first moment of the polarised structure function g_1 by $\Gamma_N = \int dx g_1^N(x, Q^2)$. Then, using the value for the PEST potential in table 4.1, we can rewrite the left hand side of Eq. (6.11) as:

$$\frac{\frac{M_A}{\int_0^m \left(g_1^{^3\text{H}}(x, Q^2) - g_1^{^3\text{He}}(x, Q^2) \right) dx}}{\int_0^1 \left(g_1^p(x, Q^2) - g_1^n(x, Q^2) \right) dx} = (P_n - 2P_p) \frac{\tilde{\Gamma}_p - \tilde{\Gamma}_n}{\Gamma_p - \Gamma_n} = 0.921 \frac{\tilde{\Gamma}_p - \tilde{\Gamma}_n}{\Gamma_p - \Gamma_n}. \quad (6.13)$$

Since off-shell corrections [49] slightly decrease the value of the structure function g_1 we have $(\tilde{\Gamma}_p - \tilde{\Gamma}_n)/(\Gamma_p - \Gamma_n) < 1$, and thus this theoretical prediction underestimates the result of Eq. (6.11). Note that if we do not include off-shell corrections, the right hand side of Eq. (6.13) becomes $P_n - 2P_p = 0.921$ which also underestimates the ratio of Bjorken sum rules. This simple computation demonstrates the needs for new nuclear effects that are not included in the convolution formula (6.7) and (6.8).

Our theoretical result from Eq. (6.13) underestimates the experimental result from Eq. (6.11) by about 3.5%. An effect has been proposed that can make up for this discrepancy [72]. The direct correspondence between the calculations of the Gamow-Teller matrix element in the triton β -decay

and the Feynman diagrams of DIS on ${}^3\text{He}$ and ${}^3\text{H}$ suggests that two-body exchange currents should play an equal role in both processes. Of particular interest is the fact that analyses [78] have shown that the two-body exchange currents involving a $\Delta(1232)$ isobar increase the theoretical prediction for the axial vector coupling of the triton ($g_A({}^3\text{H})$) by about 4%, making it consistent with the experimental value. In the same way, this process should increase the value of the Bjorken sum rule in the tri-nucleon system, making the theoretical value of Eq. (6.13) consistent with the experimental value given in Eq. (6.11).

The $\Delta(1232)$ isobar contributes to $g_1^{{}^3\text{He}}$ and $g_1^{{}^3\text{H}}$ through Feynman diagrams involving the non diagonal transitions: $n \rightarrow \Delta^0$ and $p \rightarrow \Delta^+$. This requires the introduction of new polarised structure functions, $g_1^{n \rightarrow \Delta^0}$ and $g_1^{p \rightarrow \Delta^+}$, as well as the corresponding light-cone momentum distributions, $\Delta f_{n \rightarrow \Delta^0}$ and $\Delta f_{p \rightarrow \Delta^+}$. If we suppose that these light-cone momentum distributions are peaked enough around y equal one, then we can replace them by the effective polarisations¹ $P_{n \rightarrow \Delta^0}$ and $P_{p \rightarrow \Delta^+}$ times the delta function $\delta(1 - y)$. With this addition Eqs. (6.7) and (6.8) become:

$$g_1^{{}^3\text{He}}(x, Q^2) = \int_x^{\frac{M_A}{m}} \frac{dy}{y} \left(\Delta f_n(y) \tilde{g}_1^n\left(\frac{x}{y}, Q^2\right) + 2\Delta f_p(y) \tilde{g}_1^p\left(\frac{x}{y}, Q^2\right) \right) + 2P_{n \rightarrow \Delta^0} g_1^{n \rightarrow \Delta^0} + 4P_{p \rightarrow \Delta^+} g_1^{p \rightarrow \Delta^+}, \quad (6.14)$$

$$g_1^{{}^3\text{H}}(x, Q^2) = \int_x^{\frac{M_A}{m}} \frac{dy}{y} \left(\Delta f_n(y) \tilde{g}_1^n\left(\frac{x}{y}, Q^2\right) + 2\Delta f_p(y) \tilde{g}_1^p\left(\frac{x}{y}, Q^2\right) \right) - 2P_{n \rightarrow \Delta^0} g_1^{p \rightarrow \Delta^+} - 4P_{p \rightarrow \Delta^+} g_1^{n \rightarrow \Delta^0}. \quad (6.15)$$

The minus sign in front of the contribution from the Δ in the formula for $g_1^{{}^3\text{H}}$ comes from the convention that $P_{n \rightarrow \Delta^0} \equiv P_{n \rightarrow \Delta^0/{}^3\text{He}} = -P_{p \rightarrow \Delta^+/{}^3\text{H}}$ and $P_{p \rightarrow \Delta^+} \equiv P_{p \rightarrow \Delta^+/{}^3\text{He}} = -P_{n \rightarrow \Delta^0/{}^3\text{H}}$.

In the quark parton model, the interference structure functions $g_1^{n \rightarrow \Delta^0}$ and $g_1^{p \rightarrow \Delta^+}$ can be related to the usual structure functions g_1^p and g_1^n thanks to the general form of the $SU(6)$ nucleon wave function [79]:

$$g_1^{n \rightarrow \Delta^0} = g_1^{p \rightarrow \Delta^+} = \frac{2\sqrt{2}}{5} (g_1^p - 4g_1^n). \quad (6.16)$$

This relation is valid in the domain of x and Q^2 where the contributions from sea quarks and gluons to g_1 can be omitted, that is for $0.2 \leq x \leq 0.8$ and

¹Those effective polarisations are defined as the integral over x of the corresponding light-cone momentum distributions.

$0.5 \leq Q^2 \leq 5 \text{ GeV}^2$ in the case of the parametrisation GSRV00. However, as shown in Ref. [81], this expression can be extended to all x , as it provides a satisfactory value for the following sum rule $\int (g_1^{n \rightarrow \Delta^0}(x) + g_1^{p \rightarrow \Delta^+}(x)) dx$, when the integral is performed over all x .

Effective polarisations $P_{n \rightarrow \Delta^0}$ and $P_{p \rightarrow \Delta^+}$, as well as the corresponding light-cone momentum distributions, could be computed with the help of a tri-nucleon wave function including the Δ resonance. This would require the computation of new wave functions and would involve computational methods beyond the scope of the present study. Instead, we will fix the effective polarisation by requiring that the ratio of Bjorken sum rules is consistent with the experimental result. This leads to the following condition:

$$-2(P_{n \rightarrow \Delta^0} + 2P_{p \rightarrow \Delta^+}) \frac{\int dx (g_1^{n \rightarrow \Delta^0}(x) + g_1^{p \rightarrow \Delta^+}(x))}{\Gamma_p - \Gamma_n} = 0.956 - 0.921 \frac{\tilde{\Gamma}_p - \tilde{\Gamma}_n}{\Gamma_p - \Gamma_n}. \quad (6.17)$$

Then using Eq. (6.16) to link the interference structure functions to the off-shell neutron and proton polarised structure functions g_1 we have:

$$2(P_{n \rightarrow \Delta^0} + 2P_{p \rightarrow \Delta^+}) = \frac{0.814(\tilde{\Gamma}_p - \tilde{\Gamma}_n) - 0.845(\Gamma_p - \Gamma_n)}{\tilde{\Gamma}_p - 4\tilde{\Gamma}_n} = -0.024. \quad (6.18)$$

The numerical value in Eq. (6.18) has been computed at 4 GeV^2 with the standard NLO parametrisation of GSRV00 for the quark distributions. This correction has also been computed with the PEST potential and other potentials could yield slightly different results.

6.4 The neutron in ${}^3\text{He}$

Computing $g_1^{3\text{He}}$ using Eq. (6.7) and our three usual potentials, we found that the results are sufficiently close that we can limit ourselves to the PEST potential in the following. We will compute the polarised structure function g_1 of ${}^3\text{He}$ for three cases:

- Simple convolution using Eq. (6.7) but without off-shell corrections.
- Convolution including off-shell corrections as per Eq. (6.7).
- Same as above plus corrections from the inclusion of the Δ resonance as per Eq. (6.14) and using the results of Eqs. (6.16) and (6.18).

In Fig. 6.1 we show four curves at $Q^2 = 4 \text{ GeV}^2$: $xg_1(x)$ for the free neutron and $xg_1(x)$ for ${}^3\text{He}$ for each one of our three cases. As one can see, the four

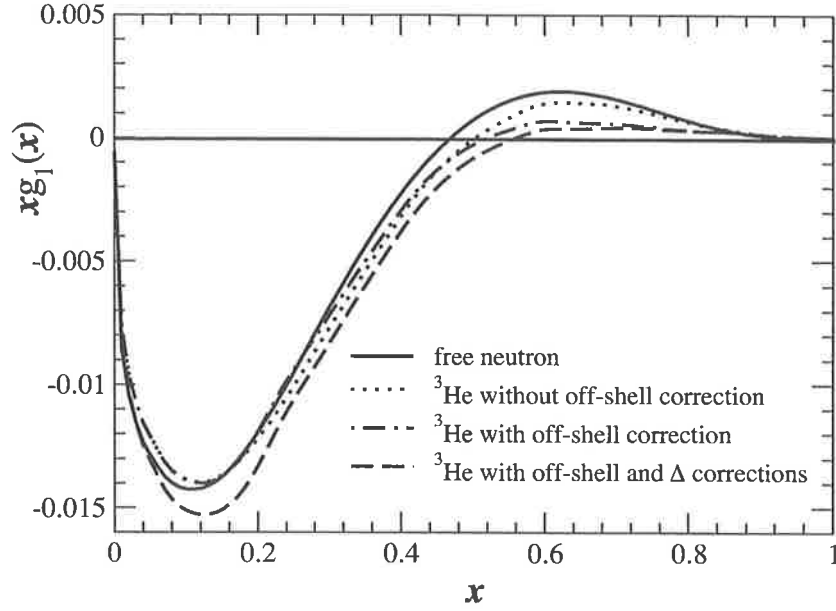


Figure 6.1: Comparison of several calculations of $xg_1(x)$ for ^3He and the free neutron at $Q^2 = 4 \text{ GeV}^2$.

curves are quite close. There are two main sources of complications when one tries to extract g_1^n from ^3He . As one can see from Fig. 6.1, the contribution of the Δ resonance can be important for values of x less or equal to 0.2. Another complication is the contribution of the proton. The free proton spin structure function is very big compared with that of the neutron, so while the proton contribution in ^3He is severely reduced by the low effective polarisation, it may not be negligible. One way to estimate the size of the contribution of the proton is to compare $g_1^{^3\text{He}}$ with a formula often used in experimental analysis²:

$$g_1^{^3\text{He}} \approx \Delta_n g_1^n + 2\Delta_p g_1^p. \quad (6.19)$$

If the contribution of the proton to $g_1^{^3\text{He}}$ is negligible, Eq. (6.19) is equivalent to: $g_1^{^3\text{He}} \approx \Delta_n g_1^n$. To estimate the effect of the proton contribution in the extraction of g_1^n , we plotted the following differences:

$$\Delta_g = \frac{g_1^{^3\text{He}} - 2\Delta_p g_1^p}{\Delta_n} - g_1^n, \quad (6.20)$$

²There are several ways to find this result. One would be to use the same argument we already used for the Δ isobar in the previous section. See Ref. [19] for another derivation.

and

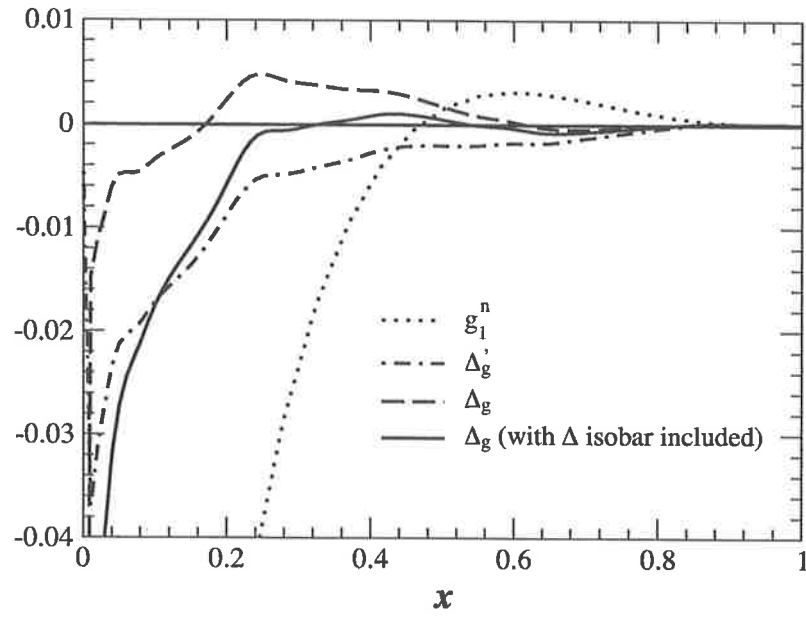
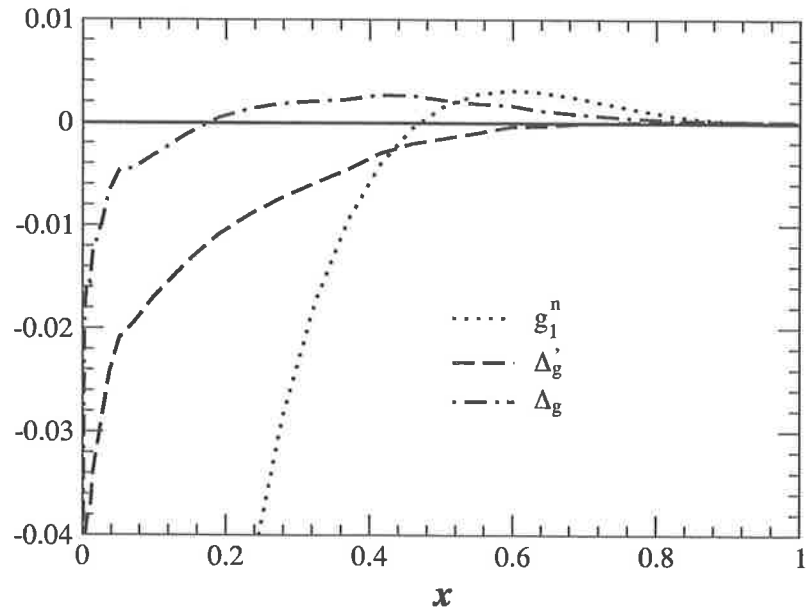
$$\Delta'_g = \frac{g_1^{^3\text{He}}}{\Delta_n} - g_1^n. \quad (6.21)$$

In Figs. 6.2 and 6.3 we plot Δ_g , Δ'_g and g_1^n . We have plotted g_1^n as one ultimately wants to extract it and one needs to have an idea of the relative size of the error. In Fig. 6.2 the dotted curve is g_1^n , the dash-dotted curve is Δ'_g , where $g_1^{^3\text{He}}$ has been computed with Eq. (6.7), including the off-shell effects of Ref. [49], the dashed curve is Δ_g , where $g_1^{^3\text{He}}$ is the same as for the dash-dotted curve, finally the solid curve is Δ_g where $g_1^{^3\text{He}}$ has been computed as per Eq. (6.14), that is, with both off-shell effects and the Δ isobar. In Fig. 6.3 we plotted the same curves as in Fig. 6.2 (except the solid curve), without including the off-shell effects of Ref. [49] in the computation of $g_1^{^3\text{He}}$. These computations have been done at $Q^2 = 4 \text{ GeV}^2$. We do not plot the ratio of structure functions because in both the neutron and ^3He cases g_1 can be zero, leading to singularities in the plots.

If we do not include off-shell effects, it is clear from Fig. 6.4, that one gets more accurate results for most values of x , by taking into account the contribution of the protons. In Fig. 6.2, one can see that once we turn on the off-shell effects of Ref. [49], one gets more accurate results on $0.5 \leq x \leq 0.8$ by including the contribution of the protons. However on $0.2 \leq x \leq 0.5$ both computations give similar errors. Surprisingly, when we include the contribution of the Δ isobar, Eq. (6.19) is very accurate for $x \geq 0.2$. In this case the inclusion of the protons contribution is essential as without it, we get a far greater error than with any other computations. In all cases, the relative error is at its biggest, for $0.2 \leq x \leq 0.8$, around the point where g_1^n cross the x -axis.

For values of x below 0.2, all computations give big absolute differences and one clearly needs some other tools to accurately extract the free neutron structure function, even if the relative difference seems to be small. For values of x over 0.8, the differences are all very small, but so is the structure function g_1^n . For those values of x , Fermi motion effects are significant, but this cannot be shown on a difference plot. Fermi motion effects will be more apparent for ^3H , in the next section. We find similar curves for other parton distributions, such as those from Refs. [54, 48].

In Figs. 6.4 and 6.5, we apply our previous results to experimental data. Fig. 6.4 shows results from E154 [82] while Fig. 6.5 shows results from HERMES [52]. In the following we compute the value of Δ_g , defined in Eq. (6.20), using the standard NLO parton distribution of Ref. [70], for each experimental point, including the various corrections we studied previously. Then we apply this correction, Δ_g , to the experimental data. In both figures the white

Figure 6.2: Δ_g , Δ'_g and g_1^n at $Q^2 = 4 \text{ GeV}^2$.Figure 6.3: Δ_g , Δ'_g and g_1^n , without off-shell corrections, at $Q^2 = 4 \text{ GeV}^2$.

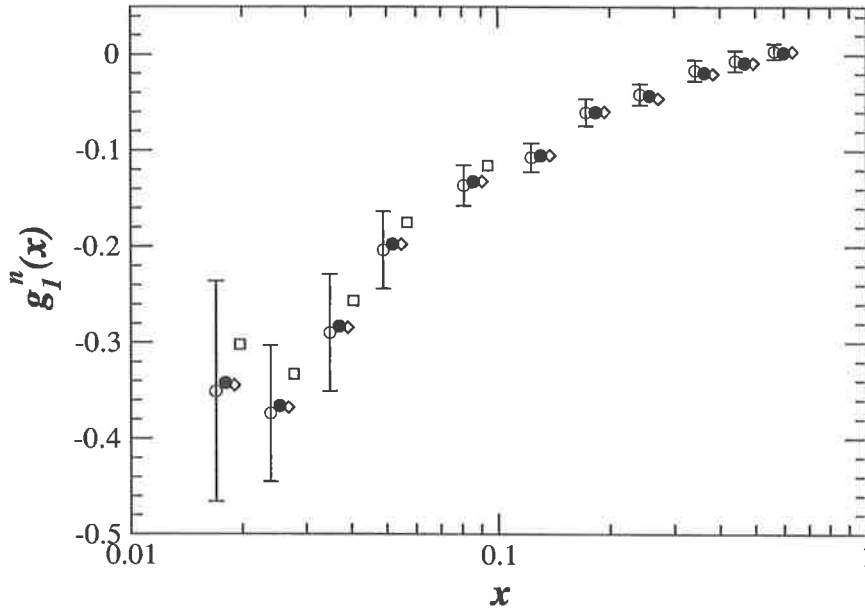


Figure 6.4: Corrections to g_1^n data from E154. White circles represent the original data. Black circles are corrected for binding energy and nuclear effects. Diamonds have all corrections from the black circles as well as off-shell corrections. Squares have all the corrections from the diamonds as well as Δ isobar corrections. The error bars are statistical errors.

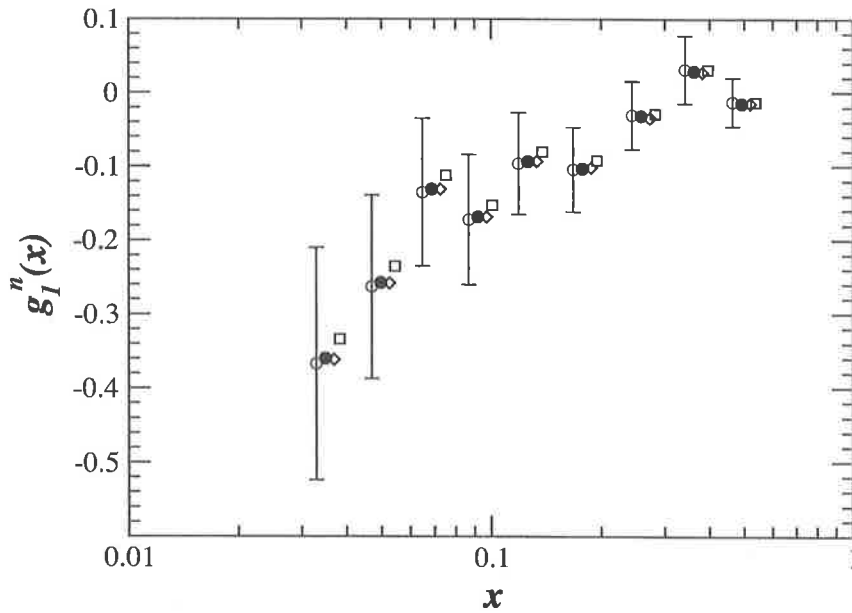


Figure 6.5: Corrections to g_1^n data from HERMES. White circles represent the original data. Black circles are corrected for binding energy and nuclear effects. Diamonds have all corrections from the black circles as well as off-shell corrections. Square have all the corrections from the diamond as well as Δ isobar corrections. The error bars are statistical errors.

circles represent the original data given in Refs. [52, 82] and are assumed to have been extracted as per Eq. (6.19). One gets the black circles by correcting for the nuclear effects included in the convolution formalism. One gets the diamonds by including the off-shell effects of Ref. [49], and finally, one gets the squares by including the correction from the Δ isobar discussed in section 6.3.

In Fig. 6.4, we did not apply the correction associated with the Δ isobar on all points, as for points with $x \geq 0.1$ the corresponding Q^2 is more than 6 GeV^2 which is outside the range of application of the model used. The E154 collaboration has evolved its data to $Q^2 = 5 \text{ GeV}^2$ which would be in the limit of applicability of the model, however, we believe that data should be corrected before being evolved. So, we will not use the evolved data of E154. In Fig. 6.5 we did apply the Δ isobar correction to the last point, $x = 0.464$ and $Q^2 = 5.25 \text{ GeV}^2$, as it is not far off the limit of applicability of our model. Both figures show that the most important correction comes from the inclusion of the Δ isobar for values of x smaller than 0.2. All other corrections are small and well within error bars. However at small x , one probably needs to take into account some other physics to get a good description of the system. This suggests that we can make an accurate extraction of g_1^n from ^3He data for medium and large values of x . In the small x region, however, one may need other tools to perform an accurate extraction of g_1^n from $g_1^{^3\text{He}}$.

6.5 The proton in tritium

For tritium we will compute the polarised structure function g_1 using Eqs. (6.8) and (6.15). In this case one can plot a ratio, as g_1^p and $g_1^{^3\text{H}}$ do not change sign. Therefore, to illustrate the effect of the neutron contribution in this case one can plot:

$$R_g = \frac{g_1^{^3\text{H}} - 2\Delta_n g_1^n}{\Delta_p g_1^p}, \quad (6.22)$$

and

$$R'_g = \frac{g_1^{^3\text{H}}}{\Delta_p g_1^p}. \quad (6.23)$$

In Fig. 6.6 we show both ratios (R_g is the solid line and R'_g is the dashed line) without including the off-shell corrections [49] as well as R_g with the off-shell corrections (dot-dashed line). In this figure we can clearly see that on most of the interval the contribution of the neutron is negligible, some difference appearing for small x . This is expected simply because g_1^n is significantly smaller than g_1^p for most values of x , but starts to grow at small

x in most parametrisations. For the next figure we will concentrate on R'_g . Since this ratio does not depend on the structure function of the neutron it may be more accurately compared with experiment.

In Fig. 6.7 we study the impact of off-shell corrections and Δ isobar corrections on R'_g . On this figure there are three curves. The dotted curve is identical to the dashed one in Fig. 6.6 and does not include any corrections. The dashed line includes the off-shell corrections of Ref. [49] for $0.2 \leq x \leq 0.8$. As one can see, on this curve there is a correction of at least 5% for all x . One can also see that there is also a big drop of R'_g for $x \approx 0.8$. At its lowest point, in this dip we have $R'_g \approx 0.68$. If apply these off-shell corrections for all x this dip is present and we have $R'_g \approx 0.44$ at its lowest point. This dip is almost certainly spurious and may come from the inclusion of the off-shell correction outside its domain of validity. If we limit the off-shell corrections to $0.2 \leq x \leq 0.7$ the dip remains but its lowest point is now $R'_g \approx 0.85$, which is more credible. We also note that we now have a “jump” in R'_g at $x = 0.2$, so the behaviour at small x is not clearly determined as the transition should be smoother. The solid line includes corrections from both off-shell effects and Δ isobar. The Δ isobar has no effects on the dip around $x \approx 0.8$, but it reduces the contribution of off-shell effects for $0.2 \leq x \leq 0.6$. For $x \leq 0.2$ the Δ increases $g_1^{3\text{H}}$ compare to g_1^p , however, as in the case of ^3He one probably needs to take into account some additional physics, such as shadowing and meson exchange currents, in order to get an accurate description of $g_1^{3\text{H}}$.

From Fig. 6.7 we can conclude that any corrections from the nuclear medium can probably be put in evidence in the ratio R'_g at moderate x . In the high x region the behaviour of this ratio is still unclear. The dip observed in Fig. 6.7 can have two origins. One is that off-shell corrections are not properly handled at high x , which is why we tried to reduce the range on which we apply the correction. The second may be a breakdown of the convolution formalism we used for those values. However, if both the convolution formalism and the off-shell corrections hold for values of x as high as 0.8 we would have a very big effect on the ratio that could definitely be measured. In fact even if the off-shell corrections applies to a smaller range of x , a dip may still be spotted – basically because the effects from off-shell corrections act against the effect of Fermi motion³

³In Ref. [71] where the OSC were put by taking the inverse of Eq. (6.5), the effects of OSC goes in the same way as the Fermi motion and thus there is no dip, but the effect is added to the Fermi motion making it seem to start earlier and be bigger.

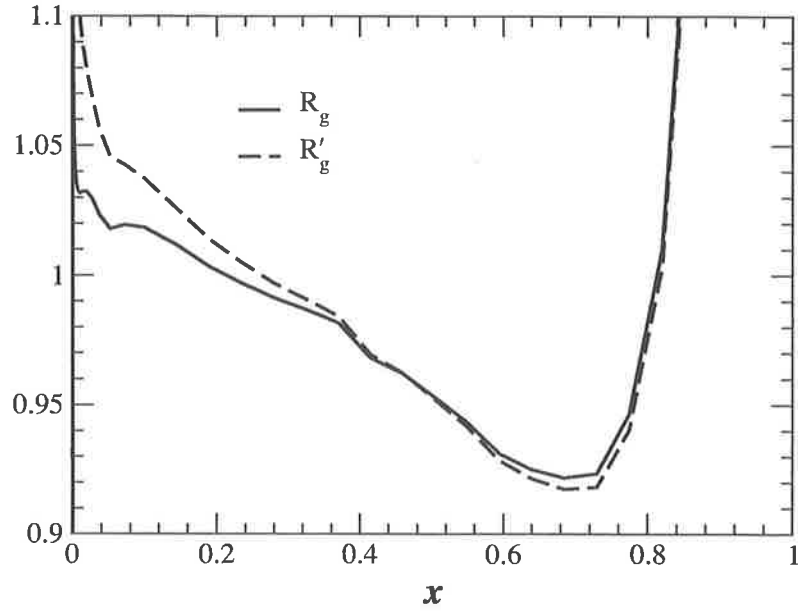


Figure 6.6: The ratio R_g and R'_g of Eqs. (6.22) and (6.23) at 4 GeV^2 , without any off-shell corrections.

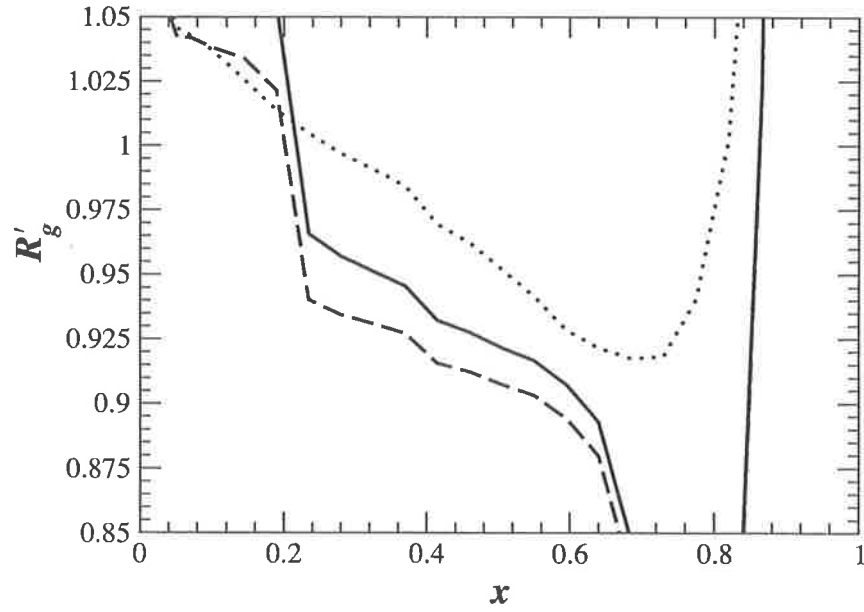


Figure 6.7: The ratio R'_g of Eq. (6.23) at 4 GeV^2 . The dotted line is without off-shell corrections. The dashed line is with off-shell corrections and the solid line include both off-shell corrections and Δ isobar corrections.

Chapter 7

Conclusions

In the first part of this work we have shown how to derive the Faddeev equation and how to write them down in order to be used with a separable potential. We have used these equations to get the wave function of the three nucleon system with several potentials. We compared the figures for the binding energy and the contribution of the different partial waves to the wave function. We have concluded that most realistic potentials under-bind the three nucleon system. This problem may have several origins, such as the lack of a contribution from genuine three-body forces in our computation or from a misrepresentation of the short range behaviour of the two-body potential. However, these kinds of potentials have proved to be able to give a good description of a wide range of phenomena both in the two-nucleon and the three-nucleon sector. While in that chapter we have focused on systems made up of identical particles, this work can be easily extended to systems made of different kinds of particles.

Then, we presented, how from first principles one can write the cross-section of an electromagnetic probe with a nuclear target of spin $1/2$. We pointed out that such a cross-section depends on four nuclear unknowns, the structure functions. We then presented a short derivation of the convolution formalism. This formalism gave us basic tools to link the structure functions of simple objects like the nucleons to the structure functions of more complex objects, made of nucleons, like ^3He and ^3H . During the presentation of this formalism we have carefully enumerated the hypotheses and approximations made in its derivation. This formalism supposes that only one photon exchange occurs and that there is no rescattering. It is known that in the small x region multiple scattering is likely to occur, so the convolution formalism cannot be used to make predictions for small x . It also supposes that there is no interaction between the components of the final state of the reaction. If it is known that such interactions are important then, it is likely to have consequences for the applicability of the formalism.

We moved on to the computation of the fundamental ingredients of the convolution formalism: the light-cone momentum distributions. We have shown how one can compute those quantities from the tri-nucleon wave function we first computed. The light-cone momentum distributions we get from different potentials are very similar, curves computed from the PEST and RSC potentials are very close, while there is some discrepancy between those and the Yamaguchi type of potential. These discrepancies were already present in the computed value of the binding energy of the wave function and it was likely to have an influence on the light-cone momentum distribution. We also studied the figures for the polarisation of the nucleon in ^3He and saw that they were in agreement with the figures given in the literature, with the exception of the polarisation of the proton, which is very slightly

underestimated.

Next, we studied the structure functions of the three nucleon system. We started with the unpolarised structure functions. Using the QPM, we wrote down the expression of the structure functions of the free nucleons in terms of quark distribution. Using the convolution we then computed the unpolarised structure functions of both ^3He and ^3H . We, then, used these results to compute the EMC effect in the three nucleon system (*i.e.* for both ^3He and ^3H). We studied the dependence of the EMC effect to both the potential used and the quark distribution. We found that all the potentials we used give similar results. In fact, we found that our predictions for the EMC effect are more dependent on the quark distributions used than the potential. After computing the EMC effect we evaluated the Gottfried sum rule in the (^3He , ^3H) system. We found, that according to our model, the nuclear medium in the three nucleon system had little effect on the Gottfried sum rule. This implied that the flavour asymmetry of the quark sea in the tri-nucleon system is the same as in the nucleons.

At last, in this chapter we have shown how one can extract the structure function F_2 of the neutron by measuring the EMC effect in both ^3He and ^3H . This work led to a proposal for an experiment at TJNAF [56, 94] to cross check previous results from deuteron experiments and to determine the behaviour of F_2^n at high x . This, in turn, could lead to re-analysis of most current quark distributions which enforce the following behaviour: $d/u \rightarrow 0$ as $x \rightarrow 1$. However, computations from perturbative QCD predict the following behaviour: $d/u \rightarrow 1/5$ as $x \rightarrow 1$. This experiment will help clarify the behaviour of the ratio d/u as x goes towards 1. Our perspective on the behaviour of quark distribution in the limit $x \rightarrow 1$ could be changed completely by this experiment.

After studying the unpolarised structure functions of the three nucleon system we moved to the study of the polarised one. One of the main interests in the study of the polarised structure functions of ^3He , is the extraction of the neutron ones. So, we have analysed the usual formula used to extract g_1^n from $g_1^{^3\text{He}}$ and the effects of the most important corrections that one can make in this extraction. First, the convolution formalism required the use of off-shell structure functions. In this work we have studied the effect of novel off-shell corrections computed with the help of the QMC [49, 50]. We also included the contribution of the resonance $\Delta(1232)$ in the computation of the $g_1^{^3\text{He}}$. This contribution is needed if one wants to recover the Bjorken sum rule in the tri-nucleon system. In the absence of the contribution of the Δ resonance the convolution formalism, with or without the inclusion of off-shell corrections, cannot satisfy this sum rule. We found that the results from the experiments HERMES [52] and E154 [82] were almost not changed

by our corrections except at small x were the applicability of our method is uncertain. This shows that the data extracted from these experiments are quite reliable.

In the last part of this chapter we have shown that one could detect effects of the nuclear medium on the proton in ^3H . As polarised ^3He behaves almost as a polarised neutron, polarised ^3H behaves almost like a polarised proton. However, while in ^3He we must be careful to include the contribution from the proton to $g_1^{^3\text{He}}$, in ^3H we can discard totally the small contribution of the neutron to $g_1^{^3\text{H}}$. So, ^3H is a perfect target to measure effects of the light nuclear medium on the polarised proton structure function. Using the same corrections discussed for ^3He we have shown that for $0.7 \leq x \leq 0.8$ there is a very big discrepancy between results computed with and without off-shell corrections. This shows that measurements of the polarised structure function of ^3H could help us understand the effect of the light nuclear medium on nucleons. Such an experiment, while technically possible at TJNAF, cannot be done safely at the moment. Thus, it constitutes a future test of the QMC.

This work can have several natural extensions. First, as the Faddeev equations can be cast for a system made several kinds of particle, we could explicitly break the isospin symmetry we have used in most of this thesis and use different potential for proton-proton, neutron-proton and neutron-neutron interactions. Some potentials, for example, include the Coulomb corrections in their proton-proton potential. In this work, we neglected the second polarised structure function g_2 . While the study of g_2 is more difficult than the study of g_1 , one can derive a convolution formula for it and study the relationship between g_2 in the tri-nucleon system and g_2 of the free nucleon, and g_2^n in particular.

To extract the structure functions of the neutron, ^3He is not the only choice of target. Of course, deuterium has already been used, and will probably be used again for that purpose. But, some other target like ^6Li , may be used for that purpose as well. In first approximation, ^6Li can be described as an α -particle plus two nucleons (one proton and one neutron) more weakly bound. This system can be described as a three-body system provided that one does not probe the α -particle very deeply. In that case, one can hope that the weakly bound peripheral neutron can give useful information on the free neutron structure functions.

Such a study would re-use the Faddeev equations, for two different kinds of particles this time (α -particle and nucleon), to compute the wave function of ^6Li and the same convolution formalism. If one does not break the α -particle, the final state of the reaction can only be a scattering state (if one nucleon or the α -particle is struck) or a deuteron state (if the α -particle is

struck). This similarly to the case of ^3He . Good care should be taken of the fact that ^6Li is not a spin $1/2$ target but a spin 1 target. However, similar studies have been done on the deuteron which has the same spin, and should be readily usable. A similar study to that performed on $g_1^3\text{H}$ could be done in the hope of finding a clear signature of the effects of nuclear medium on free nucleon, such a study could be done with the help of off-shell corrections computed with the QMC and readily available [49].

Appendix A

The kernel of the homogeneous Faddeev equation

We now review the derivation of the kernel of the homogeneous Faddeev equation, $Z_{\ell_\alpha N_\alpha; \ell_\beta N_\beta}^{JJ}$. We note that the derivation of the permutation term will be very similar. First of all we will use the following notation for the z-projections of the various angular momenta: m_α , m_β and m_γ for the z-projections of j_α , j_β and j_γ ; σ_α for s_α ; \bar{m}_α for \bar{j}_α ; λ_α for ℓ_α ; Λ_α for L_α ; Σ_α for S_α and M for J . If for simplicity we forget isospin and use the notation $\hat{J} = \sqrt{2J+1}$, we have

$$\begin{aligned}
Z_{\ell_\alpha N_\alpha; \ell_\beta N_\beta}^J(p_\alpha, p_\beta, E) &\equiv \langle g_{\ell_\alpha}^{n_\alpha}; \ell_\alpha N_\alpha; p_\alpha | G_0(E) | p_\beta; \ell_\beta N_\beta; g_{\ell_\beta}^{n_\beta} \rangle \\
&= \frac{1}{\hat{J}^2} \sum_{\substack{\text{all} \\ \text{z-projections}}} \langle j_\beta m_\beta j_\gamma m_\gamma | s_\alpha \sigma_\alpha \rangle \langle j_\gamma m_\gamma j_\alpha m_\alpha | s_\beta \sigma_\beta \rangle \\
&\quad \times \langle \ell_\alpha \lambda_\alpha s_\alpha \sigma_\alpha | \bar{j}_\alpha \bar{m}_\alpha \rangle \langle \ell_\beta \lambda_\beta s_\beta \sigma_\beta | \bar{j}_\beta \bar{m}_\beta \rangle \\
&\quad \times \langle \bar{j}_\alpha \bar{m}_\alpha j_\alpha m_\alpha | S_\alpha \Sigma_\alpha \rangle \langle \bar{j}_\beta \bar{m}_\beta j_\beta m_\beta | S_\beta \Sigma_\beta \rangle \\
&\quad \times \langle L_\alpha \Lambda_\alpha S_\alpha \Sigma_\alpha | J M \rangle \langle L_\beta \Lambda_\beta S_\beta \Sigma_\beta | J M \rangle \\
&\quad \times \langle g_{\ell_\alpha}^{n_\alpha}; \mathcal{Y}_{\ell_\alpha \lambda_\alpha}; \mathcal{Y}_{L_\alpha \Lambda_\alpha}; p_\alpha | G_0(E) | p_\beta; \mathcal{Y}_{\ell_\beta \lambda_\beta}; \mathcal{Y}_{L_\beta \Lambda_\beta}; g_{\ell_\beta}^{n_\beta} \rangle.
\end{aligned} \tag{A.1}$$

The last term in Eq. (A.1) is given by

$$\begin{aligned}
\mathcal{G} &= \langle g_{\ell_\alpha}^{n_\alpha}; \mathcal{Y}_{\ell_\alpha \lambda_\alpha}; \mathcal{Y}_{L_\alpha \Lambda_\alpha}; p_\alpha | G_0(E) | p_\beta; \mathcal{Y}_{\ell_\beta \lambda_\beta}; \mathcal{Y}_{L_\beta \Lambda_\beta}; g_{\ell_\beta}^{n_\beta} \rangle \\
&= \int d^3 \vec{p}'_\alpha d^3 \vec{q}'_\alpha d^3 \vec{p}'_\beta d^3 \vec{q}'_\beta \mathcal{Y}_{\ell_\alpha \lambda_\alpha}(\hat{q}_\alpha) \mathcal{Y}_{L_\alpha \Lambda_\alpha}(\hat{p}'_\alpha) \mathcal{Y}_{\ell_\beta \lambda_\beta}^*(\hat{q}_\beta) \mathcal{Y}_{L_\beta \Lambda_\beta}^*(\hat{p}'_\beta) \\
&\quad \times \frac{g_{\ell_\beta}^{n_\beta \dagger}(q_\beta) g_{\ell_\alpha}^{n_\alpha}(q_\alpha)}{E - \frac{p_\alpha'^2}{2m} - \frac{p_\beta'^2}{2m} - \frac{(\vec{p}'_\alpha + \vec{p}'_\beta)^2}{2m}} \frac{\delta(p'_\alpha - p_\alpha)}{p_\alpha^2} \frac{\delta(p'_\beta - p_\beta)}{p_\beta^2} \\
&\quad \times \delta^3(\vec{q}_\alpha - (\vec{p}'_\beta + \rho_\alpha \vec{p}'_\alpha)) \delta^3(\vec{q}_\beta - (-\vec{p}'_\alpha - \rho_\beta \vec{p}'_\beta)).
\end{aligned} \tag{A.2}$$

In the last equation the integrals are only on \hat{p}'_α and \hat{p}'_β . \vec{q}_α and \vec{q}_β are completely determined once we know \vec{p}'_α and \vec{p}'_β , as shown by the delta functions present in the integral. For a system of particles with identical masses we have $\rho_\alpha = \rho_\beta = 1/2$ in Eq. (A.2). Since \hat{p}'_α and \hat{p}'_β are the only indepent variables in Eq. (A.2), one needs to express every components of the integral in terms of them. The spherical harmonics in \hat{q}_α and \hat{q}_β can be expressed in terms of \hat{p}'_α and \hat{p}'_β using the following [1]

$$\begin{aligned}
p^\ell \mathcal{Y}_{\ell m}(\hat{p}) &= \sum_{\substack{ab \\ m_a m_b}} \delta_{\ell, a+b} \sqrt{\frac{4\pi(2\ell+1)!}{(2a+1)!(2b+1)!}} \langle a m_a b m_b | \ell m \rangle \\
&\quad \times (\alpha q)^a \mathcal{Y}_{a m_a}(\hat{q}) (\beta r)^b \mathcal{Y}_{b m_b}(\hat{r}),
\end{aligned} \tag{A.3}$$

with $\vec{p} = \alpha\vec{q} + \beta\vec{r}$. To completely eliminate the dependence on \hat{q}_α and \hat{q}_β of \mathcal{G} , one needs to expand the products of the Green's function with the form factors in terms of spherical harmonics in \hat{p}'_α and \hat{p}'_β . That is

$$\frac{q_\beta^{-\ell_\beta} g_{\ell_\beta}^{n_\beta \dagger}(q_\beta) g_{\ell_\alpha}^{n_\alpha}(q_\alpha) q_\alpha^{-\ell_\alpha}}{E - \frac{p_\alpha^2}{2m} - \frac{p_\beta^2}{2m} - \frac{(\vec{p}'_\alpha + \vec{p}'_\beta)^2}{2m}} = 4\pi \sum_{\mathcal{L}M_\mathcal{L}} F_{n_\alpha, n_\beta}^{\mathcal{L}, \ell_\alpha, \ell_\beta}(p_\alpha, p_\beta, E) \mathcal{Y}_{\mathcal{L}M_\mathcal{L}}^*(\hat{p}'_\beta) \mathcal{Y}_{\mathcal{L}M_\mathcal{L}}(\hat{p}'_\alpha), \quad (\text{A.4})$$

with

$$F_{n_\alpha, n_\beta}^{\mathcal{L}, \ell_\alpha, \ell_\beta}(p_\alpha, p_\beta, E) = \frac{1}{2} \int_{-1}^{+1} dx \frac{q_\beta^{-\ell_\beta} g_{\ell_\beta}^{n_\beta \dagger}(q_\beta) g_{\ell_\alpha}^{n_\alpha}(q_\alpha) q_\alpha^{-\ell_\alpha}}{E - \frac{p_\alpha^2}{2m} - \frac{p_\beta^2}{2m} - \frac{(\vec{p}'_\alpha + \vec{p}'_\beta)^2}{2m}} P_\mathcal{L}(x), \quad (\text{A.5})$$

where $P_\mathcal{L}$ is the Legendre polynomial of order \mathcal{L} and $x = \hat{p}'_\alpha \cdot \hat{p}'_\beta$. Using all the previous equations leads to an expression for \mathcal{G} that contains 4 spherical harmonics in both \hat{p}'_α and \hat{p}'_β . Those can be reduced, using the following formula [2, 3]

$$\mathcal{Y}_{\ell_1 m_1}(\hat{p}) \mathcal{Y}_{\ell_2 m_2}(\hat{p}) = \sum_{\ell, m} \sqrt{\frac{(2\ell_1 + 1)(2\ell_2 + 1)(2\ell + 1)}{4\pi}} \times \begin{pmatrix} \ell_1 & \ell_2 & \ell \\ m_1 & m_2 & m \end{pmatrix} \begin{pmatrix} \ell_1 & \ell_2 & \ell \\ 0 & 0 & 0 \end{pmatrix} \mathcal{Y}_{\ell m}^*(\hat{p}), \quad (\text{A.6})$$

to a product of two spherical harmonics in each variable, for which we can use standard orthogonality relation between spherical harmonics. The result involves several vector coupling coefficients and 3-j symbols. Summing over some z-projections with the help of Eqs. (2.20) and (3.21) of Ref [2] one finds:

$$\begin{aligned} \mathcal{G} = & (-1)^{\ell_\alpha + \lambda_\alpha + \Lambda_\alpha} \hat{\ell}_\alpha \hat{\ell}_\beta \hat{L}_\alpha \hat{L}_\beta \sum_{\mathcal{L}} (-1)^\mathcal{L} \hat{\mathcal{L}}^2 F_{n_\alpha, n_\beta}^{\mathcal{L}, \ell_\alpha, \ell_\beta}(p_\alpha, p_\beta, E) \\ & \times \sum_{aa'bb'} \delta_{\ell_\alpha, a+b} \delta_{\ell_\beta, a'+b'} \rho_\alpha^a \rho_\beta^{b'} p_\alpha^{a+a'} p_\beta^{b+b'} \sqrt{\frac{(2\ell_\alpha + 1)!(2\ell_\beta + 1)!}{(2a)!(2b)!(2a')!(2b')!}} \\ & \times \sum_{\Lambda\Lambda'f} (\hat{f}\hat{\Lambda}\hat{\Lambda}')^2 \begin{pmatrix} a & a' & \Lambda \\ 0 & 0 & 0 \end{pmatrix} \begin{pmatrix} b & b' & \Lambda' \\ 0 & 0 & 0 \end{pmatrix} \begin{pmatrix} \Lambda & \mathcal{L} & L_\alpha \\ 0 & 0 & 0 \end{pmatrix} \begin{pmatrix} \Lambda' & \mathcal{L} & L_\beta \\ 0 & 0 & 0 \end{pmatrix} \\ & \times \left\{ \begin{matrix} L_\alpha & L_\beta & f \\ \Lambda' & \Lambda & \mathcal{L} \end{matrix} \right\} \left\{ \begin{matrix} \ell_\alpha & \ell_\beta & f \\ a & a' & \Lambda \end{matrix} \right\} \sum_{m_f} \begin{pmatrix} \ell_\alpha & \ell_\beta & f \\ -\lambda_\alpha & \lambda_\beta & m_f \end{pmatrix} \begin{pmatrix} L_\alpha & L_\beta & f \\ \Lambda_\alpha & -\Lambda_\beta & m_f \end{pmatrix}. \quad (\text{A.7}) \end{aligned}$$

Going back to the expression for the kernel one can replace all Clebsch-Gordan coefficients by 3-j symbols¹ and then use the following relations to simplify the expression:

$$\begin{aligned} \sum_{\Lambda_\alpha \Lambda_\beta M} (-1)^{\Lambda_\beta - 2M} \begin{pmatrix} L_\alpha & L_\beta & f \\ \Lambda_\alpha & -\Lambda_\beta & m_f \end{pmatrix} \begin{pmatrix} L_\alpha & S_\alpha & J \\ \Lambda_\alpha & \Sigma_\alpha & -M \end{pmatrix} \begin{pmatrix} L_\beta & S_\beta & J \\ \Lambda_\beta & \Sigma_\beta & -M \end{pmatrix} \\ = (-1)^{J-f+\Sigma_\alpha} \begin{pmatrix} S_\alpha & S_\beta & f \\ -\Sigma_\alpha & \Sigma_\beta & m_f \end{pmatrix} \left\{ \begin{matrix} S_\alpha & S_\beta & f \\ L_\beta & L_\alpha & J \end{matrix} \right\}, \quad (\text{A.8}) \end{aligned}$$

and

$$\begin{aligned} \sum_{\substack{\text{all} \\ \text{z-projections}}} (-1)^{-\Sigma_\alpha - \bar{m}_\alpha - \bar{m}_\beta - \sigma_\alpha - \sigma_\beta + \lambda_\alpha} \begin{pmatrix} S_\alpha & S_\beta & f \\ -\Sigma_\alpha & \Sigma_\beta & m_f \end{pmatrix} \begin{pmatrix} \ell_\alpha & \ell_\beta & f \\ -\lambda_\alpha & \lambda_\beta & m_f \end{pmatrix} \\ \times \begin{pmatrix} \bar{j}_\alpha & j_\alpha & S_\alpha \\ \bar{m}_\alpha & m_\alpha & -\Sigma_\alpha \end{pmatrix} \begin{pmatrix} \bar{j}_\beta & j_\beta & S_\beta \\ \bar{m}_\beta & m_\beta & -\Sigma_\beta \end{pmatrix} \begin{pmatrix} \ell_\alpha & s_\alpha & \bar{j}_\alpha \\ \lambda_\alpha & \sigma_\alpha & -\bar{m}_\alpha \end{pmatrix} \begin{pmatrix} \ell_\beta & s_\beta & \bar{j}_\beta \\ \lambda_\beta & \sigma_\beta & -\bar{m}_\beta \end{pmatrix} \\ \times \begin{pmatrix} j_\beta & j_\gamma & s_\alpha \\ m_\beta & m_\gamma & -\sigma_\alpha \end{pmatrix} \begin{pmatrix} j_\gamma & j_\alpha & s_\beta \\ m_\gamma & m_\alpha & -\sigma_\beta \end{pmatrix} \\ = (-1)^{2f+2S_\beta+2\ell_\alpha+2\bar{j}_\beta-s_\alpha+2s_\beta-j_\alpha+2j_\beta} \left\{ \begin{matrix} j_\alpha & S_\alpha & S_\beta & j_\beta \\ \bar{j}_\alpha & f & \bar{j}_\beta & j_\gamma \\ s_\alpha & \ell_\alpha & \ell_\beta & s_\beta \end{matrix} \right\}, \quad (\text{A.9}) \end{aligned}$$

where the 12-j symbol is defined by Ord-Smith[58]. One can find these relations using the diagrammatic procedures of Ref. [4]. In the end the kernel can be expressed in the following way:

$$\begin{aligned} Z_{\ell_\alpha N_\alpha; \ell_\beta N_\beta}^{JI} &\equiv \langle g_{\ell'_\alpha}^{n_\alpha}; \Omega_{\ell'_\alpha N_\alpha}^{JI} | G_0(E) | \Omega_{\ell_\beta N_\beta}^{JI}; g_{\ell_\beta}^{n_\beta} \rangle \\ &= p_\beta^{\ell_\alpha} p_\alpha^{\ell_\beta} B_{N_\alpha N_\beta} \sum_{\mathcal{L}} F_{n_\alpha, n_\beta}^{\mathcal{L} \ell_\alpha \ell_\beta}(p_\alpha, p_\beta, E) \sum_{a=0}^{l_\alpha} \sum_{b=0}^{l_\beta} A_{\ell_\alpha N_\alpha; \ell_\beta N_\beta}^{\mathcal{L}, a, b} \left(\frac{p_\alpha}{p_\beta} \right)^{a-b}. \end{aligned} \quad (\text{A.10})$$

The coefficients $A_{\ell_\alpha N_\alpha; \ell_\beta N_\beta}^{\mathcal{L}, a, b}$ which result from the recoupling of the spin and

¹We have the following relation between Clebsch-Gordan and 3-j symbol:
 $\langle j_1 m_1 j_2 m_2 | j m \rangle = (-1)^{-j_1+j_2-m} \sqrt{2j+1} \begin{pmatrix} j_1 & j_2 & j \\ m_1 & m_2 & -m \end{pmatrix}.$

orbital angular momentum are given by

$$\begin{aligned}
A_{\ell_\alpha N_\alpha; \ell_\beta N_\beta}^{\mathcal{L}, a, b} &= (-1)^R \hat{\ell}_\alpha \hat{\ell}_\beta \hat{L}_\alpha \hat{L}_\beta \hat{S}_\alpha \hat{S}_\beta \hat{J}_\alpha \hat{J}_\beta \hat{s}_\alpha \hat{s}_\beta \hat{\mathcal{L}}^2 \rho_\alpha^a \rho_\beta^b \\
&\times \sqrt{\frac{(2\ell_\alpha+1)!(2\ell_\beta+1)!}{(2a)!(2b)!(2\ell_\alpha-2a)!(2\ell_\beta-2b)!}} \\
&\times \sum_{f\Lambda\Lambda'} \left(\hat{f} \hat{\Lambda} \hat{\Lambda}' \right)^2 \begin{Bmatrix} S_\alpha & S_\beta & f \\ L_\beta & L_\alpha & J \end{Bmatrix} \begin{Bmatrix} L_\alpha & L_\beta & f \\ \Lambda' & \Lambda & \mathcal{L} \end{Bmatrix} \\
&\times \begin{Bmatrix} j_\alpha & S_\alpha & S_\beta & j_\beta \\ \bar{j}_\alpha & f & \bar{j}_\beta & j_\gamma \\ s_\alpha & \ell_\alpha & \ell_\beta & s_\beta \end{Bmatrix} \begin{Bmatrix} \ell_\alpha & \ell_\beta & f \\ a & \ell_\beta - b & \Lambda \\ \ell_\alpha - a & b & \Lambda' \end{Bmatrix} \\
&\times \begin{pmatrix} a & \ell_\beta - b & \Lambda \\ 0 & 0 & 0 \end{pmatrix} \begin{pmatrix} \Lambda' & \mathcal{L} & L_\beta \\ 0 & 0 & 0 \end{pmatrix} \begin{pmatrix} \Lambda & \mathcal{L} & L_\alpha \\ 0 & 0 & 0 \end{pmatrix} \begin{pmatrix} \ell_\alpha - a & b & \Lambda' \\ 0 & 0 & 0 \end{pmatrix},
\end{aligned} \tag{A.11}$$

with the phase R defined as

$$R = -J + L_\alpha + L_\beta + S_\alpha + S_\beta + \bar{j}_\alpha + \bar{j}_\beta - j_\alpha + s_\beta + \ell_\alpha + \mathcal{L}. \tag{A.12}$$

Finally, the isospin recoupling coefficient $B_{N_\alpha N_\beta}$ is given in terms of a 6-j symbol by the relation

$$B_{N_\alpha N_\beta} = (-1)^{i_\alpha + i_\gamma - \bar{i}_\beta + 2I} \hat{i}_\alpha \hat{i}_\beta \begin{Bmatrix} i_\beta & i_\gamma & \bar{i}_\alpha \\ i_\alpha & I & \bar{i}_\beta \end{Bmatrix}. \tag{A.13}$$

Appendix B

The permutation term

This section is devoted to the extraction of the form of Eq. (2.23). We call it the permutation term because it originates from Eq. (2.1). Its derivation has a lot of similarities with the derivation of the kernel. The contribution of a given channel ($\ell_\beta N_\beta$) to a given channel ($\ell_\alpha N_\alpha$) can be written as the sum over all z-projections over the same series of clebsch-gordan. Only the term we called \mathcal{G} in the previous section will be different. For this reason we will call it \mathcal{G}' . We have

$$\begin{aligned}
\mathcal{G}' &= \langle \mathcal{Y}_{\ell_\alpha \lambda_\alpha}; \mathcal{Y}_{L_\alpha \Lambda_\alpha}; p_\alpha q_\alpha | \mathcal{Y}_{\ell_\beta \lambda_\beta}; \mathcal{Y}_{L_\beta \Lambda_\beta}; \eta_{\ell_\beta N_\beta}^{JI1} \rangle \\
&= \int d^3 \vec{p}'_\alpha d^3 \vec{q}'_\alpha d^3 \vec{p}_\beta d^3 \vec{q}_\beta \mathcal{Y}_{\ell_\alpha \lambda_\alpha}(\vec{q}'_\alpha) \mathcal{Y}_{L_\alpha \Lambda_\alpha}(\vec{p}'_\alpha) \mathcal{Y}_{\ell_\beta \lambda_\beta}^*(\vec{q}_\beta) \mathcal{Y}_{L_\beta \Lambda_\beta}^*(\vec{p}_\beta) \\
&\quad \times \eta_{\ell_\beta N_\beta}^{JI1}(p_\beta, q_\beta) \frac{\delta(p'_\alpha - p_\alpha)}{p_\alpha^2} \frac{\delta(q'_\alpha - q_\alpha)}{q_\alpha^2} \\
&\quad \times \delta^3(\vec{p}_\beta - (\vec{q}'_\alpha - \varrho_\alpha \vec{p}'_\alpha)) \delta^3(\vec{q}_\beta - (-\varrho_\beta \vec{q}'_\alpha - \varrho_\gamma \vec{p}'_\alpha)), \tag{B.1}
\end{aligned}$$

with $\varrho_\alpha = 1/2$, $\varrho_\beta = 1/2$ and $\varrho_\gamma = 3/4$, for a system of particles with identical masses. Here the integral is really only on \vec{p}'_α and \vec{q}'_α , the same way that the integral in Eq. (A.2) depends only on \vec{p}'_α and \vec{p}'_β . However we can use the delta function in Eq. (B.1) to make it an integral over \vec{p}'_α and \vec{p}_β instead. The advantage being that we can reuse our derivation of the kernel to express the permutation term. The only significative difference will be in the expression of the coefficient F given by Eq. (A.5). What we want to express as an expansion in spherical harmonics here, is

$$\begin{aligned}
\int dp_\beta \left(\frac{p_\beta}{q_\alpha} \right)^2 \frac{p_\beta^{\ell_\alpha + b - a}}{q_\alpha^{\ell_\alpha} q_\beta^{\ell_\beta}} \eta_{\ell_\beta N_\beta}^{JI1}(p_\beta, q_\beta) \delta(q'_\alpha - q_\alpha) = \\
4\pi \sum_{\mathcal{L} M_\mathcal{L}} Q_{\ell_\beta N_\beta; \ell_\alpha}^{\mathcal{L}, a, b}(p_\alpha, q_\alpha) \mathcal{Y}_{\mathcal{L} M_\mathcal{L}}(\vec{p}'_\alpha) \mathcal{Y}_{\mathcal{L} M_\mathcal{L}}^*(\vec{p}_\beta), \tag{B.2}
\end{aligned}$$

where we have

$$\begin{aligned}
Q_{\ell_\beta N_\beta; \ell_\alpha}^{\mathcal{L}, a, b}(p_\alpha, q_\alpha) = \\
\int_{-1}^{+1} dx \int dp_\beta \left(\frac{p_\beta}{q_\alpha} \right)^2 \frac{p_\beta^{\ell_\alpha + b - a}}{q_\alpha^{\ell_\alpha} q_\beta^{\ell_\beta}} \eta_{\ell_\beta N_\beta}^{JI1}(p_\beta, q_\beta) \delta(q'_\alpha - q_\alpha) P_\mathcal{L}(x), \tag{B.3}
\end{aligned}$$

where $x = \vec{p}'_\alpha \cdot \vec{p}_\beta$. We have to put the integral on p_β in the coefficient because p_β is dependent on x through the delta function $\delta(q'_\alpha - q_\alpha)$. From the integral on \vec{q}'_α and \vec{q}_β we have $\vec{q}'_\alpha = \vec{p}_\beta + \varrho_\alpha \vec{p}'_\alpha$ (see Eq. (A.2)). Therefore we have

$q'_\alpha = \sqrt{p_\beta^2 + \rho_\alpha^2 p_\alpha'^2 + 2\rho_\alpha x p'_\alpha p_\beta}$ and p_β is dependent on x and q_α . So one can finally write the equivalent of Eq. (A.7) for \mathcal{G}'

$$\begin{aligned}
\mathcal{G}' = & (-1)^{\ell_\alpha + \lambda_\alpha + \Lambda_\alpha} \hat{\ell}_\alpha \hat{\ell}_\beta \hat{L}_\alpha \hat{L}_\beta \sum_{\mathcal{L}} (-1)^{\mathcal{L}} \hat{\mathcal{L}}^2 \sum_{a=0}^{\ell_\alpha} \sum_{b=0}^{\ell_\beta} \\
& \times Q_{\ell_\beta N_\beta; \ell_\alpha}^{\mathcal{L}, a, b}(p_\alpha, q_\alpha) \rho_\alpha^a \rho_\beta^b p_\alpha^{\ell_\alpha + a - b} \sqrt{\frac{(2\ell_\alpha + 1)!(2\ell_\beta + 1)!}{(2a)!(2b)!(2\ell_\alpha - 2a)!(2\ell_\beta - 2b)!}} \\
& \times \sum_{\Lambda \Lambda' f} \left(\hat{f} \hat{\Lambda} \hat{\Lambda}' \right)^2 \begin{pmatrix} a & \ell_\beta - b & \Lambda \\ 0 & 0 & 0 \end{pmatrix} \begin{pmatrix} \ell_\alpha - a & b & \Lambda' \\ 0 & 0 & 0 \end{pmatrix} \begin{pmatrix} \Lambda & \mathcal{L} & L_\alpha \\ 0 & 0 & 0 \end{pmatrix} \begin{pmatrix} \Lambda' & \mathcal{L} & L_\beta \\ 0 & 0 & 0 \end{pmatrix} \\
& \times \left\{ \begin{matrix} L_\alpha & L_\beta & f \\ \Lambda' & \Lambda & \mathcal{L} \end{matrix} \right\} \left\{ \begin{matrix} \ell_\alpha & \ell_\beta & f \\ a & \ell_\beta - b & \Lambda \\ \ell_\alpha - a & b & \Lambda' \end{matrix} \right\} \sum_{m_f} \begin{pmatrix} \ell_\alpha & \ell_\beta & f \\ -\lambda_\alpha & \lambda_\beta & m_f \end{pmatrix} \begin{pmatrix} L_\alpha & L_\beta & f \\ \Lambda_\alpha & -\Lambda_\beta & m_f \end{pmatrix}. \quad (\text{B.4})
\end{aligned}$$

Finally using the same formula as in appendix A, one can write the permutation term

$$\langle p_\alpha q_\alpha; \Omega_{\ell_\alpha N_\alpha}^{JI} | \Omega_{\ell_\beta N_\beta}^{JI} \rangle | \eta_{\ell_\beta N_\beta}^{JI1} \rangle = p_\alpha^{\ell_\alpha} B_{N_\alpha N_\beta} \sum_{\mathcal{L}} \sum_{a=0}^{\ell_\alpha} \sum_{b=0}^{\ell_\beta} p_\alpha^{a-b} Q_{\ell_\beta N_\beta; \ell_\alpha}^{\mathcal{L}, a, b} A_{\ell_\alpha N_\alpha; \ell_\beta N_\beta}^{\mathcal{L}, a, b}, \quad (\text{B.5})$$

where the coefficients $A_{\ell_\alpha N_\alpha; \ell_\beta N_\beta}^{\mathcal{L}, a, b}$ and $B_{N_\alpha N_\beta}$ are given by Eqs. (A.11) and (A.13).

Bibliography

- [1] M. Moshinsky, Nucl. Phys. **13**,104 (1959).
- [2] M. Rotenberg, R. Bivins, N. Metropolis and J. K. Wooten, Jr : *The 3-j and 6-j symbols* (The Technology Press, MIT 1959).
- [3] A. J. Edmonds : *Angular momentum in Quantum Mechanics* (Princeton University Press 1957).
- [4] A. P. Yutsis, I. B. Levinson, V. V. Vanagas : *Mathematical Apparatus of the Theory of Angular Momentum* (Israel Program for Scientific Translations, Jerusalem 1962).
- [5] J. Haidenbauer and W. Plessas, Phys. Rev. **C 30**, 1822 (1984); *ibid.* **C 32**, 1424 (1985).
- [6] M. Lacombe, B. Loiseau, J. M. Richard, R. Vinh Mau, J. Côté, P. Pirès, and R. de Tournell, Phys. Rev. **C 21**, 861 (1980).
- [7] W. C. Parke, Y. Koike, D. R. Lehman and L. C. Maximon, Few Body Syst. **11**, 89 (1991).
- [8] T. Y. Saito and I. R. Afnan, Phys. Rev. **C 50**, 2756 (1994); Few Body Syst. **18**, 101 (1995).
- [9] I. R. Afnan and J. M. Read, Aust. J. Phys. **26** 725 (1973); Phys. Rev. **C 8**,1294 (1973).
- [10] R. V. Reid, Ann. Phys. (N.Y.) **50**, 411 (1968).
- [11] Y. Yamaguchi and Y. Yamaguchi, Phys. Rev. **95**, 1635 (1954).
- [12] I. R. Afnan and A. W. Thomas: "Fundamentals of Three-Body Scattering Theory" in *Modern Three-Hadron Physics*, ed. A. W. Thomas (Springer-Verlag, Berlin Heidelberg New York, 1977).
- [13] C. Lovelace, Phys. Rev. **135B**, 1225 (1964).
- [14] I. R. Afnan and N. D. Birrell, Phys. Rev. **C 16**, 823 (1977).
- [15] R. Machleidt, F. Sammarruca and Y. Song, Phys. Rev. **C 53**, 1483 (1996) [nucl-th/9510023].
- [16] B. F. Gibson, Nucl. Phys. **A 543**, 1e (1992); M. T. Peña, P. U. Sauer, A. Stalder and G. Gortemeyer, Phys. Rev. **C 48**, 2208 (1993); S. A. Coon and M. T. Peña, Phys. Rev. **C 48**, 2559 (1993); T. Y. Saito and J. Haidenbauer, Eur. Phys. J **A 7**,559 (2000).

- [17] D. F. Geesaman, K. Saito and A. W. Thomas, *Ann. Rev. Nucl. Part. Sci.* **45**, 337 (1995).
- [18] B. Lampe and E. Reya, *Phys. Rept.* **332**, 1 (2000).
- [19] M. Anselmino, A. Efremov and E. Leader, *Phys. Rept.* **261**, 1 (1995).
- [20] R. -W. Schulze and P. U. Sauer, *Phys. Rev. C* **48**, 38 (1993).
- [21] R. -W. Schulze and P. U. Sauer, *Phys. Rev. C* **56**, 2293 (1997).
- [22] L. Heller and A. W. Thomas, *Phys. Rev. C* **41**, 2756 (1990).
- [23] H. Meier-Hadjuk, U. Oelfke and P. U. Sauer, *Nucl. Phys. A* **499**, 637 (1989).
- [24] U. Oelfke, P. U. Sauer and F. Coester, *Nucl. Phys. A* **518**, 593 (1990).
- [25] T. Uchiyama and K. Saito, *Phys. Rev. C* **38**, 2245 (1988).
- [26] L. L. Frankfurt and M. I. Strikman, *Phys. Lett. B* **64**, 433 (1976); *Phys. Lett. B* **65**, 51 (1976); *Phys. Lett. B* **76**, 333 (1978) ; *Nucl. Phys. B* **148**, 107; *Phys. Rept.* **76**, 215 (1981).
- [27] H-M. Jung and G. A. Miller, *Phys. Lett. B* **200**, 351 (1988).
- [28] C. Ciofi degli Atti and S. Liuti, *Phys. Rev. C* **41**, 1100 (1990).
- [29] C. Ciofi degli Atti, E. Pace and G. Salmè, *Phys. Lett* **141B**, 14 (1984).
- [30] S. Frullani and J. Mougey, *Adv. in Nucl. Phys.* **14**, 1 (1984).
- [31] A. E. L. Dieperink and T. de Forest Jr., *Ann. Rev. Nucl. Sc.* **25**, 1 (1975).
- [32] J. L. Friar, B. F. Gibson and G. L. Payne, *Phys. Rev. C* **37**, 2869 (1988).
- [33] J. L. Friar, B. F. Gibson, G. L. Payne, A. M. Bernstein and T. E. Chupp, *Phys. Rev. C* **42**, 2310 (1990).
- [34] A. W. Thomas, *Phys. Lett. B* **126**, 97 (1983).
- [35] R. D. Field and R. P. Feynman, *Phys. Rev. D* **15**, 2590 (1977).
- [36] A. I. Signal and A. W. Thomas, *Phys. Rev. D* **40**, 2832 (1989).
- [37] H. L. Lai et al., *Eur. Phys. J. C* **12**, 375 (2000).

- [38] New Muon Collaboration, M. Arnadeo et al., Phys. Rev. **D 50**, R1 (1994).
- [39] FNAL E866/NuSea Collaboration, J. C. Peng et al, Phys. Rev. **D 58**, 092004 (1998).
- [40] A. Kievsky, E. Pace, G. Salme and M. Viviani, Phys. Rev. **C 56**, 64 (1997) [nucl-th/9704050].
- [41] C. Ciofi degli Atti, E. Pace and G. Salme, Phys. Rev. **C 51**, 1108 (1995) [nucl-th/9411006].
- [42] J. J. Aubert *et al.*, Phys. Lett. **123B**, 275 (1983).
- [43] M. Glück, E. Reya and A. Vogt, Z. Phys. **C 67**, 433 (1995).
- [44] A. Donnachie and P. V. Landshoff, Z. Phys. **C 61**, 139 (1994).
- [45] J. T. Londergan and A. W. Thomas, Prog. Part. Nucl. Phys. **41**, 49 (1998).
- [46] R. M. Woloshyn, Nucl. Phys. **A 496**, 749 (1989); B. Blankleider and R. M. Woloshyn, Phys. Rev. **C 29**, 538 (1984).
- [47] Y. Goto *et al.* [Asymmetry Analysis collaboration], Phys. Rev. **D 62**, 034017 (2000) [hep-ph/0001046].
- [48] M. Glück, E. Reya, M. Stratmann and W. Vogelsang, Phys. Rev. **D 53**, 4775 (1996).
- [49] F. M. Steffens, K. Tsushima, A. W. Thomas and K. Saito, Phys. Lett. **B 447**, 233 (1999).
- [50] P. A. M. Guichon, K. Saito, E. Rodionov and A. W. Thomas, Nucl. Phys. **A601**, 349 (1996) [nucl-th/9509034]; K. Saito and A. W. Thomas, Phys. Rev. **C 51**, 2757 (1995) [nucl-th/9410031]; P. A. Guichon, Phys. Lett. **B 200**, 235 (1988).
- [51] P. L. Anthony *et al.* [E142 Collaboration], Phys. Rev. **D 54**, 6620 (1996) [hep-ex/9610007].
- [52] K. Ackerstaff *et al.* [HERMES Collaboration], Phys. Lett. **B 404**, 383 (1997) [hep-ex/9703005].
- [53] C. Ciofi degli Atti, S. Scopetta, E. Pace and G. Salme, Phys. Rev. **C 48**, 968 (1993) [nucl-th/9303016].

- [54] T. Gherman and W. J. Stirling, Z. Phys. **C 65**, 461 (1995).
- [55] I. R. Afnan *et al.*, Phys. Lett. **B 493**, 36 (2000) [nucl-th/0006003].
- [56] G. G. Petratos *et al.*, Jefferson Lab proposal (July 2000)
- [57] E. Pace, G. Salme and S. Scopetta, Nucl. Phys. **A 689**, 453 (2001).
- [58] R. J. Ord-Smith, Phys. Rev. **94**, 1227 (1954).
- [59] R. G. Roberts: *The structure of the proton* (Cambridge University Press, 1990).
- [60] R. L. Jaffe: "Deep inelastic scattering with application to nuclear targets", in *Los Alamos School on Relativistic Dynamics and Quark-Nuclear Physics*, ed. M. B. Jackson and A. Picklesimer (Jhon Wiley and Sons, New York, 1985).
- [61] P. V. Landshoff and J. C. Polkinghorne, Phys. Rep. **5c**, 1 (1972).
- [62] C. G. Callan and D. J. Gross, Phys. Rev. Lett. **22**, 156 (1969).
- [63] G. B. West, Phys. Lett. **37B**, 509 (1971); W. B. Atwood and G. B. West, Phys. Rev. **D 7**, 773 (1973).
- [64] L. P. Kaptari, A. Yu. Umnikov, Phys. Lett. **B 259**, 155 (1991); M. A. Braun, M. V. Tokarev, Phys. Lett. **B 320**, 381 (1994).
- [65] W. Melnitchouck, A. W. Schreiber and A. W. Thomas, Phys. Lett. **B 335**, 11 (1994).
- [66] W. Melnitchouck and A. W. Thomas, Phys. Lett. **B 377**, 11 (1996).
- [67] K. Abe *et al*, Phys. Rev **D 58**, 112003 (1998).
- [68] P. L. Anthony *et al.*, Phys. Lett. **B 463**, 339 (1999).
- [69] R. L. Jaffe, Nucl. Phys. **19**, 239 (1990).
- [70] M. Glück, E. Reya, M. Stratmann and W. Vogelsang, Phys. Rev. **D 63**, 094005 (2001).
- [71] I. R. Afnan, F. Bissey and A. W. Thomas, Phys. Rev. **C 64**, 024004 (2001).
- [72] L. Frankfurt, V. Guzey and M. Strickman, Phys. Lett. **B 381**, 379 (1996).

- [73] J. D. Bjorken, Phys. Rev. **148**, 1467 (1966).
- [74] Particle Data Group, C. Caso *et al.*, Eur. Phys. J. **C 3**, 1 (1998).
- [75] B. Budick, J. Chen and H. Lin, Phys. Rev. Lett. **67**, 2630 (1991).
- [76] S. J. Brodsky, M. Burkardt and I. Schmidt, Nucl. Phys. **B 441**, 197 (1995).
- [77] W. Melnitchouk and A. W. Thomas, Phys. Lett. **B 377**, 11 (1994); W. Melnitchouk and J. C. Peng, Phys. Lett. **B 400**, 220 (1997); U. K. Yang and A. Bodek, Phys. Rev. Lett. **82**, 2467 (1999); M. Boglione and E. Leader, [hep-ph/0005092] .
- [78] T. Y. Saito, Y. Wu, S. Ishikawa and T. Sasakawa, Phys. Lett. **B 242**, 12 (1990); J. Carlson, D. Riska, R. Schiavilla and R. B. Wiringa, Phys. Rev. **C 44**, 619 (1991).
- [79] F. E. Close and A. W. Thomas, Phys. Lett. **B 212**, 227 (1988); C. Boros and A. W. Thomas, Phys. Rev. **D 60**, 074017 (1999).
- [80] J. L. Friar, E. I. Tomusiak, B. F. Gibson and G. L. Payne, Phys. Rev. **C 24**, 677 (1981); G. Derrick and J. M. Blatt, Nucl. Phys. **8**, 310 (1958).
- [81] C. Boros, V. Guzey, M. Strikman and A. W. Thomas, Phys. Rev. **D 64**, 014025 (2001); F. Bissey, V. Guzey, M. Strikman and A. W. Thomas, [hep-ph/0109069].
- [82] E154 Collab., K. Abe *et al.*, Phys. Lett. **B 404**, 339 (1997); K. Abe *et al.*, *ibid.* **405**, 180 (1997); Phys. Rev. Lett. **79**, 26 (1997).
- [83] H. Geiger and E. Marsden, Proc. Roy. Soc. Lond. **82**, 495 (1909); E. Rutherford, Philos. Mag. **21**, 669 (1911).
- [84] R. Hofstadter and R. W. McAllister, Phys. Rev. **98**, 217 (1955); R. Hofstadter, Rev. Mod. Phys. **28**, 214 (1956).
- [85] M. Gell-Mann, Phys. Lett. **8**, 214 (1964); G. Zweig, CERN-8182/Th.401 (1964), unpublished; G. Zweig, CERN-8419/Th.412 (1964), unpublished.
- [86] Y. Ne'eman, Nucl. Phys. **26**, 222 (1961); M. Gell-Mann and Y. Ne'eman, *The Eightfold Way* (Benjamin, New York, 1964).
- [87] M. Y. Han and Y. Nambu, Phys. Rev. **139**, 1006B (1965).

- [88] E. D. Bloom *et al.*, Phys. Rev. Lett. **23**, 930 (1969); M. Breidenbach *et al.*, *ibid.* **23**, 935 (1969).
- [89] R. P. Feynman, Phys. Rev. Lett. **23**, 1415 (1969).
- [90] D. Gross and F. Wilczek, Phys. Rev. Lett. **30**, 1343 (1973); D. Politzer, *ibid.* **30**, 1346 (1973).
- [91] M. Alguard *et al.*, Phys. Rev. Lett. **37**, 1258 (1976); *ibid.* **37**, 1261 (1976); *ibid.* **41**, 70 (1976).
- [92] J. Ashman *et al.*, Phys. Lett. **B 206**, 364 (1988); Nucl. Phys. **B 328**, 1 (1989).
- [93] P. L. Anthony *et al.*, Phys. Rev. Lett. **71**, 959 (1993).
- [94] I. R. Afnan, F. Bissey, J. Gomez, A. T. Katramatou, W. Melnitchouk, G. G. Petratos and A. W. Thomas, Phys. Lett. **B 493**, 36 (2000); G. G. Petratos, I. R. Afnan, F. Bissey, J. Gomez, A. T. Katramatou, W. Melnitchouk and A. W. Thomas, [nucl-ex/0010011].
- [95] S. C. Bhatt, J. S. Levinger and E. Harms, Phys. Lett. **40B**, 23 (1972); Nucl. Phys. **A 197**, 33 (1972).
- [96] R. Machleidt, Nucl. Phys. **A 689**, 11 (2001).
- [97] O. W. Greenberg, Phys. Rev. Lett. **13**, 598 (1964).
- [98] H. Fritzsch, M. Gell-Mann and H. Leutwyler, Phys. Lett. **47B**, 365 (1973).
- [99] K. Ackerstaff *et al.*, Phys. Lett. **B 464**, 123 (1999).
- [100] F. M. Steffens and A. W. Thomas, Phys. Rev. **C 55**, 900 (1997).

List of Publications

Published papers

- **Comments on "Parton distributions, d/u , and Higher Twist Effects at High x ".**
Published in Phys. Rev. Lett. **84**, 5455 (2000).
- **Neutron structure functions and $A = 3$ mirror nuclei.**
Published in Phys. Lett. B **493**, 36 (2000).
- **Deep inelastic scattering on asymmetric nuclei.**
Published in Phys. Lett. B **493**, 288 (2000).
- **Structure functions for the three-nucleon system.**
Published in Phys. Rev. C **64**, 024004 (2001).

Contribution to conferences

- **Extracting nucleon spin structure functions from nuclear data.**
Talk given to the "Circum-Pan-Pacific RIKEN Symposium On High-Energy Spin Physics (Pacific Spin 99)", Wako, Japan, 4 - 6 Nov. 1999.
Published in Riken. Rev. **28**, 90 (2001).
- **Measurements of the F_2^n/F_2^p and d/u ratios in deep inelastic electron scattering off ^3H and ^3He .**
Invited talk at "Workshop on Nucleon Structure in High x -Bjorken Region (HiX2000)", Philadelphia, Pennsylvania, 30 Mar. - 1 Apr. 2000.
Unpublished. [nucl-ex/0010011].

Submitted papers

- **Complete analysis of the spin structure function g_1 of ^3He .**
Submitted to Phys. Rev. C. [hep-ph/0109069].

Comment on "Parton Distributions, d/u , and Higher Twist Effects at High x "

In a recent Letter, Yang and Bodek [1] presented results of a new analysis of proton and deuteron structure functions in which the free neutron structure function, F_2^n , was extracted at large x . Relating nuclear structure functions to those of free nucleons is, however, not straightforward because at large x nuclear effects become quite sizable. In particular, omitting nuclear binding or off-shell corrections can introduce errors of up to 50% [2] in F_2^n/F_2^p already at $x \sim 0.75$.

Rather than follow the conventional procedure of subtracting Fermi motion and binding effects in the deuteron via standard two-body wave functions, Yang and Bodek instead extract F_2^n using "a model proposed by Frankfurt and Strikman [3], in which all binding effects in the deuteron and heavy nuclear targets are assumed to scale with the nuclear density" [1]. Here we point out why this approach is ill-defined for light nuclei and why it introduces a large theoretical bias into the extraction of F_2^n at large x .

For heavy nuclei the nuclear EMC effect is observed to scale with the nuclear density, ρ_A [3],

$$\frac{R_{A_1} - 1}{R_{A_2} - 1} = \frac{\rho_{A_1}}{\rho_{A_2}} \quad (1)$$

where $R_A = F_2^A/F_2^d$ and $\rho_A = 3A/(4\pi R_e^3)$, with $R_e^2 = (5/3)\langle r^2 \rangle$ and $\langle r^2 \rangle^{1/2}$ is the nuclear rms radius. Assuming that an analog of Eq. (1) holds also for F_2^A/F_2^N ($F_2^N = F_2^p + F_2^n$), Frankfurt and Strikman [3] derive $F_2^d/F_2^N \approx 1 + (R_A - 1)\rho_d/(\rho_A - \rho_d)$, from which the free F_2^n is then extracted [1].

While the correlation of EMC ratios with nuclear densities is empirical for heavy nuclei, application of Eq. (1) to light nuclei, $A < 4$, is fraught with ambiguities in defining physically meaningful nuclear densities for few body nuclei. Firstly, the relevant density in Eq. (1) is the nuclear matter density, while in practice ρ_A is usually calculated from the charge radius [1] — for heavy nuclei the difference is negligible, but for light nuclei it can be significant. Secondly, treating the deuteron as a system with radius $\langle r^2 \rangle^{1/2} \approx 2$ fm means that one includes *both* nucleons in the average density felt by one of them, even though one nucleon obviously cannot influence its own structure. Therefore what one should consider is the probability of one nucleon overlapping the other, which is simply the deuteron wave function at the origin. This has zero weight, however, so the only sensible definition of mean density for the deuteron is zero. Strictly speaking, the nuclear density extrapolation then predicts *no nuclear EMC effect in the deuteron*.

In Ref. [3] Frankfurt and Strikman argue that for heavy nuclei the average potential energy is proportional to the average nuclear density, and hence for x below 0.5–0.6 the nuclear EMC effect should scale with average nuclear density. If one applies the idea from heavy

nuclei to the deuteron, one finds that the EMC effect in d is $(F_2^d/F_2^N - 1) = 0.25 (F_2^{Fe}/F_2^d - 1)$. For light nuclei ($A = 2, 3$), however, no justification for this assumption is provided, and for $x \gtrsim 0.6$, where nuclear Fermi motion effects become large, Frankfurt and Strikman caution that this estimate is only a qualitative one [3].

The size of the EMC effect in the deuteron cannot be tested directly in any inclusive deep-inelastic scattering experiment on the deuteron, as it requires knowledge of F_2^n , which itself must be extracted from deuteron data. If, on the other hand, the EMC effect scales with nuclear density even for the deuteron, as assumed in [1,3], it must also scale with ρ_A for all $A > 2$. In particular, it must predict the size of the EMC effect in three-body nuclei. In fact, for $A = 3$ the nuclear density extrapolation makes quite a dramatic prediction: since the three-body nuclear densities calculated from the charge radii are $\rho_{^3\text{He}} = 0.049 \text{ fm}^{-3}$ and $\rho_{^3\text{H}} = 0.068 \text{ fm}^{-3}$, the EMC effect in ^3H is 40% larger than that in ^3He . This is to be compared with standard many-body calculations in terms of Faddeev wave functions which predict a $\lesssim 10\%$ difference between the EMC effects in $A = 3$ mirror nuclei. A proposal to perform deep-inelastic scattering experiments from ^3He and ^3H targets is currently being discussed at Jefferson Lab [4].

The point is that one would never think of using a density extrapolation to extract the neutron's electromagnetic form factors from quasielastic scattering on the deuteron or ^3He , for example, and there is no reason to believe this method is any more reasonable for structure functions.

This work was supported by the Australian Research Council, and by DOE under Contract No. DE-AC05-84ER40150.

W. Melnitchouk,^{1,2} I. R. Afnan,³ F. Bissey,¹
and A. W. Thomas¹

¹Special Research Centre for the Subatomic Structure
of Matter
and Department of Physics and Mathematical Physics
University of Adelaide
Adelaide 5005, Australia

²Jefferson Lab
12000 Jefferson Avenue
Newport News, Virginia 23606

³School of Physical Sciences
The Flinders University of South Australia
Bedford Park, South Australia 5042, Australia

Received 2 December 1999

PACS numbers: 13.60.Hb, 12.38.Qk, 24.85.+p, 25.30.Mr

- [1] U. K. Yang and A. Bodek, Phys. Rev. Lett. **82**, 2467 (1999).
- [2] W. Melnitchouk and A. W. Thomas, Phys. Lett. B **377**, 11 (1996).
- [3] L. Frankfurt and M. Strikman, Phys. Rep. **160**, 235 (1988).
- [4] G. Petratos *et al.*, in Proceedings of Workshop on Experiments with Tritium at JLab, Jefferson Lab, 1999 (to be published).

Neutron structure function and $A = 3$ mirror nuclei

I.R. Afnan^a, F. Bissey^{b,c}, J. Gomez^d, A.T. Katramatou^e, W. Melnitchouk^{b,d,*},
G.G. Petratos^e, A.W. Thomas^b

^a School of Physical Sciences, Flinders University of South Australia, Bedford Park 5042, Australia

^b Special Research Centre for the Subatomic Structure of Matter, and Department of Physics and Mathematical Physics,
Adelaide University, Adelaide 5005, Australia

^c Laboratoire de Physique Corpusculaire, Université Blaise Pascal, CNRS/IN2P3, 24 avenue des Landais,
63177 Aubière cedex, France

^d Jefferson Lab, 12000 Jefferson Avenue, Newport News, VA 23606, USA

^e Kent State University, Kent, OH 44242, USA

Received 5 June 2000; received in revised form 9 August 2000; accepted 31 August 2000

Editor: W. Haxton

Abstract

We investigate deep inelastic scattering from ^3He and ^3H within a conventional convolution treatment of binding and Fermi motion effects. Using realistic Faddeev wave functions together with a nucleon spectral function, we demonstrate that the free neutron structure function can be extracted in deep-inelastic scattering from $A = 3$ mirror nuclei, with nuclear effects canceling to within 2% for $x \lesssim 0.85$. © 2000 Elsevier Science B.V. All rights reserved.

One of the most fundamental properties of the nucleon is the structure of its valence quark distributions. Unlike the sea, which is generated via both perturbative and non-perturbative mechanisms, the valence quark structure reflects entirely large distance dynamics in the nucleon, which cannot be described within perturbative quantum chromodynamics.

Experimentally, most of the recent studies of nucleon structure have emphasized the small- x region populated mainly by sea quarks (x being the fraction of momentum of the nucleon carried by the quark), while the valence quark structure has for some time now been thought to be understood. This is to some extent true, albeit with one major exception — the so-called deep valence region, at very large x , $x \gtrsim 0.7$.

Recently it has become more widely appreciated that knowledge of quark distributions at large x is essential for a number of reasons. Not least of these is the necessity of understanding backgrounds in collider experiments, such as in searches for new physics beyond the standard model [1]. Furthermore, the behavior of the d/u quark distribution ratio in the limit $x \rightarrow 1$ is a critical test of the mechanism of spin-flavor symmetry breaking in the nucleon, and of the onset of perturbative behavior in large- x structure functions.

The most widely used source of information about the valence quark distributions in the nucleon has been the proton structure function, F_2^p , which at large x measures a charge-squared weighted combination of the valence u and d distributions. Because the u quark is weighted by a factor 4 : 1 compared with the d , the F_2^p structure function most directly constrains the u quark distribution.

* Corresponding author.

E-mail address: wmelnitc@nlab.org (W. Melnitchouk).

To determine the individual isospin distributions separately requires a second linear combination of u and d , which traditionally is obtained from the neutron structure function, F_2^n , and which could in principle constrain the d quark distribution as well as the u . However, the absence of free neutron targets means that usually the deuteron is used as an effective neutron, with the neutron structure function approximated by $F_2^n \approx F_2^d - F_2^p$. While this approximation is valid at moderate x , it breaks down dramatically for $x \gtrsim 0.4$ due to Fermi motion and nuclear binding effects in the deuteron [2–5].

The problem of extracting neutron structure functions from nuclear data is rather old [2], although recently the discussion has been revived with the realization [5] that F_2^n , extracted from F_2^d by taking into account Fermi motion and binding (off-shell) effects, could be significantly larger than that extracted in earlier analyses in which only Fermi motion corrections were applied. In particular, omitting nuclear binding corrections can introduce errors of up to 50% [5,6] in F_2^n/F_2^p already at $x \sim 0.75$. Such a difference is of the same order of magnitude as the variation of the behavior of the F_2^n/F_2^p ratio predicted in the $x \rightarrow 1$ limit, which ranges from $1/4$ in non-perturbative models where the d quark is suppressed relative to u [7], to $3/7$ in perturbative QCD-inspired models which emphasize helicity aligned configurations of the quark and nucleon [8].

Although one can make a strong argument that a proper treatment of nuclear corrections in the deuteron should account for both Fermi motion as well as binding effects, the question can ultimately be settled only by experiment. In this Letter we suggest how this can be achieved by using a novel method which maximally exploits the mirror symmetry of $A = 3$ nuclei. Regardless of the absolute value of the nuclear EMC effects in ${}^3\text{He}$ or ${}^3\text{H}$, the differences between these will be small — on the scale of charge symmetry breaking in the nucleus — which allows a relatively clean determination of F_2^n over a large range of x essentially free of nuclear contamination.

The argument is actually rather simple. In the absence of the Coulomb interaction and in an isospin symmetric world the properties of a proton (neutron) bound in a ${}^3\text{He}$ nucleus would be identical to that of a neutron (proton) bound in ${}^3\text{H}$. If, in addition, the proton and neutron distributions in ${}^3\text{He}$ (and in ${}^3\text{H}$)

were identical, the neutron structure function could be extracted with no nuclear corrections, regardless of the size of the EMC effect in ${}^3\text{He}$ or ${}^3\text{H}$ separately.

In practice, ${}^3\text{He}$ and ${}^3\text{H}$ are of course not perfect mirror nuclei — their binding energies for instance differ by some 10% — and the p and n distributions are not quite identical. However, the $A = 3$ system has been studied for many years, and modern realistic $A = 3$ wave functions are known to rather good accuracy. In a self-consistent framework one can use the same NN interaction which describes the two-nucleon system (e.g., NN scattering, deuteron form factors, quasi-elastic ed scattering) to provide the basic input interaction into the three-nucleon calculation. Therefore the wave functions can be tested against a large array of observables which put rather strong constraints on the models.

Defining the EMC-type ratios for the F_2 structure functions of ${}^3\text{He}$ and ${}^3\text{H}$ (weighted by corresponding isospin factors) by:

$$R({}^3\text{He}) = \frac{F_2^{3\text{He}}}{2F_2^p + F_2^n}, \quad (1a)$$

$$R({}^3\text{H}) = \frac{F_2^{3\text{H}}}{F_2^p + 2F_2^n}, \quad (1b)$$

one can write the ratio of these as:

$$\mathcal{R} = \frac{R({}^3\text{He})}{R({}^3\text{H})}. \quad (2)$$

Inverting this expression directly yields the ratio of the free neutron to proton structure functions:

$$\frac{F_2^n}{F_2^p} = \frac{2\mathcal{R} - F_2^{3\text{He}}/F_2^{3\text{H}}}{2F_2^{3\text{He}}/F_2^{3\text{H}} - \mathcal{R}}. \quad (3)$$

We stress that F_2^n/F_2^p extracted via Eq. (3) does not depend on the size of the EMC effect in ${}^3\text{He}$ or ${}^3\text{H}$, but rather on the *ratio* of the EMC effects in ${}^3\text{He}$ and ${}^3\text{H}$. If the neutron and proton distributions in the $A = 3$ nuclei are not dramatically different, one might expect $\mathcal{R} \approx 1$. To test whether this is indeed the case requires an explicit calculation of the EMC effect in the $A = 3$ system.

The conventional approach employed in calculating nuclear structure functions in the valence quark region, $x \gtrsim 0.3$, is the impulse approximation, in which

the virtual photon scatters incoherently from individual nucleons in the nucleus [9]. The nuclear cross section is determined by factorizing the γ^* -nucleus interaction into γ^* -nucleon and nucleon–nucleus amplitudes. In the absence of relativistic and nucleon off-shell corrections [10,11], the structure function of a nucleus, F_2^A , can then be calculated by folding the nucleon structure function, F_2^N , with a nucleon momentum distribution in the nucleus, $f_{N/A}$:

$$F_2^A(x) = \int dy f(y) F_2^N(x/y) \equiv f(x) \otimes F_2^N(x), \quad (4)$$

where y is the fraction of the “plus”-component of the nuclear momentum carried by the interacting nucleon, and the Q^2 dependence in the structure functions is implicit. The convolution expression in Eq. (4) is correct in the limit of large Q^2 ; at finite Q^2 there are additional contributions to F_2^A from the nucleon F_1^N structure function, although these are suppressed by powers of M^2/Q^2 , where M is the nucleon mass. Corrections to the impulse approximation appear in the guise of final state interactions, multiple rescattering (nuclear shadowing), NN correlations and 6-quark clusters, however, these are generally confined to either the small- x [12], or very large- x ($x \gtrsim 0.9$) [13] regions.

The distribution $f(y)$ of nucleons in the nucleus is related to the nucleon spectral function $S(p)$ by [9]:

$$f(y) = \int d^4p \left(1 + \frac{p_z}{p_0}\right) \delta\left(y - \frac{p_0 + p_z}{M}\right) S(p), \quad (5)$$

where p is the four-momentum of the bound nucleon, and is normalized such that $\int dy f(y) = 1$. The spectral function includes final state interactions between the two spectator nucleons, either as a deuteron or in the continuum. In the latter case, this includes an integration over interacting final state NN wave functions, as distinct from a calculation in terms of a simple momentum distribution (see Ref. [14] for a definition of the three-body spectral function). For an $A = 3$ nucleus the spectral function is evaluated from the three-body nuclear wave function, calculated by solving the homogeneous Faddeev equation with a given two-body interaction. Details of the computation of the wave functions can be found in Ref. [15]. To examine the model dependence of the distribution function we use several different potentials, namely the “EST” (Ernst–Shakin–Thaler) separable approximation to the Paris potential [16] (referred to as “PEST”),

the unitary pole approximation [17] to the Reid Soft Core (RSC) potential, and the Yamaguchi potential [18] with 7% mixing between 3S_1 and 3D_1 waves.

In terms of the proton and neutron momentum distributions, the F_2 structure function for ^3He is given by:

$$F_2^{^3\text{He}} = 2f_{p/^3\text{He}} \otimes F_2^p + f_{n/^3\text{He}} \otimes F_2^n. \quad (6a)$$

Similarly for ^3H , the structure function is evaluated from the proton and neutron momentum distributions in ^3H :

$$F_2^{^3\text{H}} = f_{p/^3\text{H}} \otimes F_2^p + 2f_{n/^3\text{H}} \otimes F_2^n. \quad (6b)$$

Because isospin symmetry breaking effects in nuclei are quite small, one can to a good approximation relate the proton and neutron distributions in ^3He to those in ^3H :

$$f_{n/^3\text{H}} \approx f_{p/^3\text{He}}, \quad (7a)$$

$$f_{p/^3\text{H}} \approx f_{n/^3\text{He}}, \quad (7b)$$

although in practice we consider both the isospin symmetric and isospin symmetry breaking cases explicitly. Note that even in the isospin symmetric case the proton and neutron distributions in ^3He will be different because while the neutron in ^3He is accompanied by a spectator pp , the spectator system of the proton is either an uncorrelated pn pair or a recoiling deuteron.

The ratio \mathcal{R} of EMC ratios for ^3He and ^3H is shown in Fig. 1 for the various nuclear model wave functions (PEST, RSC and Yamaguchi), using the CTEQ parameterization [19] of parton distributions at $Q^2 = 10 \text{ GeV}^2$ for F_2^N . The EMC effects are seen to largely cancel over a large range of x , out to $x \sim 0.85$ – 0.9 , with the deviation from a “central value” $\mathcal{R} \approx 1.01$ within $\pm 1\%$. Furthermore, the dependence on the nuclear wave function is very weak. In practice, the exact shape of \mathcal{R} will not be important for the purposes of extracting F_2^n/F_2^p from the $F_2^{^3\text{He}}/F_2^{^3\text{H}}$ ratio; rather, it is essential that, as we find, the model dependent deviation of \mathcal{R} from the central value should be small.

The dependence of \mathcal{R} on the input nucleon structure function parameterization is illustrated in Fig. 2, where several representative curves at $Q^2 = 10 \text{ GeV}^2$ are given: apart from the standard CTEQ fit (solid), the results for the GRV [20] (dot-dashed), Donnachie–Landshoff (DL) [21] (dashed), and BBS [22] (dotted) parameterizations are also shown (the latter at

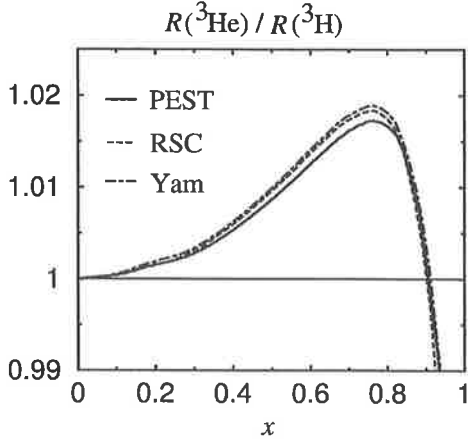


Fig. 1. Ratio of nuclear EMC ratios for ^3He and ^3H for various nuclear models: PEST (solid), Reid Soft Core (dashed), Yamaguchi (dot-dashed).

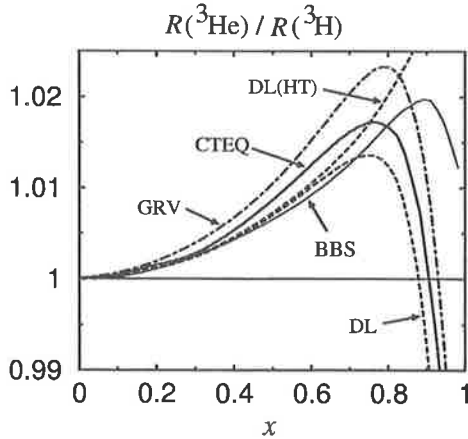


Fig. 2. Ratio of nuclear EMC ratios for ^3He and ^3H with the PEST wave functions, using various nucleon structure function parameterizations: CTEQ (solid), GRV (dot-dashed), BBS (dotted), and Donnachie–Landshoff (DL) with leading twist only, and with higher twist (HT) correction (dot-dashed).

$Q^2 = 4 \text{ GeV}^2$). For $x \lesssim 0.6$ there is little dependence ($\lesssim 0.5\%$) in the ratio on the structure function input. For $0.6 \lesssim x \lesssim 0.85$ the dependence is greater, but still with $\lesssim \pm 1\%$ deviation away from the central value $\mathcal{R} \approx 1.01$. The spread in this region is due mainly to the poor knowledge of the neutron structure function at large x . Beyond $x \approx 0.85$ there are few data in the deep-inelastic region on either the neutron or proton

structure functions, so here both the d and u quark distributions are poorly determined.

A standard assumption in most global fits of parton distributions is that $d/u \rightarrow 0$ as $x \rightarrow 1$. This assumption has recently been questioned on theoretical and phenomenological grounds [5,23,24]. The BBS parameterization [22], on the other hand, incorporates constraints from perturbative QCD, and forces $d/u \rightarrow 0.2$ as $x \rightarrow 1$ [8]. The effect of the different large- x behavior of the d quark is apparent only for $x \gtrsim 0.85$, where it gives a difference of $\sim 1\text{--}2\%$ in \mathcal{R} compared with the fits in which $d/u \rightarrow 0$. One can also modify the standard CTEQ fit, for example, by applying a correction factor [23] to enforce $d/u \rightarrow 0.2$, however, this also produces differences in \mathcal{R} which are $\lesssim 2\%$ for $x < 0.9$.

Despite the seemingly strong dependence on the nucleon structure function input at very large x , this dependence is actually artificial. In practice, once the ratio $F_2^{3\text{He}}/F_2^{3\text{H}}$ is measured, one can employ an iterative procedure to eliminate this dependence altogether. Namely, after extracting F_2^n/F_2^p from the data using some calculated \mathcal{R} , the extracted F_2^n can then be used to compute a new \mathcal{R} , which is then used to extract a new and better value of F_2^n/F_2^p . This procedure is iterated until convergence is achieved and a self-consistent solution for the extracted F_2^n/F_2^p and \mathcal{R} is obtained (see also Ref. [25]).

All of the structure functions discussed thus far have been calculated assuming leading twist dominance at $Q^2 = 10 \text{ GeV}^2$. To test the sensitivity of the ratio to possible effects beyond leading twist, we have calculated \mathcal{R} using the fit to the total F_2 structure function from Donnachie and Landshoff [21], which has an explicit higher twist ($\propto 1/Q^2$) component in addition to the leading twist. The result is indicated by the upper dot-dashed curve DL(HT) in Fig. 2. The difference between the leading twist only and leading + higher twist curves is negligible for $x \lesssim 0.8$, increasing to $\sim 1.5\%$ at $x \sim 0.85$, where higher twist effects are known to be more important. The size of the higher twist corrections can be determined by taking measurements at several values of Q^2 and observing any $1/Q^2$ dependence of the structure function. In particular, since the Q^2 dependence of F_2^p has been measured in a number of earlier experiments [26], the Q^2 dependence of the extracted F_2^n/F_2^p can be used to

separate the leading twist from the non-leading twist components of F_2^n .

We conclude therefore that the effect on \mathcal{R} from the present lack of knowledge of the nucleon structure function is $\lesssim 2\%$ for $x \lesssim 0.85$. However, this uncertainty can in principle be eliminated altogether via an iteration procedure, so that the only model dependence of \mathcal{R} will be from the nuclear interaction in the $A = 3$ nucleus.

The ratios in Fig. 1 were calculated using three-nucleon wave functions neglecting the Coulomb interaction and working in an isospin basis (we also omit possible three-body forces since these are expected to have a negligible effect on \mathcal{R}). To estimate the effect of neglecting the Coulomb interaction in ${}^3\text{He}$ and at the same time correct the long range part of the three-body wave function due to the change in the binding energy, we have modified the 1S_0 potential in ${}^3\text{He}$ and ${}^3\text{H}$ to reproduce their respective experimental binding energies. In this way the 3S_1 – 3D_1 interaction responsible for the formation of the deuteron is unchanged. This approximation spreads the effect of the Coulomb interaction over both the pp and np interaction in the 1S_0 channel. To that extent, it shifts some of the Coulomb effects in the neutron distribution in ${}^3\text{He}$ to the proton distribution. However, this simple modification to the 1S_0 interaction will allow us to study explicitly the possible effects associated with the differences in the binding energies of ${}^3\text{He}$ and ${}^3\text{H}$.

The ratio \mathcal{R} calculated with the PEST wave function modified according to this prescription is shown in Fig. 3, labeled PEST(E) (dashed curve). (The CTEQ parameterization of the nucleon structure function at $Q^2 = 10 \text{ GeV}^2$ is used.) The result of this modification is a shift of approximately 0.5–1% shift in \mathcal{R} , with the net effect still being a ratio which deviates by $< 2\%$ from unity.

Also shown in Fig. 3 is the prediction of the nuclear density model, extrapolated from heavy nuclei to $A = 3$ [27]. The nuclear density model, which has proven successful for studying the A -dependence of the EMC effect for heavy nuclei, stems from the empirical observation that for heavy nuclei the deviation from unity in the EMC ratio is assumed to scale with nuclear density:

$$\frac{R(A_1) - 1}{R(A_2) - 1} = \frac{\rho(A_1)}{\rho(A_2)}, \quad (8)$$

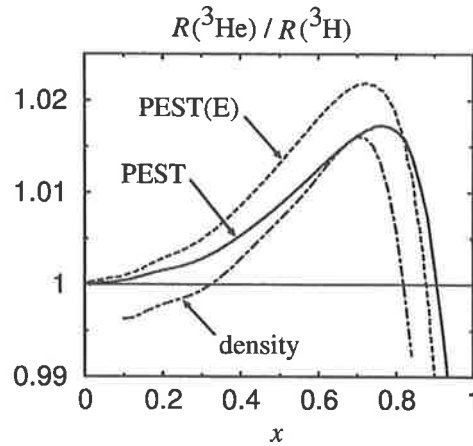


Fig. 3. Ratio of nuclear EMC ratios for ${}^3\text{He}$ and ${}^3\text{H}$ for the PEST wave function (solid), modified PEST to reproduce the experimental binding energies (dashed), and the density extrapolation model (dot-dashed).

where $\rho(A)$ is the mean nuclear density. From the empirical $A = 3$ charge radii one finds that $\rho({}^3\text{H})/\rho({}^3\text{He}) \approx 140\%$, so that the EMC effect in ${}^3\text{H}$ is predicted to be $\sim 40\%$ bigger than in ${}^3\text{He}$. However, assuming that $R({}^3\text{He})$ can be extrapolated from the measured EMC ratios for heavy nuclei such as ${}^{56}\text{Fe}$, one still finds that ratio $|\mathcal{R} - 1| < 2\%$ for all $x \lesssim 0.85$. Although there are questions about the meaning of nuclear density for a few-body system [28], it is reassuring to see that practically the entire range of models of the nuclear EMC effect predict that \mathcal{R} is within 1–2% of unity for all $x \lesssim 0.85$.

The ideal place to carry out a high- x deep-inelastic scattering (DIS) experiment on ${}^3\text{He}$ and ${}^3\text{H}$ [29,30] is Jefferson Lab (JLab) with its proposed energy upgrade to 12 GeV. Since the ratio of longitudinal to transverse photoabsorption cross sections $R = \sigma_L/\sigma_T$ is the same for ${}^3\text{He}$ and ${}^3\text{H}$, measurements of the ${}^3\text{He}$ and ${}^3\text{H}$ DIS cross sections under identical conditions can provide a direct measurement of the ratio of the F_2 structure functions of the two nuclei: $\sigma({}^3\text{H})/\sigma({}^3\text{He}) = F_2({}^3\text{H})/F_2({}^3\text{He})$. The key issue for the experiment will be the availability of a high density ${}^3\text{H}$ tritium target similar to those used in the past to measure the elastic form factors of ${}^3\text{H}$ at Saclay [31] and MIT-Bates [32]. The high intensity of the JLab beam and the large acceptance of existing or proposed JLab spectrometers will facilitate high statistics DIS

cross section measurements ($\leq \pm 0.25\%$) over a large x range ($0.10 \leq x \leq 0.83$) and valuable systematic checks in a data taking period of just a few weeks.

The measured $F_2^{3\text{H}}/F_2^{3\text{He}}$ ratio is expected to be dominated by experimental uncertainties that do not cancel in the DIS cross section ratio of ^3H to ^3He , and the theoretical uncertainty in the calculation of \mathcal{R} . Assuming that the target densities can be known to the $\simeq 0.5\%$ level and that the relative difference in the ^3H and ^3He radiative corrections would be $\simeq 0.5\%$, the total experimental error in the DIS cross section ratio of ^3H to ^3He should be $\leq 1.0\%$ (similar to the error of past DIS measurements of the proton to deuteron cross section ratio [33]). Such an error is comparable to the present theoretical uncertainty in the calculation of the ratio \mathcal{R} .

Fig. 4 shows the presently available data on F_2^n/F_2^p , adjusted for the JLab 12 GeV kinematics, as extracted

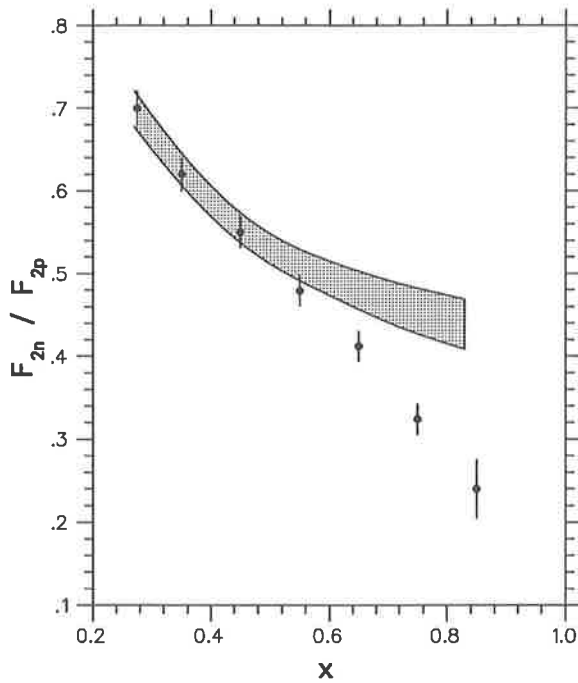


Fig. 4. F_2^n/F_2^p ratio extracted from previous deep-inelastic p and d cross sections using a Fermi-smearing model [6] (solid circles). The shaded band represents a \pm one standard deviation error for the proposed ^3H and ^3He DIS JLab experiment, with the central values of the band corresponding to F_2^n/F_2^p extracted assuming an EMC effect in deuterium (see text).

from the SLAC deep-inelastic $\sigma(p)$ and $\sigma(d)$ cross sections using a Fermi-smearing model with the Paris nucleon–nucleon potential [6]. To indicate the quality of the proposed F_2^n/F_2^p ratio determination from the $\sigma(^3\text{H})/\sigma(^3\text{He})$ measurement, we plot in Fig. 4 the \pm one standard deviation projected error band for the x range accessible with a 12 GeV upgraded JLab beam. The band includes both projected experimental and theoretical uncertainties. The central values of the band represent F_2^n/F_2^p determined using the density model [27] for the nuclear EMC effect and data on EMC ratios for heavy nuclei from the SLAC experiment E139 [34]. It is evident, therefore, that the proposed measurement will be able to unambiguously distinguish between the two different methods of extracting the F_2^n/F_2^p ratio from proton and deuterium DIS measurements, and determine its value for large x with an excellent precision in an (almost) independent model way.

As well as offering a relatively clean way to extract F_2^n/F_2^p , DIS from the $^3\text{He}/^3\text{H}$ system can also determine the absolute size of the EMC effect in $A \leq 3$ nuclei. With F_2^n determined from the combined $F_2^{3\text{He}}/F_2^{3\text{H}}$ and F_2^p structure functions, the size of the EMC effect in the deuteron (namely, $F_2^d/(F_2^p + F_2^n)$) can be deduced from the measured F_2^d/F_2^p ratio. This would settle a question which has remained controversial since the early 1970s. Furthermore, data on the absolute values of $F_2^{3\text{He}}$ and $F_2^{3\text{H}}$ will also allow the absolute value of the EMC effect in $A = 3$ nuclei to be determined. To date the only data on $F_2^{3\text{He}}$ in existence are those from the HERMES experiment [35], which measured the ratio $\sigma(^3\text{He})/(\sigma(d) + \sigma(p))$, although the focus there was the region of small x and Q^2 .

In summary, we have demonstrated the effectiveness of using $A = 3$ mirror nuclei to extract the ratio of the neutron to proton structure functions, F_2^n/F_2^p , essentially free of nuclear effects for all $x \lesssim 0.85$. A successful program of DIS measurements of $A = 3$ cross sections at an energy-upgraded Jefferson Lab would not only settle a “text-book” issue which has eluded a definitive resolution for nearly 30 years, but would also allow the completion of the empirical study of nuclear effects in deep-inelastic scattering over the full range of mass numbers.

Acknowledgements

We would like to thank S. Liuti, G. Salme, S. Scopetta and S. Simula for helpful discussions and communications. This work was supported by the Australian Research Council, the US Department of Energy contract DE-AC05-84ER40150, and the US National Science Foundation grant PHY-9722640.

References

- [1] S. Kuhlmann et al., Phys. Lett. B 476 (2000) 291.
- [2] G.B. West, Phys. Lett. 37B (1971) 509;
W.B. Atwood, G.B. West, Phys. Rev. D 7 (1973) 773.
- [3] L.P. Kaptari, A.Yu. Umnikov, Phys. Lett. B 259 (1991) 155;
M.A. Braun, M.V. Tokarev, Phys. Lett. B 320 (1994) 381.
- [4] W. Melnitchouk, A.W. Schreiber, A.W. Thomas, Phys. Lett. B 335 (1994) 11.
- [5] W. Melnitchouk, A.W. Thomas, Phys. Lett. B 377 (1996) 11.
- [6] L.W. Whitlow et al., Phys. Lett. B 282 (1992) 475.
- [7] R.P. Feynman, Photon Hadron Interactions, Benjamin, Reading, MA, 1972;
F.E. Close, Phys. Lett. 43B (1973) 422;
R. Carlitz, Phys. Lett. 58B (1975) 345;
F.E. Close, A.W. Thomas, Phys. Lett. B 212 (1988) 227;
N. Isgur, Phys. Rev. D 59 (1999) 034013.
- [8] G.R. Farrar, D.R. Jackson, Phys. Rev. Lett. 35 (1975) 1416.
- [9] S.V. Akulinichev, S.A. Kulagin, G.M. Vagradov, Phys. Lett. B 158 (1985) 485;
G.V. Dunne, A.W. Thomas, Nucl. Phys. A 455 (1986) 701;
E.L. Berger, F. Coester, Annu. Rev. Nucl. Part. Sci. 37 (1987) 463;
T. Uchiyama, K. Saito, Phys. Rev. C 38 (1988) 2245;
R.P. Bickerstaff, A.W. Thomas, J. Phys. G 15 (1989) 1523;
C. Ciofi degli Atti, S. Liuti, Phys. Rev. C 41 (1990) 1100;
C. Ciofi degli Atti, S. Liuti, Phys. Rev. C 44 (1991) 1269;
C. Ciofi degli Atti, S. Scopetta, E. Pace, G. Salme, Phys. Rev. C 48 (1993) 968;
S.A. Kulagin, G. Piller, W. Weise, Phys. Rev. C 50 (1994) 1154;
D.F. Geesaman, K. Saito, A.W. Thomas, Annu. Rev. Nucl. Part. Sci. 45 (1995) 337.
- [10] W. Melnitchouk, A.W. Schreiber, A.W. Thomas, Phys. Rev. D 49 (1994) 1183.
- [11] F. Gross, S. Liuti, Phys. Rev. C 45 (1992) 1374;
S.A. Kulagin, W. Melnitchouk, G. Piller, W. Weise, Phys. Rev. C 52 (1995) 932;
W. Melnitchouk, G. Piller, A.W. Thomas, Phys. Lett. B 346 (1995) 165;
W. Melnitchouk, G. Piller, A.W. Thomas, Phys. Rev. C 54 (1996) 894.
- [12] G. Piller, W. Weise, Phys. Rep. 330 (2000) 1;
W. Melnitchouk, A.W. Thomas, Phys. Rev. D 47 (1993) 3783;
W. Melnitchouk, A.W. Thomas, Phys. Lett. B 317 (1993) 437.
- [13] C. Ciofi degli Atti, S. Liuti, Phys. Lett. B 225 (1989) 215;
C. Ciofi degli Atti, S. Simula, L.L. Frankfurt, M.I. Strikman, Phys. Rev. C 44 (1991) R7;
S. Simula, Few-Body Systems 9 (Suppl.) (1995) 466.
- [14] C. Ciofi degli Atti, E. Pace, G. Salme, Phys. Rev. C 21 (1980) 805;
C. Ciofi degli Atti, E. Pace, G. Salme, Phys. Lett. 141B (1984) 14.
- [15] F. Bissey, A.W. Thomas, I.R. Afnan, in preparation.
- [16] J. Haidenbauer, W. Plessas, Phys. Rev. C 30 (1984) 1822.
- [17] T.Y. Saito, I.R. Afnan, Few-Body Systems 18 (1995) 101.
- [18] Y. Yamaguchi, Phys. Rev. 95 (1954) 1628.
- [19] H.L. Lai et al., Eur. Phys. J. C 12 (2000) 375.
- [20] M. Gluck, E. Reya, A. Vogt, Eur. Phys. J. C 5 (1998) 461.
- [21] A. Donnachie, P.V. Landshoff, Z. Phys. C 61 (1994) 139.
- [22] S.J. Brodsky, M. Burkardt, I. Schmidt, Nucl. Phys. B 441 (1995) 197.
- [23] W. Melnitchouk, J.C. Peng, Phys. Lett. B 400 (1997) 220.
- [24] U.K. Yang, A. Bodek, Phys. Rev. Lett. 82 (1999) 2467;
M. Boglione, E. Leader, hep-ph/0005092.
- [25] E. Pace, G. Salme, S. Scopetta, in: Proceedings of the XVIIth European Few-Body Conference, Evora, Portugal, to appear, private communication.
- [26] P. Amaudruz et al., Nucl. Phys. B 371 (1992) 3;
M. Virchaux, A. Milsztajn, Phys. Lett. B 274 (1992) 221.
- [27] L.L. Frankfurt, M.I. Strikman, Phys. Rep. 160 (1988) 235.
- [28] W. Melnitchouk, F. Bissey, I.R. Afnan, A.W. Thomas, Phys. Rev. Lett. 84 (2000) 5455.
- [29] G.G. Petratos et al., in: Proceedings of Workshop on Experiments with Tritium at JLab, Jefferson Lab, Newport News, VA, September 1999.
- [30] W. Melnitchouk, in: Proceedings of Workshop on Experiments with Tritium at JLab, Jefferson Lab, Newport News, VA, September 1999.
- [31] A. Amroun et al., Nucl. Phys. A 579 (1994) 596.
- [32] D. Beck et al., Nucl. Instrum. Methods in Phys. Res. A 277 (1989) 323.
- [33] A. Bodek et al., Phys. Rev. D 20 (1979) 1471.
- [34] J. Gomez et al., Phys. Rev. D 49 (1994) 4348.
- [35] K. Ackerstaff et al., Phys. Lett. B 475 (2000) 386.



ELSEVIER

16 November 2000

PHYSICS LETTERS B

Physics Letters B 493 (2000) 288–292

www.elsevier.nl/locate/npe

Deep inelastic scattering on asymmetric nuclei

K. Saito ^{a,*}, C. Boros ^b, K. Tsushima ^c, F. Bissey ^{b,d}, I.R. Afnan ^c, A.W. Thomas ^b

^a *Tohoku College of Pharmacy, Sendai 981-8558, Japan*

^b *Department of Physics and Mathematical Physics, and Special Research Center for the Subatomic Structure of Matter, University of Adelaide, Adelaide 5005, Australia*

^c *School of Chemistry Physics and Earth Sciences, Flinders University, GPO Box 2100, Adelaide 5001, Australia*

^d *Laboratoire de Physique Corpusculaire, Université Blaise Pascal, CNRS/IN2P3, 24 avenue des Landais, 63177 Aubière Cedex, France*

Received 10 August 2000; accepted 3 October 2000

Editor: W. Haxton

Abstract

We study deep inelastic scattering on isospin asymmetric nuclei. In particular, the difference of the nuclear structure functions and the Gottfried sum rule for the lightest mirror nuclei, ^3He and ^3H , are investigated. It is found that such systems can provide significant information on charge symmetry breaking and flavor asymmetry in the nuclear medium. Furthermore, we propose a new method to extract the neutron structure function from radioactive isotopes far from the line of stability. We also discuss the flavor asymmetry in the Drell–Yan process with isospin asymmetric nuclei. © 2000 Elsevier Science B.V. All rights reserved.

PACS: 25.30.Mr; 21.45.+v; 24.85.+p; 24.80.+y

Keywords: Nuclear structure function; Isospin asymmetric nuclei; Flavor asymmetry; Few-body system

The distributions of quarks in a nucleus differ significantly from those in the free nucleon. This became clear when, nearly two decades ago, the European Muon Collaboration (EMC) measured the ratio of structure functions of iron and deuterium (D) in the deep inelastic scattering (DIS) of muons [1]. Since then many experiments have been performed to investigate the distributions of partons in nuclei [2], and a large amount of data on (flavor) singlet nuclear struc-

ture functions has been collected. However, relatively less attention has been paid to the nonsinglet structure functions of a nucleus. Measurements of the nonsinglet part of nuclear structure functions could shed light on many phenomena involving nonperturbative QCD in nuclei, such as SU(3) symmetry breaking, the flavor asymmetry and so on.

It is, therefore, very interesting and important to measure the structure functions of nuclei with large asymmetry in proton (p) and neutron (n) numbers ($Z \neq N$). In particular, if DIS with high energy electrons on neutron or proton rich nuclei (for example, the RIKEN–MUSES project [3]) could be realized in the future, it would be possible to get interesting information on the nonperturbative quark structure of nuclei. In this paper, we study structure functions of nuclei

* Corresponding author.

E-mail addresses: ksaito@nucl.phys.tohoku.ac.jp (K. Saito), cboros@physics.adelaide.edu.au (C. Boros), ktsushim@physics.adelaide.edu.au (K. Tsushima), fbissey@physics.adelaide.edu.au (F. Bissey), i.r.afnan@flinders.edu.au (I.R. Afnan), athomas@physics.adelaide.edu.au (A.W. Thomas).

with $Z \neq N$, including the radioactive isotopes (RI) which will be studied at RIKEN [3,4].

Until recently it was usually assumed (see, however, Ref. [5]) that the sea quark distributions in the (free) nucleon were flavor symmetric. However, the New Muon Collaboration (NMC) at CERN [6] and the E866 Drell–Yan experiments at Fermilab [7], in particular, have revealed a clear asymmetry in the sea distributions by using proton and deuteron targets. If the quark and antiquark pairs in the sea are created perturbatively and charge symmetry breaking (CSB) effects ($m_d > m_u \sim 5$ MeV) are very small [8] in the free nucleon, it is not possible to explain the measured flavor asymmetry. This fact strongly suggests that non-perturbative QCD process, such as chiral symmetry breaking or the Pauli exclusion principle, must play an important role in the flavor asymmetry [9].

The flavor asymmetry in the sea was observed in the difference between the structure functions of the free proton and neutron, $F_2^p - F_2^n$, and it is simply expressed in terms of the u and d quark distributions, $u(x)$ and $d(x)$, and the antiquark distributions, $\bar{u}(x)$ and $\bar{d}(x)$, in the free proton as

$$F_2^p(x) - F_2^n(x) = \frac{1}{3}x[u(x) - d(x)] + \frac{1}{3}x[\bar{u}(x) - \bar{d}(x)], \quad (1)$$

where we assume charge symmetry in the parton distributions [8]. (The structure functions and distributions depend on the 4-momentum transfer squared, Q^2 , which is suppressed here.) Then, the difference gives the Gottfried sum, I_G^N , for the nucleon as

$$I_G^N(z) = \int_z^1 dx \frac{1}{x} [F_2^p(x) - F_2^n(x)]. \quad (2)$$

Using the normalization condition for the valence quark distributions, we finally find

$$I_G^N(0) = \frac{1}{3} + \frac{2}{3} \int_0^1 dx [\bar{u}(x) - \bar{d}(x)], \quad (3)$$

which provides a measure of flavor asymmetry. If the sea were flavor symmetric, namely $\bar{u}(x) = \bar{d}(x)$, the Gottfried sum rule (GSR) is given by $I_G^N(0) = 1/3$. However, the experimental value measured by NMC was $I_G^N(0) = 0.235 \pm 0.026$ (at $Q^2 = 4 \text{ GeV}^2$) [6],

which is clearly less than $1/3$, and implies that $\bar{d}(x)$ overcomes $\bar{u}(x)$ in the free proton [6,7]:

$$\int_0^1 dx [\bar{d}(x) - \bar{u}(x)] = 0.148 \pm 0.039. \quad (4)$$

The origin of the flavor asymmetry in the proton may be attributed to either the pion cloud required by chiral symmetry [5,10,11] or to the Pauli exclusion principle at quark level [12,13] (or both) — since the proton consists of uud quarks, $u\bar{u}$ pair creation may be suppressed by the Pauli exclusion effect more than $d\bar{d}$ pair creation.

It is a very interesting problem to see how the GSR changes in a nucleus. Studying the flavor asymmetry of a bound nucleon may provide an opportunity to learn details about the nonperturbative structure of the nucleon inside nuclear matter. To this end we consider DIS of an electron or muon off a pair of mirror nuclei. We consider the “nuclear Gottfried sum” defined by

$$I_G^{AA'}(z) = \int_z^A \frac{dx}{x} [F_2^A(x) - F_2^{A'}(x)], \quad (5)$$

where (A, A') is a pair of mirror nuclei: $A = Z + N$ ($Z > N$) (proton rich) and $A' = Z' + N'$ ($N' > Z'$) (neutron rich).

We now turn to the simplest example of this kind, namely the lightest mirror nuclei, ${}^3\text{He}$ and ${}^3\text{H}$. The fact that these are mirror nuclei means that the nuclear corrections are very similar and this has already been exploited in a proposal to extract F_{2p}/F_{2n} from a measurement of $F_2({}^3\text{He})/F_2({}^3\text{H})$ [14]. The three-body system offers the advantage that it can be treated exactly by solving the Faddeev equations [2,15]. However, since it is not easy to handle the Coulomb interaction in the full Faddeev approach, we treat it approximately by adjusting the strength of the 1S_0 nucleon–nucleon potential so as to fit the observed binding energies: $E_b = -7.72$ and -8.48 MeV for ${}^3\text{He}$ and ${}^3\text{H}$, respectively [16].

Using the spectral function given by the solution of the Faddeev equation with the PEST potential [17], we have calculated the difference between the nuclear structure functions of ${}^3\text{He}$ and ${}^3\text{H}$ (at $Q^2 = 10 \text{ GeV}^2$), which is shown in Fig. 1. For the free nucleon structure function we have used the CTEQ5 parametrization

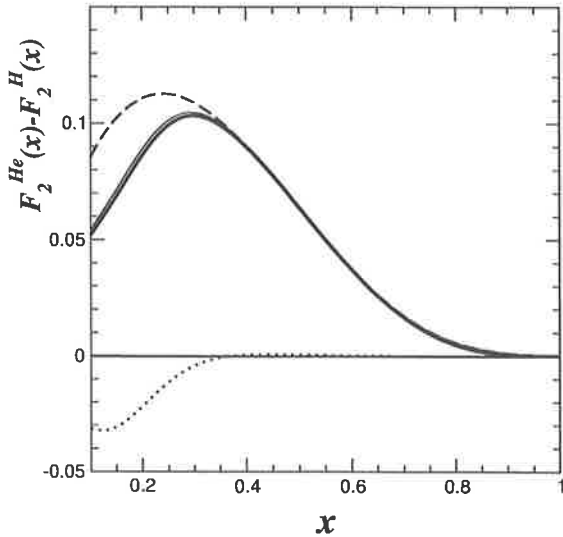


Fig. 1. Difference between the nuclear structure functions of ^3He and ^3H (at $Q^2 = 10 \text{ GeV}^2$). The solid (dashed) [dotted] curves show the total (valence) [sea] contributions. The thin, solid curve presents the difference between the free proton and neutron structure functions (CTEQ5 [18]).

which incorporates the measured flavor asymmetry in the free nucleon [18]. We do not show the structure functions below $x = 0.1$ because in the small x region we should include nuclear shadowing [19]. Since we want to keep the present discussion simple in order to emphasize the key physics ideas, for the present we concentrate on the nuclear structure functions in the region $x > 0.1$. We may expect that since the difference between the nuclear structure functions is (isovector) nonsinglet the nuclear shadowing effect should not be large — the pomeron does not directly couple to the isovector, nonsinglet part.

The effect of CSB in nuclei [20] is to break the nuclear Gottfried sum rule (NGSR):

$$I_G^{AA'}(0) = Y \times I_G^N(0), \quad (6)$$

with $Y (= Z - N = N' - Z')$ the excess proton number in A . (Eq. (6) holds if the nuclear environment does not affect the flavor asymmetry at all.) In the present calculation we find that, at $Q^2 = 10 \text{ GeV}^2$, $I_G^N(0.1) = 0.152$ (from CTEQ5 [18]), while $I_G^{\text{He,H}}(0.1) = 0.150$, which may imply that CSB in the $A = 3$ system gives very little change in the distribution of $\bar{d} - \bar{u}$ (see also Ref. [21]).

While the major source of CSB is the Coulomb force, the main physics interest is in the possible additional sources of flavor asymmetry in nuclei, such as:

1. The probability of finding pions in the in-medium nucleon may be different from that in free space. It is certainly natural to expect that hadronic properties should change in a nuclear medium [22,23]. For example, the distribution of virtual pions per bound nucleon may change, leading to a different flavor asymmetry in nuclei [24]. The nuclear structure functions of mirror nuclei far from the line of stability may provide us significant information on flavor asymmetry and pion dynamics in nuclei. There will be many possible candidates for such mirror nuclei at facilities such as the proposed radioactive ion beam collider at RIKEN [3,4]: for example, (^{22}Mg , ^{22}Ne , $Y = 2$), (^{13}O , ^{13}B , $Y = 3$), (^{17}Ne , ^{17}N , $Y = 3$), (^{20}Mg , ^{20}O , $Y = 4$), etc. Those neutron rich or proton rich nuclei give rise to a large asymmetry in the N/Z ratio.
2. There is the much anticipated possibility of finding exotic configurations, such as 6-quark states, in nuclei. As one consequence, the effect of the Pauli exclusion principle at the quark level may be different because of quark percolation. In the naive counting estimate the ground state of the free proton has 4 vacant states for u quarks and 5 vacant states for d quarks. Thus, the expected flavor asymmetry is $\bar{d}/\bar{u} \simeq 5/4$ [12,13]. However, in a nuclear medium there may be some probability for two nucleons to overlap. Suppose that the valence quarks from two protons are put into one confining potential. In this case, there are 2 vacant states (in the lowest energy level) for u quarks and 4 vacant states for d quarks. Then, the asymmetry becomes $\bar{d}/\bar{u} \simeq 2$, which implies that the flavor asymmetry would be enhanced in nuclei. It may be possible to investigate these nonperturbative phenomena by measuring the nuclear structure functions of mirror nuclei.

DIS off mirror nuclei with large isospin asymmetry should be possible in the future. Our calculation for $A = 3$ represents the standard calculation without any of the possible new contributions. The observation of some deviation from the calculations shown here

would stimulate a great deal of work which may eventually lead to genuinely new information on the dynamics of nuclear systems.

We would like to add some comments on isospin asymmetric nuclei (or nuclei far from the line of stability). First, it is very important to extract the neutron structure function from nuclear experimental data. The system traditionally used for this is the deuteron but the $A = 3$ case is also being seriously considered now [14]. The proposed MUSES project at RIKEN [3] will provide a number of attractive alternatives for extracting the neutron structure function using radioactive ions rich in neutrons.

As an example, let us consider a series of Li nuclei. There exist five RI observed at RIKEN: ${}^6\text{Li}$, ${}^7\text{Li}$, ${}^8\text{Li}$, ${}^9\text{Li}$, ${}^{11}\text{Li}$. Then, we shall consider a ratio

$$R_n(i) = \frac{F_2({}^i\text{Li}) - F_2({}^{i-1}\text{Li})}{F_2^D - F_2^P}, \quad (7)$$

where $F_2({}^i\text{Li})$ is the structure function of ${}^i\text{Li}$, and i runs from 7 to 9. (For $i = 11$, we may take $[F_2({}^{11}\text{Li}) - F_2({}^9\text{Li})]/2$ as the numerator of the ratio.) This $R_n(i)$ means the ratio of the neutron structure function bound in the Li nucleus to that in D (if those were the same the ratio would be unity). We suppose that the deuteron structure function itself is already understood.

Varying the atomic number i successively (i.e., varying the binding effect on the neutron in Li) and comparing the i -series of those ratios, we may get useful information on the neutron structure function, its nuclear binding effect (shell structure dependence) [4] and the off-mass shell effect [19]. In particular, the last neutron in the halo nuclei (like ${}^{11}\text{Li}$) is bound very weakly — some hundred keV [3,4], which is much weaker than in D. The RI series of Be, B, C, O, Na and Mg [3,4] are also of great interest.

Finally, we turn to the nuclear Drell–Yan (DY) process as an alternative method to study the sea quark distributions [25]. We first define the p – n asymmetry, C_{DY}^N , in the free nucleon as

$$C_{\text{DY}}^N = \frac{2\sigma^{pp} - \sigma^{pD}}{\sigma^{pD}} \simeq \frac{\sigma^{pp} - \sigma^{pn}}{\sigma^{pp} + \sigma^{pn}}, \quad (8)$$

where σ^{AB} is the DY cross section for the lepton pair production of $A + B \rightarrow \ell^+ \ell^- + X$, and we assume that the nuclear binding effect in D can be neglected. Then, if we take a large $x_F (= |x_A - x_B|)$ the p – n asymmetry

becomes

$$C_{\text{DY}}^N \rightarrow \frac{[4u(x_A) - d(x_A)][\bar{u}(x_B) - \bar{d}(x_B)]}{[4u(x_A) + d(x_A)][\bar{u}(x_B) + \bar{d}(x_B)]}, \quad (9)$$

where $u(x_i)$ ($d(x_i)$) is the u (d) quark distribution with momentum fraction x_i in i ($= A$ or B). This ratio is sensitive to the flavor asymmetry in B .

In order to check the flavor asymmetry in a nucleus, we shall again use a pair of mirror nuclei, (A, A') , and define the p – n asymmetry in nuclei as

$$C_{\text{DY}}^{AA'} = \frac{\sigma^{pA} - \sigma^{pA'}}{\sigma^{pD}}. \quad (10)$$

If A and A' simply consist of protons and neutrons and we assume that the nuclear binding effect is small, the p – n asymmetry in nuclei becomes

$$C_{\text{DY}}^{AA'} = Y \times C_{\text{DY}}^N, \quad (11)$$

with the excess proton number Y . If we take the (double) ratio as

$$D_{\text{DY}} = \frac{C_{\text{DY}}^{AA'}}{C_{\text{DY}}^N} = Y, \quad (12)$$

it gives just Y if the flavor asymmetry is not changed by the nuclear medium. The deviation from Y in actual measurements should be a sensitive signature for the flavor asymmetry and nuclear binding in a nucleus.

Moreover, we can see the flavor asymmetry by using a single RI. We suppose a ratio

$$R_{\text{DY}}^A = \frac{2}{A} \left(\frac{\sigma^{pA}}{\sigma^{pD}} \right), \quad (13)$$

and again assume that the nucleus, A , is a simple collection of Z protons and N neutrons. We then find

$$\begin{aligned} R_{\text{DY}}^A &\simeq \frac{2}{A} \left(\frac{Z\sigma^{pp} + N\sigma^{pn}}{\sigma^{pp} + \sigma^{pn}} \right), \\ &\simeq 1 - \frac{(N - Z)}{A} \left(\frac{\sigma^{pp} - \sigma^{pn}}{\sigma^{pp} + \sigma^{pn}} \right), \\ &\sim 1 - \frac{(N - Z)}{A} \\ &\quad \times \frac{[4u(x_A) - d(x_A)][\bar{u}(x_B) - \bar{d}(x_B)]}{[4u(x_A) + d(x_A)][\bar{u}(x_B) + \bar{d}(x_B)]}, \end{aligned} \quad (14)$$

for large x_F . This is also sensitive to the flavor asymmetry in the nucleus. In particular, nuclei far from the line of stability are very interesting because

they give large asymmetries — i.e., large values of $(N - Z)/A$.

In summary, we have studied the nuclear structure functions and the Gottfried sum rule for a pair of mirror nuclei which could give very significant information on CSB and flavor asymmetry in the nuclear medium. For the present we have restricted our study to the region $x > 0.1$, in order to make the discussion simple. It will be very interesting to extend this work to calculate the nuclear structure functions including shadowing, in order to complete the discussion of the NGSF and flavor asymmetry in nuclei. Furthermore, we have proposed a new method to extract the neutron structure function from RI far from the line of stability, and discussed the flavor asymmetry in the nuclear DY process. If DIS with high energy electrons (or muons) off nuclei with large isospin asymmetry becomes possible in the future, we could get a lot of valuable information on the non-perturbative quark structure of atomic nuclei.

Acknowledgements

We would like to thank W. Melnitchouk for many useful discussions. K.S. would also like to thank J.T. Londergan for providing a lot of useful information on flavor asymmetry. This work was partly supported by the Australian Research Council.

References

- [1] EMC Collaboration, J.J. Aubert, Phys. Lett. B 123 (1983) 275.
- [2] D.F. Geesaman, K. Saito, A.W. Thomas, Annu. Rev. Nucl. Part. Sci. 45 (1995) 337; M. Arneodo, Phys. Rep. 240 (1994) 301.
- [3] MUSES (Multi-Use Experimental Storage-rings) project at RIKEN, see the RIKEN home page (<http://www.rarf.riken.go.jp>).
- [4] I. Tanihata, Nucl. Phys. A 654 (1999) 235c.
- [5] A.W. Thomas, Phys. Lett. B 126 (1983) 97.
- [6] New Muon Collaboration, M. Arneodo et al., Phys. Rev. D 50 (1994) R1.
- [7] FNAL E866/NuSea Collaboration, J.C. Peng et al., Phys. Rev. D 58 (1998) 092004.
- [8] C. Boros, F.M. Steffens, J.T. Londergan, A.W. Thomas, Phys. Lett. B 468 (1999) 161; J.T. Londergan, A.W. Thomas, Prog. Part. Nucl. Phys. 41 (1998) 49.
- [9] S. Kumano, Phys. Rep. 303 (1998) 183; J. Speth, A.W. Thomas, Adv. Nucl. Phys. 24 (1998) 83; J.C. Peng, G.T. Garvey, hep-ph/9912370, LA-UR-99-5003, to be published in: Trends in Particle and Nuclear Physics, Vol. 1, Plenum Press, New York.
- [10] E.M. Henley, G.A. Miller, Phys. Lett. B 251 (1990) 453; S. Kumano, J.T. Londergan, Phys. Rev. D 44 (1991) 717; A. Signal, A.W. Schreiber, A.W. Thomas, Mod. Phys. Lett. A 6 (1991) 271; M. Ericson, A.W. Thomas, Phys. Lett. B 148 (1984) 191.
- [11] A.W. Thomas, W. Melnitchouk, F.M. Steffens, hep-ph/0005043.
- [12] R.D. Field, R.P. Feynman, Phys. Rev. D 15 (1977) 2590.
- [13] A.I. Signal, A.W. Thomas, Phys. Rev. D 40 (1989) 2832.
- [14] I.R. Afnan, F. Bissey, J. Gomez, A.T. Katramatou, W. Melnitchouk, G.G. Petratos, A.W. Thomas, nucl-th/0006003.
- [15] T. Uchiyama, K. Saito, Phys. Rev. C 38 (1988) 2245; C. Ciofi degli Atti, S. Liuti, Phys. Rev. C 41 (1990) 1100.
- [16] F. Bissey, A.W. Thomas, I.R. Afnan, manuscript in preparation.
- [17] J. Haidenbauer, W. Plessas, Phys. Rev. C 30 (1984) 1822.
- [18] H.L. Lai et al., Eur. Phys. J. C 12 (2000) 375.
- [19] For example, G. Piller, W. Weise, Phys. Rep. 330 (2000) 1.
- [20] For example, G.A. Miller, W.T.H. Van Oers, in: W.C. Haxton, E.M. Henley (Eds.), Symmetries and Fundamental Interactions in Nuclei, World Scientific, 1995, p. 127.
- [21] V.V. Burov, A.V. Molochkov, G.I. Smirnov, Phys. Lett. B 466 (1999) 1.
- [22] P.A.M. Guichon, K. Saito, E. Rodionov, A.W. Thomas, Nucl. Phys. A 601 (1996) 349; K. Saito, K. Tsushima, A.W. Thomas, Nucl. Phys. A 609 (1996) 339; K. Saito, K. Tsushima, A.W. Thomas, Phys. Rev. C 55 (1997) 2637.
- [23] Quark Matter '99, Nucl. Phys. A 661 (1999).
- [24] M. Ericson, A.W. Thomas, Phys. Lett. B 128 (1983) 112; E.L. Berger, F. Coester, Phys. Rev. D 32 (1985) 1071; C.L. Korpa, A.E.L. Dieperink, Phys. Lett. B 446 (1999) 15.
- [25] See also: S. Kumano, Phys. Lett. B 342 (1995) 339.

Structure functions for the three-nucleon system

F. Bissey,^{1,2} A. W. Thomas,¹ and I. R. Afnan³

¹*Special Research Centre for the Subatomic Structure of Matter and Department of Physics and Mathematical Physics, University of Adelaide, Adelaide 5005, Australia*

²*Laboratoire de Physique Corpusculaire, Université Blaise Pascal, CNRS/IN2P3, 24 avenue des Landais, F-63177 Aubière Cedex, France*

³*School of Chemistry Physics and Earth Science, Flinders University, GPO Box 2100, Adelaide 5001, Australia*

(Received 26 December 2000; published 10 July 2001)

The spectral functions and light-cone momentum distributions of protons and neutrons in ^3He and ^3H are given in terms of the three-nucleon wave function for realistic nucleon-nucleon interactions. To reduce computational complexity, separable expansions are employed for the nucleon-nucleon potentials. The results for the light-cone momentum distributions suggest that they are not very sensitive to the details of the two-body interaction, as long as it has reasonable short-range repulsion. The unpolarized and polarized structure functions are examined for both ^3He and ^3H in order to test the usefulness of ^3He as a neutron target. It is found that the measurement of the spin structure function of polarized ^3H would provide a very clear test of the predicted change in the polarized parton distributions of a bound proton.

DOI: 10.1103/PhysRevC.64.024004

PACS number(s): 21.45.+v, 13.60.Hb, 14.20.Dh

I. INTRODUCTION

It is well known that a polarized ^3He target can be used as a polarized neutron target. The question we would like to address is how good a polarized neutron target it is for the determination of the neutron spin structure function, g_1 , in deep inelastic scattering. There are two questions that play a central role in resolving this problem. The first is the sensitivity of the light-front momentum distribution to the three-nucleon wave function. For this we need to calculate the spectral function for realistic trinucleon wave functions. The second question is a consequence of the fact that the neutron structure function is small in comparison with the proton structure function. This raises the question of the accuracy with which one can extract the polarized neutron structure function from ^3He .

To examine these questions we need first to calculate the three-nucleon wave function for a "realistic" nucleon-nucleon potential. To simplify the problem computationally, we consider a separable expansion [1] of the Paris potential (which we call PEST) [2], that gives the same three-nucleon observables as the original Paris potential in a full multichannel Faddeev calculation [3,4]. For comparison we consider two other classes of potentials. The first is a rank one unitary pole approximation (UPA) [5] to the Reid soft core potential [6]. This has the property that it reproduces the position and residue of the poles in the 1S_0 and 3S_1 - 3D_1 channels—i.e., it reproduces the original potential's deuteron wave function. As a result, it incorporates the short range behavior of the original interaction. The second is a Yamaguchi type potential with a D -state probability of 4% and 7% [7]. These potentials do not include the short range repulsion that is commonly present in nucleon-nucleon interactions.

In Sec. II, we present the procedure used to determine the three-nucleon wave functions for these potentials, as well as the corresponding three nucleon observables. By comparing the results for these three classes of potential, we are able to determine the importance of short range correlations and the

contribution of higher partial waves to the neutron and proton spectral functions and therefore to the light-cone momentum distributions. Since we will be considering both ^3He and ^3H , we have chosen to work in an isospin basis and therefore neglect the contribution of the Coulomb interaction to the ^3He wave function. We do, however, estimate the effect of neglecting the Coulomb correction on the momentum distribution and therefore the structure functions.

In order to analyze the deep inelastic structure functions of $A=3$ nuclei, we need to determine the neutron and proton spectral functions. This is detailed in Sec. III. Here we compare the results for various two-body potentials, finding that the light-cone momentum distribution is not sensitive to the details of our three-nucleon wave function. In Sec. IV we turn to the structure functions and examine the ratio of the structure function in the three-nucleon system to that in the deuteron (the EMC effect) for the different interactions. We also examine the possible implication of neglecting the Coulomb interaction in ^3He . This opens the way for us to study the sensitivity of the unpolarized and polarized structure functions to the quark distributions in the proton and neutron and the possibility of extracting the neutron spin structure function from polarized ^3He data. Finally, in Sec. IV we present some concluding remarks.

II. THE THREE NUCLEON WAVE FUNCTION

For the three-nucleon problem we can determine the non-relativistic wave function by solving the Faddeev equations exactly for any realistic two-body interaction. However, to simplify the computational aspects of the problem, with no sacrifice in the quality of the wave function, we turn to separable expansions that have been extensively tested [3,4]. This will result in a three-nucleon wave function that can be used to calculate the spectral function and the light-cone momentum distribution. In the present section we detail the three-nucleon formalism required to evaluate the wave functions for ^3He and ^3H .

A. Notation

With the extensive literature on the Faddeev equations [8] and their use in the three-nucleon system, we restrict ourselves here to a summary of the notation used in the present analysis. The Faddeev decomposition of the three-nucleon wave function is given by

$$|\Psi\rangle = |\varphi_1\rangle + |\varphi_2\rangle + |\varphi_3\rangle = \{e + (123) + (132)\}|\varphi_3\rangle. \quad (1)$$

Here “ e ,” “(123),” and “(132)” are members of the permutation group of three objects, with e being the unit element (i.e., $e|\varphi_\alpha\rangle = |\varphi_\alpha\rangle$) and the other two being cyclic permutations of $\{1,2,3\}$. The second equality results from the requirement that we have identical particles, the wave function is then invariant under any cyclic permutation of our particles. Since we have a system of identical fermions, the total wave function must be antisymmetric under the exchange of any two particles in the system. This requirement leads to the following conditions:

$$\begin{aligned} (\alpha\beta)|\varphi_\alpha\rangle &= -|\varphi_\beta\rangle, \\ (\alpha\beta)|\varphi_\beta\rangle &= -|\varphi_\alpha\rangle, \\ (\alpha\beta)|\varphi_\gamma\rangle &= -|\varphi_\gamma\rangle. \end{aligned} \quad (2)$$

In the above equations α , β and γ are indices running from 1 to 3, and always different from each other, and $(\alpha\beta)$ is again a member of the permutation group of three objects which exchange particles α and β leaving the third one unchanged. Since we are dealing with a three-body problem, there will be only two independent momenta in the center of mass frame. All the particles have spin and isospin $\frac{1}{2}$ and one must account for their orbital angular momentum. We briefly summarize the quantum numbers and momenta used throughout this paper:

N_α is a set of quantum numbers describing a three body channel from the point of view of the particle α , which is the spectator; the set is unique for each channel.

\vec{l}_α is the orbital angular momentum between particles β and γ .

\vec{L}_α is the orbital angular momentum between particle α and the center of mass of the system consisting of particles β and γ .

$\vec{J}_\alpha, \vec{J}_\beta, \vec{J}_\gamma$ are the spins of each particle.

$\vec{t}_\alpha, \vec{t}_\beta, \vec{t}_\gamma$ are the isospins of each particle.

\vec{p}_α is the momentum of particle α in the center of mass frame.

\vec{q}_α is the relative momentum of the pair of particles β and γ , defined as $\vec{q}_\alpha = (\vec{p}_\gamma - \vec{p}_\beta)/2$.

\vec{I} and \vec{J} are, respectively, the total isospin and total angular momentum of the system.

B. The partial wave expansion

We now turn to the partial wave expansion of our wave function. To minimize the number of coupled Faddeev equations,

having truncated the interaction to a set of partial waves, we have used the following coupling scheme:

$$\begin{aligned} \vec{J}_\beta + \vec{J}_\gamma &= \vec{s}_\alpha, & \vec{l}_\alpha + \vec{s}_\alpha &= \vec{j}_\alpha, & \vec{J}_\alpha + \vec{j}_\alpha &= \vec{S}_\alpha, & \vec{L}_\alpha + \vec{S}_\alpha &= \vec{J}, \\ \vec{t}_\beta + \vec{t}_\gamma &= \vec{t}_\alpha, & \vec{t}_\alpha + \vec{t}_\alpha &= \vec{I}, \end{aligned}$$

which is known as the channel coupling scheme. With this coupling scheme the complete set of quantum number N_α describing a three-body channel is $N_\alpha = \{\vec{t}_\alpha, s_\alpha, \vec{j}_\alpha, S_\alpha, L_\alpha\}$. A subset of these quantum number that describe the two-body channels is $n_\alpha = \{\vec{t}_\alpha, s_\alpha, \vec{j}_\alpha\}$, and therefore $N_\alpha = \{n_\alpha, S_\alpha, L_\alpha\}$. We have not included l_α in the set of quantum numbers since the tensor force mixes values of l_α . This allows us to define the angular momentum and isospin basis as

$$\begin{aligned} |\Omega_{l_\alpha N_\alpha}^{IJ}\rangle &= |L_\alpha, [(l_\alpha, (j_\beta, j_\gamma) s_\alpha) \vec{j}_\alpha, J_\alpha] S_\alpha, J\rangle \\ &\times [(\vec{t}_\beta, \vec{t}_\gamma) \vec{t}_\alpha, \vec{t}_\alpha] I\rangle. \end{aligned} \quad (3)$$

These basis states satisfy the following orthogonality relation: $\langle \Omega_{l_\alpha N_\alpha}^{IJ} | \Omega_{l_\beta N_\beta}^{IJ} \rangle = \delta_{l_\alpha, l_\beta} \delta_{N_\alpha, N_\beta}$.

We are now in a position to write the partial wave expansion of the total three-nucleon wave function as

$$|\Psi\rangle = \sum_{l_\alpha N_\alpha} |\Omega_{l_\alpha N_\alpha}^{IJ}\rangle |\mathcal{U}_{l_\alpha N_\alpha}^{IJ}\rangle, \quad (4)$$

where $|\mathcal{U}_{l_\alpha N_\alpha}^{IJ}\rangle$ is defined as the radial part of the wave function corresponding to the partial wave $\{l_\alpha, N_\alpha\}$.

C. Separable potential

To reduce the dimensionality of the Faddeev integral equations from two to one, and in this way simplify the three-body wave function, we have employed a separable expansion of the nucleon-nucleon interaction. Our potential for the interaction of particles β and γ in a given partial wave is of the form [5]

$$V_{l_\alpha, l'_\alpha}^{n_\alpha} = |g_{l_\alpha}^{n_\alpha}\rangle \lambda_{l_\alpha, l'_\alpha}^{n_\alpha} \langle g_{l'_\alpha}^{n_\alpha}|, \quad (5)$$

where $|g_{l_\alpha}^{n_\alpha}\rangle$ is a “form factor” and $\lambda_{l_\alpha, l'_\alpha}^{n_\alpha}$ is the strength of the potential in that partial wave. By taking $l_\alpha \neq l'_\alpha$ we can accommodate a tensor interaction, as in the case of the 3S_1 - 3D_1 nucleon-nucleon channel. The above expression for the potential is for a rank one potential. To incorporate higher rank potentials, we turn the strength $\lambda_{l_\alpha, l'_\alpha}^{n_\alpha}$ into a matrix and as a result $|g_{l_\alpha}^{n_\alpha}\rangle$ is a row matrix. In resorting to separable expansions, we have taken the view that the expansion is a numerical procedure analogous to the use of quadratures. However, a low order expansion, such as the UPA or the use of a separable potential, is justified on the grounds that it generates the same analytic structure in the amplitude (i.e., bound or anti-bound state poles) as a corresponding realistic

potential [9]. The use of a separable potential gives rise to a separable t matrix that satisfies the Lippmann-Schwinger (LS) equation,

$$t_\alpha(E) = V_\alpha + V_\alpha G_0(E) t_\alpha(E) = (1 - G_0(E) V_\alpha)^{-1} V_\alpha, \quad (6)$$

with $G_0(E) = (E - H_0)^{-1}$ the two-body Green's function. It is simple to show that the separable t matrix in a given partial wave, resulting from a solution of the LS equation, is of the form

$$t_{l_\alpha l'_\alpha}^{n_\alpha}(E) = |g_{l_\alpha}^{n_\alpha}\rangle \tau_{l_\alpha l'_\alpha}^{n_\alpha}(E) \langle g_{l'_\alpha}^{n_\alpha}|, \quad (7)$$

where the form factor $|g_{l_\alpha}^{n_\alpha}\rangle$ is identical to that used in the separable potential. The function $\tau_{l_\alpha l'_\alpha}^{n_\alpha}(E)$, in a given channel, can be written in matrix form as

$$[\tau^{n_\alpha}(E)]^{-1} = [\lambda^{n_\alpha}]^{-1} - \langle g^{n_\alpha} | G_0(E) | g^{n_\alpha} \rangle. \quad (8)$$

This separability of the t matrix will allow us to reduce the dimensionality of the Faddeev integral equations from two to one after the partial wave expansion described in Eq. (4).

D. The three-nucleon wave function

Having determined the structure of the two-body amplitude, we now turn to the wave function for the three-nucleon system. The Schrödinger equation for this system is

$$(E - H_0) |\Psi\rangle = V |\Psi\rangle = \sum_{\alpha=1}^3 V_\alpha |\Psi\rangle. \quad (9)$$

This can be rewritten in a form that suggests the Faddeev decomposition stated in Eq. (1), i.e.,

$$|\Psi\rangle = G_0(E) V |\Psi\rangle = \sum_{\alpha=1}^3 G_0(E) V_\alpha |\Psi\rangle = \sum_{\alpha=1}^3 |\varphi_\alpha\rangle. \quad (10)$$

Here, $G_0(E) = (E - H_0)^{-1}$ is the three-body Green's function. We now can write an equation for the Faddeev components of the wave function as

$$|\varphi_\alpha\rangle = G_0(E) V_\alpha |\Psi\rangle = G_0(E) V_\alpha |\varphi_\alpha\rangle + \sum_{\gamma \neq \alpha} G_0(E) V_\alpha |\varphi_\gamma\rangle. \quad (11)$$

With the help of Eq. (6), the set of coupled integral equations for the Faddeev components of the wave function, $|\varphi_\alpha\rangle$, becomes

$$|\varphi_\alpha\rangle = G_0(E) T_\alpha(E) (|\varphi_\beta\rangle + |\varphi_\gamma\rangle). \quad (12)$$

Here $T_\alpha(E)$ is the t matrix for particles β and γ in the three-particle Hilbert space, which is related to the two-body amplitude considered in the last section by

$$T_\alpha(E) = t_\alpha(E - \epsilon_\alpha), \quad (13)$$

where ϵ_α is the energy of the spectator particle α in the three-body center of mass.¹

In Eq. (12) we have a set of coupled integral equations, known as the Faddeev equations, for the three-body bound state. For the three-nucleon system, where we have identical fermions, we take advantage of the antisymmetry, as given in Eq. (2), and the fact that $(\beta\gamma)T_\alpha = T_\alpha(\beta\gamma) = -T_\alpha$, to reduce the Faddeev equations to

$$|\varphi_\alpha\rangle = G_0(E) T_\alpha(E) (1 - (\beta\gamma)) |\varphi_\beta\rangle = 2G_0(E) T_\alpha(E) |\varphi_\beta\rangle, \quad (14)$$

with $\alpha \neq \beta$. To recast this equation into a form that will admit numerical solutions, we need to first partial wave decompose the Faddeev equations and take into consideration the separability of the two-body amplitudes. This can all be achieved by partial wave expanding the two-body amplitude in three-body Hilbert space in terms of the angular momentum states defined in Eq. (3) [10]

$$\begin{aligned} T_\alpha(E) &= \sum_{\substack{l_\alpha l'_\alpha \\ N_\alpha J I}} \int_0^\infty dp_\alpha p_\alpha^2 |\Omega_{l_\alpha N_\alpha}^{JI}; p_\alpha\rangle t_{l_\alpha l'_\alpha}^{n_\alpha}(E - \epsilon_\alpha) \langle p_\alpha; \Omega_{l'_\alpha N_\alpha}^{JI} | \\ &= \sum_{\substack{l_\alpha l'_\alpha \\ N_\alpha J I}} \int_0^\infty dp_\alpha p_\alpha^2 |\Omega_{l_\alpha N_\alpha}^{JI}; g_{l_\alpha}^{n_\alpha}\rangle \tau_{l_\alpha l'_\alpha}^{n_\alpha}(E - \epsilon_\alpha) \\ &\quad \times \langle g_{l'_\alpha}^{n_\alpha}; \Omega_{l'_\alpha N_\alpha}^{JI} |, \end{aligned} \quad (15)$$

where $\epsilon_\alpha = (3/4m)p_\alpha^2$ and

$$|\Omega_{l_\alpha N_\alpha}^{JI}; g_{l_\alpha}^{n_\alpha}\rangle = |\Omega_{l_\alpha N_\alpha}^{JI}\rangle |g_{l_\alpha}^{n_\alpha}; p_\alpha\rangle. \quad (16)$$

We now can write Eq. (14) as

$$\begin{aligned} |\varphi_\alpha\rangle &= 2G_0(E) \sum_{\substack{l_\alpha l'_\alpha \\ N_\alpha J I}} \int_0^\infty dp_\alpha p_\alpha^2 |\Omega_{l_\alpha N_\alpha}^{JI}; g_{l_\alpha}^{n_\alpha}\rangle \tau_{l_\alpha l'_\alpha}^{n_\alpha}(E - \epsilon_\alpha) \\ &\quad \times \langle g_{l'_\alpha}^{n_\alpha}; \Omega_{l'_\alpha N_\alpha}^{JI} | \varphi_\beta\rangle \\ &\equiv 2G_0(E) \sum_{\substack{l_\alpha l'_\alpha \\ N_\alpha J I}} \int_0^\infty dp_\alpha p_\alpha^2 |\Omega_{l_\alpha N_\alpha}^{JI}; g_{l_\alpha}^{n_\alpha}\rangle \tau_{l_\alpha l'_\alpha}^{n_\alpha}(E - \epsilon_\alpha) \\ &\quad \times X_{N_\alpha l'_\alpha}^{JI}(p_\alpha), \end{aligned} \quad (17)$$

with the spectator function, $X_{N_\alpha l'_\alpha}^{JI}(p_\alpha)$, satisfying the equation

¹For the three-nucleon system in a nonrelativistic formulation, $\epsilon_\alpha = (3/4m)p_\alpha^2$, where m is the nucleon mass.

$$\begin{aligned}
X_{N_\alpha l_\alpha}^{JJ}(p_\alpha) &\equiv \langle g_{l_\alpha}^{n_\alpha}; \Omega_{l_\alpha N_\alpha}^{JJ} | \varphi_\beta \rangle \\
&= 2 \sum_{\substack{l_\beta l'_\beta \\ N_\beta}} \int_0^\infty dp_\beta p_\beta^2 Z_{l_\alpha N_\alpha; l_\beta N_\beta}^{JJ}(p_\alpha, p_\beta; E) \\
&\quad \times \tau_{l_\beta l'_\beta}^{n_\beta}(E - \epsilon_\beta) X_{N_\beta l'_\beta}^{JJ}(p_\beta), \quad (18)
\end{aligned}$$

where

$$Z_{l_\alpha N_\alpha; l_\beta N_\beta}^{JJ}(p_\alpha, p_\beta; E) \equiv \langle g_{l_\alpha}^{n_\alpha}; \Omega_{l_\alpha N_\alpha}^{JJ} | G_0(E) | \Omega_{l_\beta N_\beta}^{JJ}; g_{l_\beta}^{n_\beta} \rangle, \quad (19)$$

with $\alpha \neq \beta$. In Appendix A we give an explicit expression for $Z_{l_\alpha N_\alpha; l_\beta N_\beta}^{JJ}$, for the coupling scheme used in the present analysis [8,10]. In Eq. (18) we have a set of coupled, homogeneous, integral equations for the spectator wave function, $X_{N_\alpha l_\alpha}^{JJ}(p_\alpha)$, which we can use to construct the total wave function. Here, we note that the spectator wave function is only a function of the momentum of the spectator particle and the energy of the system, which is the binding energy of ^3He or ^3H . We now turn to the total wave function for the three-nucleon system. Making use of the orthogonality of the angular functions, $|\Omega_{l_\alpha N_\alpha}^{JJ}\rangle$, we can write the total radial wave function, defined in Eq. (4), as

$$\begin{aligned}
|\mathcal{U}_{N_\alpha l_\alpha}^{JJ}\rangle &= \langle \Omega_{l_\alpha N_\alpha}^{JJ} | \Psi \rangle \\
&= \langle \Omega_{l_\alpha N_\alpha}^{JJ} | \varphi_\alpha \rangle + \langle \Omega_{l_\alpha N_\alpha}^{JJ} | \varphi_\beta + \varphi_\gamma \rangle \\
&= |\eta_{l_\alpha N_\alpha}^{JJ1}\rangle + |\eta_{l_\alpha N_\alpha}^{JJ2}\rangle, \quad (20)
\end{aligned}$$

where

$$\begin{aligned}
\eta_{l_\alpha N_\alpha}^{JJ1}(p_\alpha, q_\alpha) &\equiv \langle p_\alpha q_\alpha | \eta_{l_\alpha N_\alpha}^{JJ1} \rangle \\
&= \langle p_\alpha q_\alpha; \Omega_{l_\alpha N_\alpha}^{JJ} | \varphi_\alpha \rangle \\
&= 2G_0(q_\alpha, p_\alpha; E) g_{l_\alpha}^{n_\alpha}(q_\alpha) \\
&\quad \times \sum_{l'_\alpha} \tau_{l'_\alpha}^{n_\alpha}(E - \epsilon_\alpha) X_{N_\alpha l'_\alpha}^{JJ}(p_\alpha), \quad (21)
\end{aligned}$$

with $G_0(q_\alpha, p_\alpha; E) = [E - (1/m)(q_\alpha^2 + \frac{3}{4}p_\alpha^2)]^{-1}$. The second component of the radial wave function in Eq. (20) is given by

$$\begin{aligned}
\eta_{l_\alpha N_\alpha}^{JJ2}(p_\alpha, q_\alpha) &\equiv \langle p_\alpha q_\alpha | \eta_{l_\alpha N_\alpha}^{JJ2} \rangle \\
&= \langle p_\alpha q_\alpha; \Omega_{l_\alpha N_\alpha}^{JJ} | \varphi_\beta + \varphi_\gamma \rangle \\
&= P \sum_{l_\beta N_\beta} \int_{-1}^{+1} d\xi \Gamma_{l_\alpha N_\alpha; l_\beta N_\beta}^{JJ}(p_\alpha, p'_\beta; x) \\
&\quad \times \eta_{l_\beta N_\beta}^{JJ1}(p'_\beta, q'_\beta), \quad (22)
\end{aligned}$$

where $P = \frac{1}{2}[1 - (-1)^{l_\alpha + s_\alpha + l_\beta}]$, and

$$\begin{aligned}
p'^2_\beta &= q_\alpha^2 + \frac{1}{4}p_\alpha^2 + q_\alpha p_\alpha \xi, \quad q'^2_\beta = \frac{1}{4}q_\alpha^2 + \frac{9}{16}p_\alpha^2 - \frac{3}{4}q_\alpha p_\alpha \xi, \\
x &= -\frac{1}{p'_\beta} \left(\frac{1}{2}p_\alpha + q_\alpha \xi \right). \quad (23)
\end{aligned}$$

The function $\Gamma_{l_\alpha N_\alpha; l_\beta N_\beta}^{JJ}$ is given in Appendix A. We only observe here that the expression for $\Gamma_{l_\alpha N_\alpha; l_\beta N_\beta}^{JJ}$ differs from that for $Z_{l_\alpha N_\alpha; l_\beta N_\beta}^{JJ}$ by the absence of the separable potential form factors and the three-body Green's function. The normalization of the total wave function is then given by

$$\begin{aligned}
\langle \Psi | \Psi \rangle &= 3 \langle \varphi_\alpha | \varphi_\alpha \rangle + 6 \langle \varphi_\alpha | \varphi_\beta \rangle \\
&= 3 \sum_{l_\alpha N_\alpha} [\langle \eta_{l_\alpha N_\alpha}^{JJ1} | \eta_{l_\alpha N_\alpha}^{JJ1} \rangle + 2 \langle \eta_{l_\alpha N_\alpha}^{JJ1} | \eta_{l_\alpha N_\alpha}^{JJ2} \rangle]. \quad (24)
\end{aligned}$$

Here the sum is restricted by the two-body partial waves included in the Faddeev equations. Since the partial wave expansion of the total wave function involves an infinite sum, we need to truncate this sum such that the normalization evaluated by the truncated sum, that is,

$$\langle \Psi | \Psi \rangle = \sum_{l_\alpha N_\alpha} \langle \mathcal{U}_{N_\alpha l_\alpha}^{JJ} | \mathcal{U}_{N_\alpha l_\alpha}^{JJ} \rangle, \quad (25)$$

agrees with the result of Eq. (24). In this way we ensure that our total wave function includes all the partial waves dictated by the two-body interaction.

E. Numerical results

As a first step in the determination of our wave function, we calculate the binding energy of the three-nucleon system for the class of potentials being considered. For the UPA to the Reid soft core and the Yamaguchi potentials the interaction is restricted to the 1S_0 and 3S_1 - 3D_1 channels. This reduces the homogeneous Faddeev equations to five coupled integral equations for the spectator wave function. For the PEST potentials the number of coupled channels depends on the rank of the interaction in a given channel and the number of partial waves included. To get the optimal representation of the Paris potential we need to have achieved convergence in the rank. This varies from channel to channel. In all cases the rank has been chosen in such a way that the binding energy for a given number of channels has converged and is in agreement with the results of calculations using the Paris potential directly [4]. In Table I we present the result for the binding energy for the three classes of potentials. For the PEST potentials we have taken the 5, 10, and 18 channel potentials. The 18 channel calculation corresponds to including all nucleon-nucleon channels with $J \leq 2$. This will allow us to examine the contribution to the spectral function from higher partial waves. Here we observe that the Yamaguchi potentials overbind the three-nucleon system, while the UPA and PEST potentials underbind. Since the binding energy determines the long range part of the wave function, this

TABLE I. Binding energy for a given potential and components of the wave function.

Potential	Number of channels	Binding energy (MeV)	$P(S)$ %	$P(S')$ %	$P(D)$ %
RSC	5	-7.15	88.37%	1.88%	8.89%
YAM4	5	-9.12	93.08%	1.58%	4.97%
YAM7	5	-8.05	89.1%	1.59%	8.71%
PEST	5	-7.27	89.3%	1.88%	8.11%
PEST	10	-7.10	89.72%	1.71%	7.85%
PEST	18	-7.32	89.56%	1.66%	8.07%

difference allows us to examine the sensitivity of the structure functions to the binding energy and therefore to the tail of the wave function. A comparison of the PEST five channel and the UPA suggests that the difference between these two models is minimal. In fact, that is the case for most realistic potentials that do not include energy dependence. The higher partial waves in the PEST potential seem to have a small but significant contribution to the binding energy. Here again, this potential, in common with all realistic potentials, tends to underbind the three nucleon system. The solution to this problem may involve the short-range, velocity dependence of the two-nucleon force [11], as well as a genuine three-body force [12].

Since we have neglected the Coulomb contribution to the energy of ^3He , and our more realistic potentials underbind the three nucleon system, we have chosen to adjust the strength of the 1S_0 interaction to reproduce the experimental binding energy of both ^3He and ^3H . This procedure does not effect the deuteron wave function, but could have some influence on the continuum wave function in the 1S_0 . In this way, we may estimate the error in neglecting the Coulomb energy for ^3He , and the possible error in the tail of the wave function due to underbinding of the three nucleon system. The contribution of this correction will be discussed when considering the spectral functions and light-cone momentum distributions.

III. LIGHT CONE MOMENTUM DISTRIBUTION

Before we proceed with the discussion of light-cone momentum distributions, we should establish the relation between the cross section in charged lepton scattering and the light-cone momentum distribution. The cross section for the scattering of a charged lepton with a nucleus is proportional to the product of the leptonic tensor $L_{\mu\nu}$ with the hadronic tensor $W_{\mu\nu}$. For an unpolarized hadronic system of spin 1/2 (i.e., free nucleon, ^3He and ^3H) the hadronic tensor has the following form [13–15]:

$$\begin{aligned}
 W_{\mu\nu} = & \frac{1}{2} \sum_S \int d^4x e^{iqx} \langle PS | J_\mu(x) J_\nu(0) | PS \rangle \\
 = & \left(-g_{\mu\nu} + \frac{q_\mu q_\nu}{q^2} \right) W_1 + \left(P_\mu - \frac{P \cdot q}{q^2} q_\mu \right) \\
 & \times \left(P_\nu - \frac{P \cdot q}{q^2} q_\nu \right) \frac{W_2}{M^2}, \quad (26)
 \end{aligned}$$

where P is the four momentum of the hadronic system, S is its polarization, and M is its mass. Here, J is the electromagnetic current, and q the four momentum of the virtual photon. Finally, W_1 and W_2 are the form factors of the hadronic system. In deep inelastic scattering, one prefers to use the structure functions F_1 and F_2 instead. The relation between the form factors and the structure functions is the following:

$$F_1 = MW_1, \quad F_2 = \frac{P \cdot q}{M} W_2. \quad (27)$$

The leptonic tensor for unpolarized scattering has the following structure [13–15]:

$$\begin{aligned}
 L_{\mu\nu} = & \frac{1}{2} \sum_{s,s'} \bar{u}(k',s') \gamma_\mu u(k,s) \bar{u}(k',s') \gamma_\nu u(k,s), \\
 = & 2(k_\mu k'_\nu + k'_\mu k_\nu - g_{\mu\nu} k \cdot k'), \quad (28)
 \end{aligned}$$

with $k(k')$ and $s(s')$ the initial (final) four momentum and polarization of the lepton.

For polarized scattering one does not average over the initial polarization and the resulting tensors then have two parts; a symmetric part, identical to those of Eq. (26) and Eq. (28), and a new antisymmetric piece that is related to the polarization. The antisymmetric part of the hadronic tensor contains two new form factors, G_1 and G_2 , which are in turn linked to two new structure functions, g_1 and g_2 .

The convolution formalism gives a prescription, valid under certain conditions, to link structure functions of complex hadronic systems to structure functions of free nucleons [16,17]. In this formalism, the nucleon light cone momentum distribution in a nucleus plays a central role, in that it relates the in-medium structure function to the nucleon structure function. This relation takes the form of a convolution integral and, in the case of F_2 , given by (see Ref. [18])

$$F_2^A(x, Q^2) = \int_x^{M_A/m} dy f(y) F_2\left(\frac{x}{y}, Q^2\right). \quad (29)$$

Here, $F_2(F_2^A)$ is the free (in nuclear medium) structure function, f is the nucleon light cone momentum distribution inside the nuclear medium, M_A and m are the masses of the nucleus and of the free nucleon, respectively, finally, x is the traditional Bjorken variable and Q^2 is the momentum transfer squared ($Q^2 = -q^2$). The above relation is valid for the leading twist of the structure functions, which is why $f(y)$ has no Q^2 dependence. Another important assumption made in this formula is the impulse approximation, namely the assumption that the structure function of an off-shell nucleon is equal to the structure function of an on-shell nucleon. A more complete discussion about problems raised by this assumption can be found in Ref. [13].

The nucleon light cone momentum distribution in a nucleus, $f(y)$, is the probability to find the nucleon in the nucleus with a given fraction of the total momentum $y (=p^+/P^+)$ of the nucleus on the light front. As a result, one readily see that Eq. (29) has a simple interpretation. The structure function in the medium is the sum of all possible values of the free nucleon structure function, weighted by the probability of finding the nucleon with a given momentum

fraction y . In this section, we will show how to determine the light cone momentum distributions for the neutron or proton in the three-nucleon system.

Since the light cone momentum distribution is essentially the probability of finding a given nucleon with a particular fraction of the momentum of a nucleus, it should be related to the spectral function of the nucleon in that nucleus. In the instantaneous frame the spectral function is the combined probability of finding a nucleon with a given momentum \vec{k} while the remaining nucleus is in a state λ . We denote this spectral function by $S_\lambda(k)$. The light cone momentum distribution is then a sum over all possible states λ , and all possible k that are compatible with the fraction of momentum y . This is given by

$$f(y) = \sum_\lambda \int d^4k \left(1 + \frac{k^3}{k^0}\right) \delta\left(y - \frac{k^0 + k^3}{m}\right) S_\lambda(k). \quad (30)$$

In some cases (see Ref. [13]) a light cone momentum distribution is defined for each state λ . In Eq. (30) the factor $(1 + k^3/k^0)$ is called the flux factor. It is a relativistic correction arising from the fact that we are using a light front formalism [19,20]. Light cone momentum distributions, as well as spectral functions, can also be defined for polarized nucleons. In the following section, we will concentrate on the unpolarized spectral function and merely state the results for the polarized nucleon spectral function.

We note that the calculation of the nucleon momentum distributions presented here is very similar in spirit to the pioneering work of Ciofi degli Atti and Liuti [21]. That work used a wave function based on variational method, rather than the Faddeev equations. While the variational approach is designed to produce an accurate estimate of the binding energy of the system, one must work harder to obtain an equally accurate wave function. Indeed, for the trinucleon system this has led to the necessity to explicitly correct the proton momentum distribution, as described in Ref. [22]. We are not aware of a similar correction being applied to the neutron momentum distribution. In any case, it appears to us that it is worthwhile to make the calculation with a different technique. In addition, we can study the dependence on the assumed two-nucleon force explicitly.

A. The spectral function

To determine the light cone momentum distribution we need to know how to compute the spectral function. For the unpolarized case, the “diagonal spectral function” is given by [23,24]

$$\begin{aligned} S_\lambda(k) &= \frac{1}{2J_A + 1} \sum_{\sigma_A, \sigma} \langle \Psi, \sigma_A | a_{\sigma, N}^\dagger(\vec{k}) a_{\sigma, N}(\vec{k}) | \Psi, \sigma_A \rangle \\ &\quad \times \delta(k^0 - (m + \epsilon_\lambda - Tr_\lambda)) \\ &= \frac{1}{2J_A + 1} \sum_{\sigma_A, \sigma} |\langle \phi, \sigma_b | a_{\sigma, N}(\vec{k}) | \Psi, \sigma_A \rangle|^2 \\ &\quad \times \delta(k^0 - (m + \epsilon_\lambda - Tr_\lambda)). \end{aligned} \quad (31)$$

Here, $|\Psi, \sigma_A\rangle$ is the wave function of the initial nucleus A with spin, J_A , and spin projection, σ_A , along the z axis, while $|\phi, \sigma_b\rangle$ is the wave function of the $A-1$ system in the state σ_b . The sum over σ_b is restricted to those states allowed by the energy conserving δ function. The energy k^0 of the nucleon in this equation is given as the sum of the nucleon mass m plus the separation energy of this nucleon ϵ_λ^2 and minus the recoil kinetic energy Tr_λ of the remaining nucleus. The operator $a_{\sigma, N}^\dagger(\vec{k})$ is the creation operator for a nucleon N (proton or neutron) with spin projection σ and momentum \vec{k} .

In the following we will note the product $a_{\sigma, N}^\dagger(\vec{k}) a_{\sigma, N}(\vec{k})$ as the familiar number density operator $\rho_{\sigma, N}(\vec{k})$ and we will define it in a way similar to Ref. [25]. For example, the density of protons with spin $+1/2$ along the z axis and momentum \vec{p} , $\langle \rho_p^+(\vec{p}) \rangle$, in a trinucleon, is defined by

$$\begin{aligned} \langle \rho_p^+(\vec{p}) \rangle &= \frac{1}{2} \sum_{\sigma_A} \langle \Psi, \sigma_A | \rho_p^+(\vec{p}) | \Psi, \sigma_A \rangle, \\ &= \frac{1}{2} \sum_{\sigma_A} \sum_{i=1}^3 \int d^3\vec{q} \langle \Psi, \sigma_A(\vec{p}, \vec{q}) | \rho_{p,i}^+ | \Psi, \sigma_A(\vec{p}, \vec{q}) \rangle, \end{aligned} \quad (32)$$

with

$$\rho_{p,i}^+ = \frac{(1 + \tau_{3,i})}{2} \frac{(1 + \sigma_{z,i})}{2}. \quad (33)$$

In Eq. (33) one can recognize the number density, in the sense of Ref. [25]. The other density operators which we may use are

$$\rho_{p,i}^- = \frac{(1 + \tau_{3,i})}{2} \frac{(1 - \sigma_{z,i})}{2},$$

$$\rho_{n,i}^+ = \frac{(1 - \tau_{3,i})}{2} \frac{(1 + \sigma_{z,i})}{2},$$

$$\rho_{n,i}^- = \frac{(1 - \tau_{3,i})}{2} \frac{(1 - \sigma_{z,i})}{2}.$$

Using the notation of Sec. II, and more specifically Eq. (4), we can rewrite Eq. (32) in a slightly different way, showing explicitly how we conduct this computation with our wave function

² ϵ_λ is defined as $\epsilon_\lambda = M - M_\lambda - m$ where M_λ is the mass of the remaining nucleus.

$$\langle \rho_p^+(\vec{p}) \rangle = \frac{1}{2} \sum_{i_\alpha, N_\alpha, i_\beta, N_\beta} \left[\left(\sum_{i, \sigma_A} \int d^2 \hat{q} \langle \Omega_{i_\alpha N_\alpha}^{II}, \sigma_A(\hat{p}, \hat{q}) | \rho_{p, i}^+ | \right. \right. \\ \left. \left. \times \Omega_{i_\beta N_\beta}^{II}, \sigma_A(\hat{p}, \hat{q}) \rangle \right) \right. \\ \left. \times \left(\int dq q^2 \langle \mathcal{U}_{i_\alpha N_\alpha}^{IJ}(p, q) | \mathcal{U}_{i_\beta N_\beta}^{IJ}(p, q) \rangle \right) \right]. \quad (34)$$

B. The case of ^3He

^3He is one of simplest nuclei, along with ^3H and deuterium. It consists of two protons and one neutron. If we measure the light-cone momentum distribution of the neutron, the remaining two protons can only be in a scattering state, since there is no bound state of two protons. On the other hand, if we measure the light cone momentum distribution of the proton, the remaining two nucleons are a proton and a neutron, which can be in either a bound state, the deuteron, or a scattering state. We will therefore study first the simpler case of the neutron momentum distribution and then turn to the more difficult proton momentum distribution. In the following equations ρ_N will mean the following: $\Sigma_{i, \pm} \rho_{N, i}^\pm$. And whenever we omit the index i it means that we implicitly sum over all three particles.

1. Neutron in ^3He

In Eq. (31), the sum over σ_b is constrained by the energy conserving δ function, and for the neutron spectrum in ^3He this gives a scattering state for the final two protons with the neutron off-shell. As a result the neutron does not satisfy the on-mass-shell relation $E^2 = \vec{p}^2 + m^2$. Since we are using a nonrelativistic wave function for ^3He we will use a nonrelativistic approximation for the relation between the energy and the momentum. We then define the binding energy of the nucleus, E , by the relation $M = 3m + E$, where m is the mass of a nucleon. Since we are working with a nonrelativistic wave function, we make use of the approximation $p^0 \approx m + \vec{p}^2/(2m)$. Since we are working in the frame of the center of mass of the nucleus we have the following: $M = p_\alpha^0 + p_\beta^0 + p_\gamma^0$. As a result, the energy of the struck nucleon is $p_\alpha^0 = m + E - \vec{p}_\beta^2/(2m) - \vec{p}_\gamma^2/(2m)$. One then finds p_α^0 in terms of \vec{p}_α and q_α : $p_\alpha^0 = m + E - \vec{p}_\alpha^2/(2\mu) - \vec{q}_\alpha^2/(2\nu)$, where ν is the reduced mass of the interacting pair and μ is their total mass.³ If we compare this result with the expression given in Eq. (31), then the recoil energy Tr is $\vec{p}_\alpha^2/(2\mu)$, while the separation energy, ϵ , is $E - \vec{q}_\alpha^2/(2\nu)$. So the unpolarized spectral function for the neutron in ^3He is given by

$$S_n(p) = \frac{1}{2} \sum_{\sigma_A} \int d^3 \vec{q} \langle \Psi, \sigma_A(\vec{p}, \vec{q}) | \rho_n | \Psi, \sigma_A(\vec{p}, \vec{q}) \rangle \\ \times \delta \left(p^0 - \left(m + E - \frac{\vec{p}^2}{2\mu} - \frac{\vec{q}^2}{2\nu} \right) \right). \quad (35)$$

We stress that the two forms of Eq. (31) are equivalent and should give the same results. In order to demonstrate this we computed the light cone momentum distribution, using Eq. (30)

$$f_n(y) = \int d^4 k \left(1 + \frac{k^3}{k^0} \right) \delta \left(y - \frac{k^0 + k^3}{m} \right) S_n(k), \quad (36)$$

with the two forms of Eq. (31). For the second form of this equation, the final state $|\phi, \sigma_b\rangle$ was taken to be a plane wave plus a pair of proton interacting in the 1S_0 channel. This is by far the most important channel for the final state interaction. We found that the light cone momentum distributions computed with the two forms of Eq. (31) were identical, for all purpose.

For the polarized case there are two useful spectral functions

$$S_n^+(p) = \frac{1}{2} \sum_{\pm} \int d^3 \vec{q} \langle \Psi^\pm(\vec{p}, \vec{q}) | \rho_n^\pm | \Psi^\pm(\vec{p}, \vec{q}) \rangle \\ \times \delta \left(p^0 - \left(m + E - \frac{\vec{p}^2}{2\mu} - \frac{\vec{q}^2}{2\nu} \right) \right), \quad (37)$$

$$S_n^-(p) = \frac{1}{2} \sum_{\pm} \int d^3 \vec{q} \langle \Psi^\pm(\vec{p}, \vec{q}) | \rho_n^\mp | \Psi^\pm(\vec{p}, \vec{q}) \rangle \\ \times \delta \left(p^0 - \left(m + E - \frac{\vec{p}^2}{2\mu} - \frac{\vec{q}^2}{2\nu} \right) \right). \quad (38)$$

These spectral functions are, respectively, for a neutron with spin parallel or antiparallel to the spin of the nucleus. The “+” designates a positive projection of the spin of either the neutron or the nucleus on the z axis, and the “−” a negative projection. These computations of polarized spectral functions are similar to previous work found in Refs. [26,27]. In the same way as we obtain $f_n(y)$ we can calculate the quantities, $f_n^+(y)$ and $f_n^-(y)$, just by inserting the correct spectral functions. Then one can form the useful quantity $\Delta f_n(y) = f_n^+(y) - f_n^-(y)$, which is the equivalent of $f_n(y)$ for polarized structure functions.

2. Proton in ^3He

In the case of the proton we have two possibilities for the final state, so we also have two spectral functions. The first state is a scattering state similar to the final state encountered in the neutron case, with which it shares the formula for p^0 . The second possible final state is made of a scattered proton and a deuteron. We can find the form of the proton energy in the same way we did for the scattering state, only it is now much more simple as we have only two particles in the final state and not three. With the same nonrelativistic approximation as before, one easily finds that in this case $p_\alpha^0 = M - M_d - \vec{p}_\alpha^2/(2M_d)$, where M_d is the deuteron mass. Defining the binding energy of the deuteron, E_d , in same way we did for the trinucleon we have $M_d = 2m + E_d$ and finally,

³Note that here, in the case of two identical particles, we have $\nu = m/2$ and $\mu = 2m$.

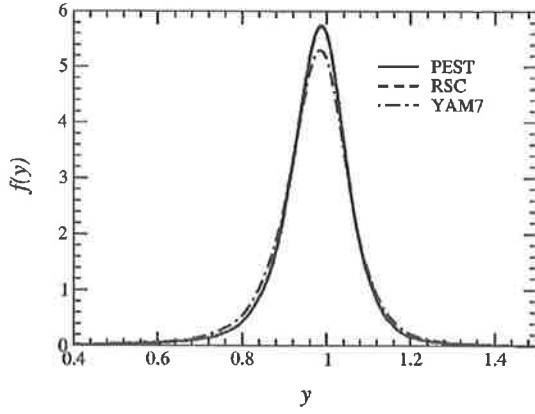


FIG. 1. Neutron light cone momentum distribution in ^3He for various potentials.

$p_\alpha^0 = m + E - E_d - \vec{p}_\alpha^2 / (2M_d)$. So we will have two spectral functions, $S_p^s(p)$ (scattering state) and $S_p^d(p)$ (deuteron state):

$$S_p^s(p) = \frac{1}{2} \sum_{\pm} \int d^3\vec{q} \langle \Psi^\pm(\vec{p}, \vec{q}) | \rho_p | \Psi^\pm(\vec{p}, \vec{q}) \rangle \times \delta\left(p^0 - \left(m + E - \frac{\vec{p}^2}{2\mu} - \frac{\vec{q}^2}{2\nu}\right)\right), \quad (39)$$

$$S_p^d(p) = \frac{1}{2} \sum_{\pm} \int d^3\vec{q} \langle \Psi^\pm(\vec{p}, \vec{q}) | \rho_p | \Psi^\pm(\vec{p}, \vec{q}) \rangle \times \delta\left(p^0 - \left(m + E - E_d - \frac{\vec{p}^2}{2M_d}\right)\right). \quad (40)$$

As in Eq. (37) and Eq. (38) the “+” and “−” indicate the nuclear spin projection on the z axis.

In term of these spectral functions we can write the light cone momentum distribution of the proton

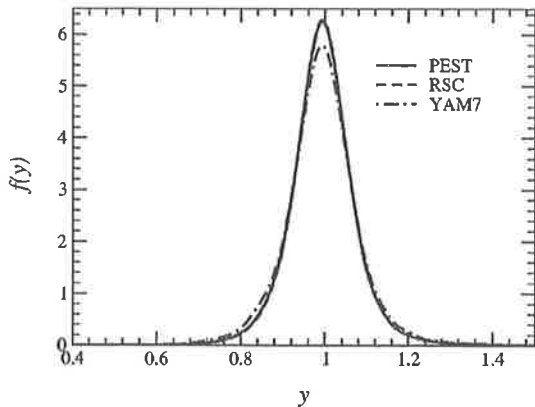


FIG. 2. Proton light cone momentum distribution in ^3He for various potentials.

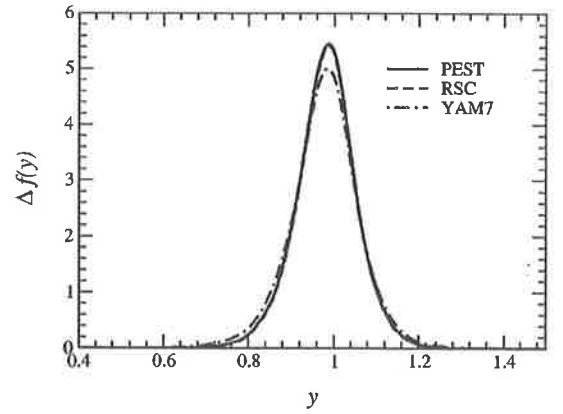


FIG. 3. Neutron polarized light cone momentum distribution in ^3He for various potentials.

$$f_p(y) = \frac{1}{2} \int d^4k \left(1 + \frac{k^3}{k^0}\right) \delta\left(y - \frac{k^0 + k^3}{m}\right) (S_p^s(k) + S_p^d(k)). \quad (41)$$

In the preceding equation we introduced a factor one-half because there are two protons in a ^3He nucleus. Without this coefficient f_p would be normalized to 2 instead of 1. In the same way we did for the neutron we can extract polarized spectral functions, $S_p^{\lambda\pm}$, for the proton by using a polarized density ρ_p^\pm in combination with the right polarization of the wave function. One can then get f_p^\pm by applying Eq. (41), with the appropriate polarized spectral functions and in the end compute $\Delta f_p(y) = f_p^+(y) - f_p^-(y)$.

C. Results

Using the formalism presented above, we have computed light cone momentum distributions for some of our three nucleon wave functions. For all those distributions we used only the first 42 three-body channels. This is because the computation of the polarized distributions involves some complicated matrix elements. However for all these wave functions the 42 first channels add up to more than 99% of the total, so one can safely assume that the contribution of

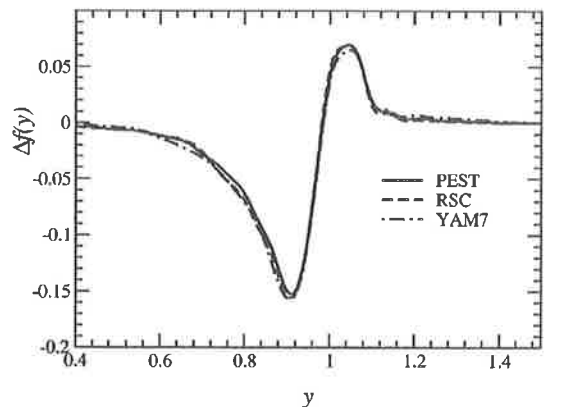


FIG. 4. Proton polarized light cone momentum distribution in ^3He for various potentials.

TABLE II. Effective polarization of the nucleons in ^3He for various potentials.

	$\Sigma P(X)$				$\int f(y)$			
	n^+	n^-	p^+	p^-	n^+	n^-	p^+	p^-
PEST	93.97%	6.03%	48.96%	51.04%	93.62%	6.32%	48.98%	50.96%
RSC	93.45%	6.55%	48.83%	51.17%	92.92%	6.79%	48.76%	50.95%
YAM7	93.66%	6.34%	48.81%	51.19%	93.25%	6.35%	48.69%	50.92%

the rest of the channels is negligible. For the unpolarized distribution the matrix elements are quite simple, so one can easily check, in this case, that the contribution from higher channels is indeed small. We compared the light cone momentum distribution for a proton and a neutron in ^3He for, respectively, 42 and 130 channels and found that for all purpose they were indistinguishable. For the PEST potential we also compared wave functions including five and 18 three-body channels and found that they were also indistinguishable. In Figs. 1 and 2 we show the proton and neutron light cone momentum distributions for our potentials (PEST, RSC and YAM7). The light cone momentum distributions given by the RSC and PEST potentials are almost indistinguishable and they cannot be separated on these figures. The YAM7 potential, however, shows some difference associated with the excess of high momentum components in D -wave wave function, in comparison with realistic potential. It is also important to note that to have consistent results one needs to use a deuteron wave function computed with the same potential as the three nucleon system.

In Figs. 3 and 4 we show the proton and neutron polarized light cone momentum distributions for the same potentials used in Figs. 1 and 2. The polarized neutron light cone momentum distribution shows the same behavior and is similar in size to its unpolarized counterpart. However, for the proton the polarized momentum distribution is far smaller than its unpolarized counterpart. In this case all the potentials gives very similar results. We note that one can extract more information from the polarized momentum distributions. While in the unpolarized case the distributions are normalized to one, in the polarized case they are normalized to the polarization of the given nucleon. From Ref. [25] one can compute these polarizations analytically in terms of the S , S' , and D waves probabilities (neglecting the small contribution of the P waves). One can compute those probabilities from the wave function and then compare them with the values extracted from the momentum distributions. From Ref. [25] we have the following relations:

$$n^+ = \int dy f_n^+(y) = 1 - \frac{1}{3}(P(S') + 2P(D)), \quad (42)$$

TABLE III. Effective polarization of the nucleons in ^3He and ^3H , with two-body interaction adjusted to produce the experimental binding energies (PEST potential only).

	$\Sigma P(X)$				$\int f(y)$			
	n^+	n^-	p^+	p^-	n^+	n^-	p^+	p^-
^3He	93.97%	6.03%	48.91%	51.09%	93.73%	6.24%	48.94%	51.02%
^3H	93.45%	6.55%	48.85%	51.15%	93.86%	6.13%	48.89%	51.10%

$$n^- = \int dy f_n^-(y) = \frac{1}{3}(P(S') + 2P(D)), \quad (43)$$

$$p^+ = \int dy f_p^+(y) = \frac{1}{2} - \frac{1}{6}(P(D) - P(S')), \quad (44)$$

$$p^- = \int dy f_p^-(y) = \frac{1}{2} + \frac{1}{6}(P(D) - P(S')). \quad (45)$$

In Table II we compare the numerical values of these two expressions in ^3He , for our various potentials. The results in quite good agreement, with the small discrepancies arising from numerical errors in the computation of many nested integrals. (Note, for example, that the overall normalization is correct to about 0.06%.) In Table III we make the same comparison but with wave functions in which we have adjusted the binding energies to the experimental values.

IV. STRUCTURE FUNCTIONS

A. Introduction

In the incoherent impulse approximation, the structure function of a nucleus is the sum of the contributions from all its constituents. As we have already said in the previous section, the convolution formalism gives a way to link the in-medium structure functions to the free ones. This formalism, however, has some limitations, especially at small Bjorken x , where other physics, like multiple scattering, becomes important. It is also only valid in the Bjorken limit, as the convolution formalism itself does not depend on Q^2 . In unpolarized scattering this formalism is a good tool to investigate the EMC effect [28], so we will use our previous results to study this effect in the three nucleon system. Another interesting result from the previous section is the fact that in ^3He , the proton polarization (i.e., $\Delta_p = p^+ - p^- \approx -2\%$) is very small and negative, while the neutron polarization (i.e., $\Delta_n = n^+ - n^- \approx 87\%$) is quite big. This is also clear from Figs. 3 and 4. This means that the neutron carries most of the spin of ^3He , so, at least for polarized scattering, this nucleus should be a good approximation to a pure neutron target. The

same argument is valid for the proton in ^3H . Since we already have a free proton target this may appear less interesting at first sight. On the other hand, it provides an ideal way to study the effect of the nuclear medium on the spin structure of a bound nucleon.

B. Unpolarized structure function and EMC effect

As we explained at the beginning of the previous section, in unpolarized deep inelastic scattering of a charged lepton on a nuclear target, all the target information is included in the two structure functions F_1 and F_2 . In a simple quark model those functions have the following form [13,15]:

$$F_1(x, Q^2) = \frac{1}{2} \sum_q e_q^2 q(x, Q^2), \quad (46)$$

$$F_2(x, Q^2) = 2xF_1(x, Q^2) = x \sum_q e_q^2 q(x, Q^2). \quad (47)$$

In these expressions $q(x)$ is the distribution of quarks of flavor q and electric charge e_q . The relation between F_1 and F_2 implies that the partons have spin 1/2 and no transverse momentum in the infinite momentum frame. A more general relation between F_1 and F_2 [13] is

$$F_2(x) = 2xF_1(x) \frac{1+R}{1+2xm_N/\nu}, \quad (48)$$

where R is the ratio of the cross section for absorbing a longitudinal photon to that for a transverse photon.

Given the relation between F_1 and F_2 , most studies concentrate on the latter. The convolution formula between the free and in medium F_2 structure functions [13,18] is

$$\tilde{F}_2^N(x, Q^2) = \int_x^{M_A/m} dy f_N(y) F_2^p\left(\frac{x}{y}, Q^2\right). \quad (49)$$

Hence the F_2 structure function of a nucleus of mass number A and proton number Z is given by

$$F_2^A(x, Q^2) = \int_x^{M_A/m} dy \left(Z f_p(y) F_2^p\left(\frac{x}{y}, Q^2\right) + (A-Z) f_n(y) F_2^n\left(\frac{x}{y}, Q^2\right) \right). \quad (50)$$

In comparing the F_2 structure functions on various targets, the European Muon Collaboration (Aubert *et al.* [28]) discovered what is now called the “EMC” effect. We define a theoretical EMC ratio as the ratio of the F_2 structure function of the nucleus to the sum of the free structure functions of the nucleons in this nucleus:

$$R_t = F_2^A / (ZF_2^p + (A-Z)F_2^n). \quad (51)$$

On the other hand, it is more common to compare the ratio of the F_2 structure function of the nucleus to that of deuterium:

$$R_x = (F_2^A/A) / (F_2^D/2). \quad (52)$$

This should be close to R_t if the deuteron is a quasifree system of a proton and a neutron and if the nucleus studied is symmetric, or almost, in its content of neutrons and protons. ^3He and ^3H are highly asymmetric nuclei, as their content in one type of nucleon is twice as much as the other. To take this into account, it is common to an isosymmetric correction so that the ratio studied is [18]

$$R_A(x, Q^2) = \frac{F_2^A(x, Q^2)}{F_2^D(x, Q^2)} I(x, Q^2), \quad (53)$$

with

$$I(x, Q^2) = \frac{F_2^p(x, Q^2) + F_2^n(x, Q^2)}{ZF_2^p(x, Q^2) + (A-Z)F_2^n(x, Q^2)}. \quad (54)$$

This ratio is, strictly speaking, the ratio of the EMC ratios of the nucleus A and the deuteron. Following the same kind of procedure used in the previous section, one can compute the light cone momentum distribution of a nucleon in the deuteron. To be consistent, this ratio has to be computed with the same interaction for both the three nucleon system and the deuteron. To compute R_A we used several parametrizations for the quark distributions.

The parametrization “CTEQ5” from the CTEQ Collaboration [29]. The collaboration gives several parametrizations, but we mainly used the one called “leading order,” and it will be the one used when we talk about the CTEQ5 parametrization, unless explicitly stated otherwise:

The “GRV” parametrization from Glück, Reya, and Vogt [30].

The “DOLA” parametrization from Donnachie and Landshoff [31].

These distributions are usually given for quarks in a proton and in order to compute neutron structure functions we used charge symmetry⁴ [32]. In Figs. 5 and 6 one can see the ratio R_3 for ^3He and ^3H , with the CTEQ5 parametrization at $Q^2 = 10 \text{ GeV}^2$, for the three potentials studied. In Fig. 7 we show R_3 in ^3He for the PEST potential alone but for all three quark distributions (again at $Q^2 = 10 \text{ GeV}^2$). We also studied the effect of adjusting the binding energy as described at the end of the first section but did not include it in Figs. 5 and 6 because it would have confused the plot. This adjustment of the binding energy caused a slightly deeper EMC effect in both ^3He and ^3H and also a slightly steeper increase at high x .

C. Polarized structure functions

If one does experiments with both a polarized lepton beam and a polarized spin 1/2 nuclear target, one needs two more structure functions, g_1 and g_2 . One can perform various measurements of cross sections with several polariza-

⁴With the exception of the DOLA distribution which gives proton and deuteron distributions. In this case we took the neutron as the difference between the deuteron and the proton.

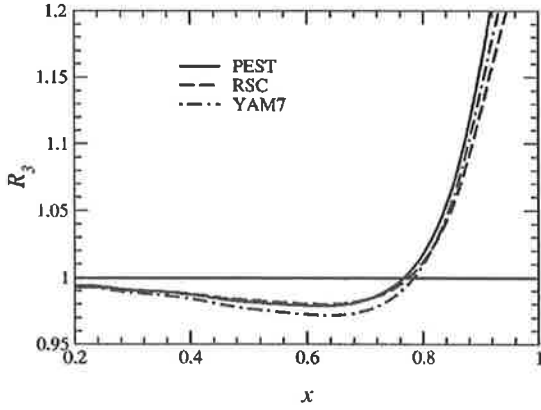


FIG. 5. The ratio R_3 , given in Eq. (53), for ${}^3\text{He}$, at $Q^2=10$ GeV^2 , calculated for various potentials using the CTEQ5 quark distributions.

tions in order to extract those two structure functions. They are smaller than F_1 and F_2 and g_2 , in particular, is often neglected. As we indicated in the Introduction, the figures for the effective polarization of the nucleons in the three nucleon system seem to indicate that the contribution to the nuclear spin structure functions from the doubly represented nucleons is severely reduced. Thus, this system should be a good approximation to a pure single nucleon target. At leading order, g_1 has the following form [14,33,34]:

$$g_1(x, Q^2) = \frac{1}{2} \sum_q e_q^2 \Delta q(x, Q^2). \quad (55)$$

In Eq. (55), Δq are the polarized quark distributions. They involve the difference between the distributions of quarks with the same and opposite helicity from that of the nucleon. It is much harder to find a simple parton interpretation for g_2 [14].

The convolution formula relating the free spin structure function to that in-medium is the following:

$$\tilde{g}_1^N(x, Q^2) = \int_x^{M_A/m} \frac{dy}{y} \Delta f_N(y) g_1^N\left(\frac{x}{y}, Q^2\right). \quad (56)$$

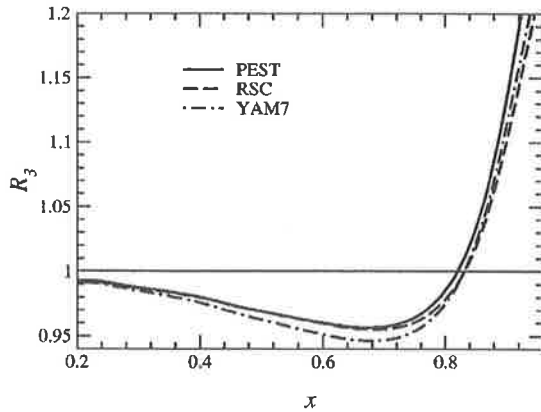


FIG. 6. The ratio R_3 , given in Eq. (53), for ${}^3\text{H}$, at $Q^2=10$ GeV^2 , calculated for various potentials using the CTEQ5 quark distributions.

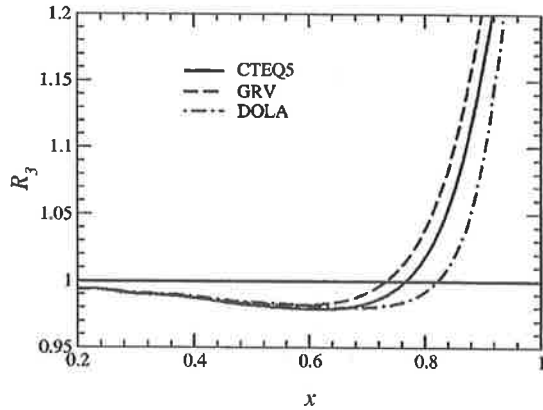


FIG. 7. The ratio R_3 , given in Eq. (53), for ${}^3\text{He}$, at $Q^2=10$ GeV^2 , calculated for the PEST potential, using various quark distributions for the nucleons.

We computed the g_1 structure function of ${}^3\text{He}$ using the same three potentials as for F_2 . The results from those potentials are sufficiently close that we will only use the results from the PEST potential hereafter. To compute g_1 we mainly used the NLO “standard scenario” of Ref. [35]. We also studied the impact of the off-shell correction from Ref. [36] on g_1 . (The off-shell correction was calculated using a local density approximation and the quark meson coupling model [37] to estimate the change of the parton distributions in a bound nucleon.) In Fig. 8 we show the following three curves at $Q^2=10$ GeV^2 : $xg_1(x)$ for the free neutron, as well as $xg_1(x)$ for ${}^3\text{He}$ with and without the off-shell correction. As one can see, the three of them are close. The main complication in the extraction of g_1 for the free neutron from ${}^3\text{He}$ is that the free proton spin structure function is very big compared with that of the neutron. So, while its contribution in ${}^3\text{He}$ is severely reduced by the low effective polarization, it is still not negligible. One way to estimate the size of the contribution of the proton is to compare $g_1({}^3\text{He})$ with a formula often used in the experimental analysis [38] (see Ref. [15] for a derivation):

$$g_1({}^3\text{He}) \approx \Delta_n g_1(n) + 2\Delta_p g_1(p). \quad (57)$$

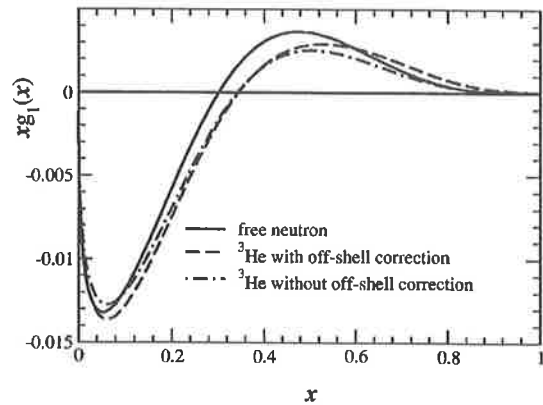


FIG. 8. Comparison of several calculations of $xg_1(x)$ for ${}^3\text{He}$, at $Q^2=10$ GeV^2 , with the parametrization of $xg_1(x)$ for the free neutron at the same energy.

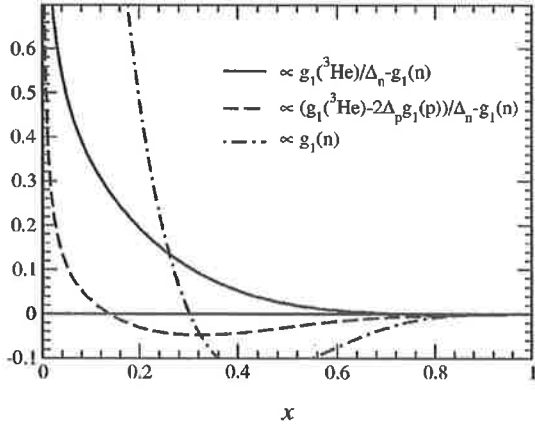


FIG. 9. Δ_g , Δ'_g , and $g_1(n)$ at $Q^2 = 10 \text{ GeV}^2$. Note that all three curves have been divided by $\int dx g_1(^3\text{He})$.

If the contribution of the proton to $g_1(^3\text{He})$ is negligible, Eq. (57) is equivalent to $g_1(^3\text{He}) \approx \Delta_n g_1(n)$. To estimate the effect of the proton contribution in the extraction of $g_1(n)$, we plotted the following differences:

$$\Delta_g = \frac{g_1(^3\text{He}) - 2\Delta_p g_1(p)}{\Delta_n} - g_1(n) \quad (58)$$

and

$$\Delta'_g = \frac{g_1(^3\text{He})}{\Delta_n} - g_1(n). \quad (59)$$

In Figs. 9 and 10 we plot both Δ_g and Δ'_g . The second plot includes the off-shell effect of Ref. [36]. Note that the curves have been divided by $\int dx g_1(^3\text{He}) (\approx -1/16)$ so that one can judge the effect on the spin sum rule. Since one ultimately wants to extract $g_1(n)$, we have also plotted that with the same normalization, so as to have an idea of the size of the

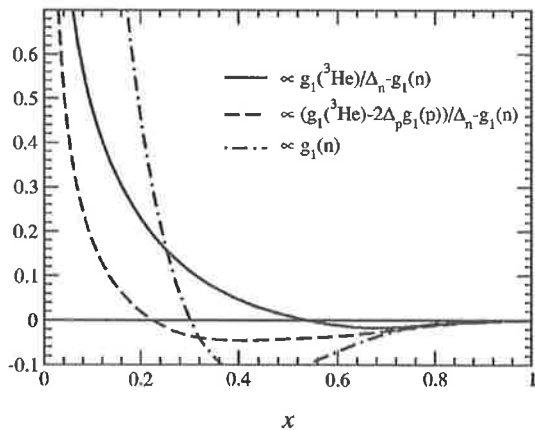


FIG. 10. Δ_g , Δ'_g , and $g_1(n)$, including off-shell corrections, at $Q^2 = 10 \text{ GeV}^2$. Note that all three curves have been divided by $\int dx g_1(^3\text{He})$.

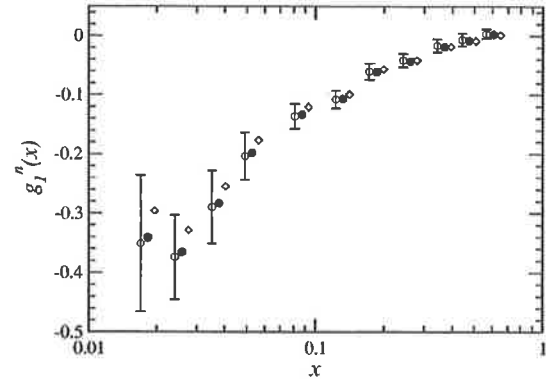


FIG. 11. Corrections to $g_1(n)$ data from E154. White circles represent the original data. Black circles are corrected for binding energy and nuclear effect. Diamonds have all corrections from the black circles as well as off-shell corrections. The error bars are statistical errors.

error in the differences.⁵ It is clear from both plots that one gets more accurate results by including the proton contribution for midrange x ($0.2 \leq x \leq 0.6$), the biggest error in this region occurring when the structure function crosses the x axis. At higher x ($x \geq 0.6$) the effect of Fermi motion is significant and this will be even more important for ^3H , below. Nevertheless, the absolute value of the structure function is small and the corrections have little effect on the spin sum rule. If we apply the corrections computed with this parametrization to the experimental results of E154 [39] and HERMES [40], we get Figs. 11 and 12. It is quite clear from those figures that it is possible to extract $g_1(n)$ from ^3He data without worrying too much about nuclear effects on most of the kinematical range. Similar results are found for other partons distributions such as those from Ref. [41]

In the case of tritium one can plot a ratio, as $g_1(p)$ does not change sign. Therefore, to illustrate the effect of the neutron contribution in this case we plot

$$R_g = \frac{g_1(^3\text{H}) - 2\Delta_n g_1(n)}{\Delta_p g_1(p)} \quad (60)$$

and

$$R'_g = \frac{g_1(^3\text{H})}{\Delta_p g_1(p)}. \quad (61)$$

In Fig. 13 we show both ratios (R_g is the solid line and R'_g is the dashed line) without including the off-shell corrections [36] as well as R_g with the off-shell corrections (dot-dashed line). In this figure we can clearly see that on most of the interval the contribution of the neutron is negligible, some difference appearing for small x . This is expected simply because $g_1(n)$ is significantly smaller than $g_1(p)$ for most values of x . On the other hand, we can also see that medium

⁵We do not plot the ratio of structure functions because in both the neutron and ^3He cases g_1 can be zero, leading to singularities in the plots.

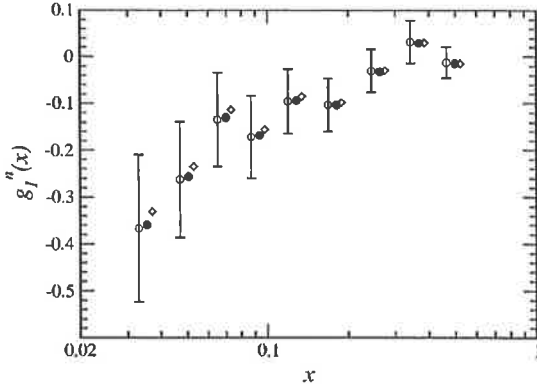


FIG. 12. Corrections to $g_1(n)$ data from HERMES. White circles represent the original data. Black circles are corrected for binding energy and nuclear effect. Diamonds have all corrections from the black circles as well as off-shell corrections. The error bars are statistical errors.

effects seem to be quite important and that the off-shell correction makes an important difference. One can also see clearly the effect of Fermi motion at high x , while it would be invisible if one were to plot differences. It is clear from these results that from a measurement of $g_1(^3\text{H})$ one can expect to extract the size of the change in the spin structure function of the bound proton and one might even hope to separate the origin of this effect.

V. CONCLUSIONS

We have computed the three-nucleon structure functions from various two body potentials. This involved calculating wave functions, light cone momentum distributions and finally the structure functions. We have presented our computations of the effects of nuclear binding and Fermi motion in the ratio R_A for both ^3He and ^3H . We have shown that those effects were quite close for various two-body potentials and quark distributions. In addition, we saw that isospin breaking would have only a small effect on these findings. This result has been used elsewhere [42] in a proposal to measure the d/u ratio at large x at Jefferson Laboratory [43,44].

From our study of the spin structure function of ^3He , we showed that it is possible to extract the structure function of

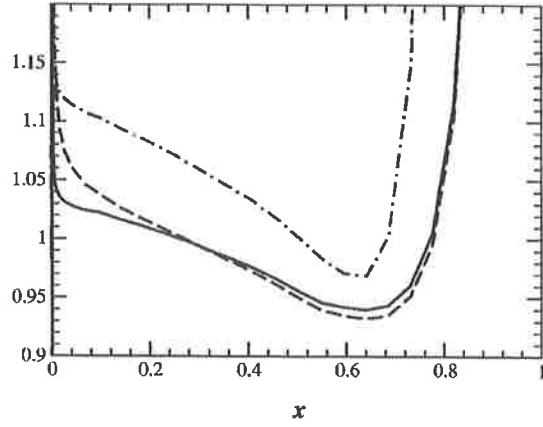


FIG. 13. The ratio of the proton spin spin structure function, g_1^p (at 10 GeV^2), extracted from ^3He data under two approximations [R_g and R'_g ; see Eqs. (60) and (61)] to the free proton g_1^p . The solid line is R_g and the dashed line is R'_g , both computed without off-shell corrections. Dash-dotted line is R_g when one includes off-shell corrections

a polarized neutron with reasonable accuracy. However, it is necessary to account for the contribution from the pair of protons which are not totally unpolarized. Turning to the polarized structure function of ^3H , we saw that while the experiment is extremely challenging it could also be very valuable. In particular, one can measure the size of the medium corrections and check experimentally the predicted modification of the spin dependent parton distributions of the bound nucleon.

ACKNOWLEDGMENTS

This work was supported by the Australian Research Council. We would like to thank W. Melnitchouk for many helpful discussions.

APPENDIX A: THE KERNEL OF THE HOMOGENEOUS FADDEEV EQUATION

For completeness, we present in this appendix the explicit expression for the kernel of the homogeneous Faddeev equation when the interaction is represented by a separable potential. The details of the derivation are in Ref. [8]. We have

$$Z_{l_\alpha N_\alpha; l_\beta N_\beta}^{II} = \langle g_{l_\alpha}^{n_\alpha}; \Omega_{l_\alpha N_\alpha}^{II} | G_0(E) | \Omega_{l_\beta N_\beta}^{II}; g_{l_\beta}^{n_\beta} \rangle = \frac{1}{2} \int_{-1}^{+1} dx \frac{g_{l_\alpha}^{n_\alpha}(q_\alpha) g_{l_\beta}^{n_\beta}(q_\beta)}{E - \frac{1}{m}(p_\alpha^2 + p_\beta^2 + p_\alpha p_\beta x)} \Gamma_{l_\alpha N_\alpha; l_\beta N_\beta}^{II}(p_\alpha, p_\beta; x), \quad (\text{A1})$$

where

$$\Gamma_{l_\alpha N_\alpha; l_\beta N_\beta}^{II}(p_\alpha, p_\beta; x) = \left(\frac{p_\beta}{q_\alpha} \right)^{l_\alpha} \left(\frac{p_\alpha}{q_\beta} \right)^{l_\beta} B_{N_\alpha N_\beta} \sum_{\mathcal{L}} P_{\mathcal{L}}(x) \sum_{a=0}^{l_\alpha} \sum_{b=0}^{l_\beta} A_{l_\alpha N_\alpha; l_\beta N_\beta}^{\mathcal{L}, a, b} \left(\frac{p_\alpha}{p_\beta} \right)^{a-b}, \quad (\text{A2})$$

with $P_{\mathcal{L}}(x)$ the Legendre polynomial of order \mathcal{L} , and

$$x = \hat{p}_\alpha \cdot \hat{p}_\beta, \quad \vec{q}_\alpha = -\vec{p}_\beta - \frac{1}{2}\vec{p}_\alpha, \quad \vec{q}_\beta = \vec{p}_\alpha + \frac{1}{2}\vec{p}_\beta. \quad (\text{A3})$$

The coefficients $A_{l_\alpha N_\alpha; l_\beta N_\beta}^{\mathcal{L}, a, b}$ which results from the recoupling of the spin and orbital angular momentum is given by

$$\begin{aligned} A_{l_\alpha N_\alpha; l_\beta N_\beta}^{\mathcal{L}, a, b} = & (-1)^R \hat{l}_\alpha \hat{l}_\beta \hat{L}_\alpha \hat{L}_\beta \hat{S}_\alpha \hat{S}_\beta \hat{J}_\alpha \hat{J}_\beta \hat{S}_\alpha \hat{S}_\beta \hat{L}^2 \rho_\alpha^a \rho_\beta^b \sqrt{\frac{(2l_\alpha+1)!(2l_\beta+1)!}{(2a)!(2b)!(2l_\alpha-2a)!(2l_\beta-2b)!}} \sum_{f\Lambda\Lambda'} (f\Lambda\Lambda')^2 \begin{Bmatrix} S_\alpha & S_\beta & f \\ L_\beta & L_\alpha & J \end{Bmatrix} \\ & \times \begin{Bmatrix} L_\alpha & L_\beta & f \\ \Lambda' & \Lambda & \mathcal{L} \end{Bmatrix} \begin{Bmatrix} j_\alpha & S_\alpha & S_\beta & j_\beta \\ \bar{J}_\alpha & f & \bar{J}_\beta & j_\gamma \end{Bmatrix} \begin{Bmatrix} l_\alpha & l_\beta & f \\ a & l_\beta-b & \Lambda \end{Bmatrix} \begin{Bmatrix} a & l_\beta-b & \Lambda \\ 0 & 0 & 0 \end{Bmatrix} \\ & \times \begin{Bmatrix} \Lambda' & \mathcal{L} & L_\beta \\ 0 & 0 & 0 \end{Bmatrix} \begin{Bmatrix} \Lambda & \mathcal{L} & L_\alpha \\ 0 & 0 & 0 \end{Bmatrix} \begin{Bmatrix} l_\alpha-a & b & \Lambda' \\ 0 & 0 & 0 \end{Bmatrix}, \quad (\text{A4}) \end{aligned}$$

where the $12-j$ symbol is that defined by Ord-Smith [45], the phase R is defined as

$$R = -J + L_\alpha + L_\beta + S_\alpha + S_\beta + \bar{J}_\alpha + \bar{J}_\beta - j_\alpha + s_\beta + l_\alpha + \mathcal{L},$$

and finally ρ_α and ρ_β are

$$\rho_\alpha = \frac{m_\beta}{m_\beta + m_\gamma} = \frac{1}{2}, \quad \rho_\beta = \frac{m_\alpha}{m_\alpha + m_\gamma} = \frac{1}{2}.$$

The isospin recoupling coefficient $B_{N_\alpha N_\beta}$ is given in terms of $6-j$ symbol by the relation

$$B_{N_\alpha N_\beta} = (-1)^{l_\alpha + l_\gamma - \bar{l}_\beta + 2l_\alpha} \hat{l}_\alpha \hat{l}_\beta \begin{Bmatrix} l_\beta & l_\gamma & \bar{l}_\alpha \\ l_\alpha & I & \bar{l}_\beta \end{Bmatrix}, \quad (\text{A5})$$

-
- [1] J. Haidenbauer and W. Plessas, Phys. Rev. C **30**, 1822 (1984); **32**, 1424 (1985).
[2] M. Lacombe, B. Loiseau, J. M. Richard, R. Vinh Mau, J. Côté, P. Pirès, and R. de Tourreil, Phys. Rev. C **21**, 861 (1980).
[3] W. C. Parke, Y. Koike, D. R. Lehman, and L. C. Maximon, Few-Body Syst., Suppl. **11**, 89 (1991).
[4] T. Y. Saito and I. R. Afnan, Phys. Rev. C **50**, 2756 (1994); Few-Body Syst., Suppl. **18**, 101 (1995).
[5] I. R. Afnan and J. M. Read, Aust. J. Phys. **26**, 725 (1973); Phys. Rev. C **8**, 1294 (1973).
[6] R. V. Reid, Ann. Phys. (N.Y.) **50**, 411 (1968).
[7] Y. Yamaguchi and Y. Yamaguchi, Phys. Rev. **95**, 1635 (1954).
[8] I. R. Afnan and A. W. Thomas, in *Modern Three-Hadron Physics*, edited by A. W. Thomas (Springer-Verlag, Berlin/Heidelberg/New York, 1977), p. 1.
[9] C. Lovelace, Phys. Rev. **135**, B1225 (1964).
[10] I. R. Afnan and N. D. Birrell, Phys. Rev. C **16**, 823 (1977).
[11] R. Machleidt, F. Sammarruca, and Y. Song, Phys. Rev. C **53**, 1483 (1996).
[12] B. F. Gibson, Nucl. Phys. **A543**, 1e (1992); M. T. Peña, P. U. Sauer, A. Stalder, and G. Gortemeyer, Phys. Rev. C **48**, 2208 (1993); S. A. Coon and M. T. Peña, *ibid.* **48**, 2559 (1993); T. Y. Saito and J. Haidenbauer, Eur. Phys. J. C **7**, 559 (2000).
[13] D. F. Geesaman, K. Saito, and A. W. Thomas, Annu. Rev. Nucl. Part. Sci. **45**, 337 (1995).
[14] B. Lampe and E. Reya, Phys. Rep. **332**, 1 (2000).
[15] M. Anselmino, A. Efremov, and E. Leader, Phys. Rep. **261**, 1 (1995).
[16] R.-W. Schulze and P. U. Sauer, Phys. Rev. C **48**, 38 (1993).
[17] R.-W. Schulze and P. U. Sauer, Phys. Rev. C **56**, 2293 (1997).
[18] T. Uchiyama and K. Saito, Phys. Rev. C **38**, 2245 (1988).
[19] L. L. Frankfurt and M. I. Strikman, Phys. Lett. **64B**, 433 (1976); **65B**, 51 (1976); **76B**, 333 (1978); Nucl. Phys. **B148**, 107 (1979); Phys. Rep. **76**, 215 (1981).
[20] H.-M. Jung and G. A. Miller, Phys. Lett. B **200**, 351 (1988).
[21] C. Ciofi degli Atti and S. Liuti, Phys. Rev. C **41**, 1100 (1990).
[22] C. Ciofi degli Atti, E. Pace, and G. Salmè, Phys. Lett. **141B**, 14 (1984).
[23] S. Frullani and J. Mougey, Adv. Nucl. Phys. **14**, 1 (1984).
[24] A. E. L. Dieperink and T. de Forest, Jr., Annu. Rev. Nucl. Sci. **25**, 1 (1975).
[25] J. L. Friar, B. F. Gibson, G. L. Payne, A. M. Bernstein, and T. E. Chupp, Phys. Rev. C **42**, 2310 (1990).
[26] A. Kievsky, E. Pace, G. Salme, and M. Viviani, Phys. Rev. C **56**, 64 (1997).
[27] C. Ciofi degli Atti, E. Pace, and G. Salme, Phys. Rev. C **51**, 1108 (1995).
[28] J. J. Aubert *et al.*, Phys. Lett. **123B**, 275 (1983).
[29] H. L. Lai, J. Huston, S. Kuhlmann, J. Morfin, F. Olness, J. Pumplin, and W. K. Tung, Eur. Phys. J. C **12**, 375 (2000).

- [30] M. Glück, E. Reya, and A. Vogt, *Z. Phys. C* **67**, 433 (1995).
- [31] A. Donnachie and P. V. Landshoff, *Z. Phys. C* **61**, 139 (1994).
- [32] J. T. Londergan and A. W. Thomas, *Prog. Part. Nucl. Phys.* **41**, 49 (1998).
- [33] R. M. Woloshyn, *Nucl. Phys. A* **496**, 749 (1989); B. Blankleider and R. M. Woloshyn, *Phys. Rev. C* **29**, 538 (1984).
- [34] Y. Goto *et al.*, Asymmetry Analysis Collaboration, *Phys. Rev. D* **62**, 034017 (2000).
- [35] M. Glück, E. Reya, M. Stratmann, and W. Vogelsang, *Phys. Rev. D* **53**, 4775 (1996).
- [36] F. M. Steffens, K. Tsushima, A. W. Thomas, and K. Saito, *Phys. Lett. B* **447**, 233 (1999).
- [37] P. A. M. Guichon, K. Saito, E. Rodionov, and A. W. Thomas, *Nucl. Phys. A* **601**, 349 (1996); K. Saito and A. W. Thomas, *Phys. Rev. C* **51**, 2757 (1995); P. A. Guichon, *Phys. Lett. B* **200**, 235 (1988).
- [38] C. Ciofi degli Atti, S. Scopetta, E. Pace, and G. Salme, *Phys. Rev. C* **48**, 968 (1993).
- [39] K. Abe *et al.*, E154 Collaboration, *Phys. Rev. Lett.* **79**, 26 (1997).
- [40] K. Ackerstaff *et al.*, HERMES Collaboration, *Phys. Lett. B* **404**, 383 (1997).
- [41] T. Gherman and W. J. Stirling, *Z. Phys. C* **65**, 461 (1995).
- [42] I. R. Afnan *et al.*, *Phys. Lett. B* **493**, 36 (2000).
- [43] G. G. Petratos *et al.*, Jefferson Lab proposal, 2000.
- [44] E. Pace, G. Salme, and S. Scopetta, *Nucl. Phys. A* **689**, 453 (2001).
- [45] R. J. Ord-Smith, *Phys. Rev.* **94**, 1227 (1954).

